Analysis of phase transformations in hydrogenated titanium metals by non-isothermal dilatometry

A thesis submitted to the Faculty of Engineering and the Built Environment, University of Cape Town, in fulfilment of the requirements for the degree of Master of Science of Engineering

By

Naseeba Abbas

Centre for Materials Engineering

2011

ABSTRACT

Hydrogen was used as a temporary alloying element in CP Ti and Ti-6Al-4V. The microstructural evolution and phase transformations were monitored, before, during and after hydrogenation with *in-situ* dilatometric testing.

Wrought CP Ti and Ti-6Al-4V specimens were pre-annealed and experienced four consecutive thermal cycles (Cycles 1-4) i.e. hydrogenation, post-hydrogenation, dehydrogenation and post-dehydrogenation, during dilatometric testing. The specimen in each thermal cycle was heated to 1000°C, heating rate 1°C/min (with an isothermal hold at 1000°C for three hours for hydrogenation and dehydrogenation cycles) and then cooled to room temperature at cooling rate of 1°C/min. Water quench experiments were performed on CP Ti during the heating step of the hydrogenation thermal cycle (Cycle 1) at 750, 825 and 940°C and at 1000°C for Ti-6Al-4V. The evolved microstructures were examined using light microscopy, SEM and EBSD.

The coefficient of thermal expansion (COTE) vs. temperature curves were plotted from the dilatometric (strain vs. temperature) curves. These curves, coupled with the use of the published Ti-H and Ti-6Al-4V-H phase diagrams were able to estimate the limit of hydrogen absorbed during the hydrogenation cycle; in CP Ti this was ±40at%H and in Ti-6Al-4V it was >15at%H. The β-transus of CP Ti, with hydrogen in solid solution was lowered to ~ 300°C as predicted by the Ti-H phase diagram.

The sequence of phase transformations for CP Ti and Ti-6Al-4V during hydrogenation could also be traced using dilatometry, SEM and EBSD analysis. The phase transformations for the two materials differed significantly. For CP Ti this was $\alpha \rightarrow \alpha_H \rightarrow \alpha_H + \beta_H \rightarrow \beta_H \rightarrow \beta_H + (G)$ and $\beta_H \rightarrow \alpha_H + hydride$ during heating and cooling respectively; for Ti-6Al-4V this was $\alpha+\beta \rightarrow \alpha_H+\beta_H \rightarrow \alpha_H+\beta_H+hydride \rightarrow \beta_H$ and $\beta_H \rightarrow \alpha_H + \beta_H + hydride$ during heating and cooling respectively. The formation of hydrides and absorption of hydrogen resulted in the lattice expansion of CP Ti and Ti-6Al-4V.

In conclusion, dilatometry coupled with light microscopy, EBSD and SEM was successfully used to monitor the real-time phase transformation behaviour of both CP Ti and Ti-6Al-4V, before, during and after hydrogenation.

ACKNOWLEDGEMENTS

First and foremost I would like to thank Almighty God for giving me the wisdom and strength to complete this project and the following people:

My supervisor Professor R.D Knutsen, for his supervision, encouragement and guidance.

Glen Newins and the all the staff at the mechanical engineering workshop for preparing my samples.

Miranda Waldron at the Electron Microscope Unit and Alon Bas for his assistance with the dilatometer.

All the staff and students at the Centre for Materials Engineering for their support and encouragement.

To my family and friends for their constant support, help, understanding and prayers.

Thank you.

DECLARATION

I, Naseeba Abbas, know the meaning of plagiarism and declare that all the work in this document, except for that which is acknowledged, is my own.

Signature: Date:

TABLE OF CONTENTS

TABLE OF FIGURES

1 INTRODUCTION

1.1 Subject of research

This project deals with monitoring the phase transformations and microstructural evolution in wrought commercially pure titanium (CP Ti) and the Ti-6Al-4V alloy, utilising hydrogen as a temporary alloying element with *in situ* dilatometry during hydrogen purging.

1.2 Background to research

Hydrogen is used as a temporary alloying element since it can be easily added and removed without melting. Titanium and its alloys have a high affinity for hydrogen and are able to absorb up to 60at% from temperatures 600°C and greater [**1**].

Hydrogen utilised during various heat treatments of CP Ti and Ti-6Al-4V alloy, lowers the β-transus temperature in order to refine the microstructure and hence, improves the mechanical properties at a lower cost. This type of processing is called thermohydrogen processing (THP) [**1**]. The hydrogen within the alloy works by modifying phase compositions, developing of metastable phases and altering the kinetics of phase transformations [**1**]. The decomposition of the metastable phases results in the refinement of the microstructure. However, contents of greater 0.02ppm of hydrogen remaining within the metal can be detrimental and leads to degradation in fracture related mechanical properties [**2**]. The removal of hydrogen after processing is thus critical in order to avoid this degradation. Removal of hydrogen is achieved by vacuum annealing where the reaction of hydrogen with the alloy is reversible owing to its positive enthalpy of solution in titanium [**3**].

Hydrogen is capable of destabilising the low temperature α phase and stabilising the more ductile high temperature β phase in the alloy [**4**]. Therefore when hydrogen is added the α-phase transforms partly into the β-phase above the eutectoid temperature, the temperature of transforming α to β phase is lowered and the temperature interval of the two phase (α+β) is increased [**1**].

The decrease in the temperature range of the (α+β) to β transformation by the addition of hydrogen, leads to a reduction in grain growth on heating into the modified β range [**5**]. The hydrogen-induced increase in the temperature interval of the α+β range allows heat treatments to be performed that would not have been possible without the addition of hydrogen. These factors in turn leads to different microstructures in the conventional Ti-6Al-4V alloy [**5**].

An increase in the more workable β-phase improves hot-workability of the alloy and decreases the hot working temperatures. The shear modulus of the β-phase increases due to hydrogen affecting dislocation interactions and thus strengthening the β-phase.

Hydrogen addition to the alloy decreases the β to α+β transus temperature, which then reduces the critical cooling rate required for martensite formation [**6**].

The conventional method of thermohydrogen processing involves i) β solution treatment before, during or after hydrogenation, ii) aging treatment below the hydrogenated β-transus for thermomechanical processing and finally iii) dehydrogenation by vacuum annealing at a lower temperature [**7**].

1.3 Objectives of the research

The objectives of the research are to:

- Successfully modify the push-rod dilatometer to act as a dual functioning dilatometer/hydrogen furnace
- Monitor the phase transformation behaviour of CP Ti and the Ti-6Al-4V alloy using the dual functioning dilatometer before, during and after hydrogenation
- Use the temporary alloying abilities of hydrogen to alter the kinetics and phase transformations of the stable CP Ti and Ti-6Al-4V alloy
- Determine the phases formed before, during and after hydrogenation
- Compare the phase transformation behaviour of CP Ti and Ti-6Al-4V before, during and after hydrogenation
- Monitor the absorption-desorption behaviour of hydrogen in CP Ti and Ti-6Al-4V and hydride formation/decomposition

1.4 Scope and limitations

The main material for this project is Ti-6Al-4V. Experiments were also performed on CP Ti to serve as a bench mark for Ti-6Al-4V. The focus of the project is to monitor the real-time phase transformations of both CP Ti and Ti-6Al-4V before, during and after hydrogenation using dilatometry. The mechanical properties arising from the different heat treatments with hydrogen and in vacuum were not evaluated. The project also focuses on the phase transformations during continuous heating and cooling. Isothermal phase transformations were not considered.

1.5 Plan of development

The project has been presented in a particular sequence. The first chapter is aimed to introduce the reader to the research project. The second chapter is a review of past research that has been conducted on heat treating and thermohydrogen processing of titanium alloys. The third chapter describes the redesign and modification of the testing facility and the fourth chapter the experimental procedure. The results and discussion are presented in chapter five, with conclusions in chapter six and finally future work in chapter seven.

2 LITERATURE REVIEW

2.1 Material

2.1.1 The history of titanium

Prior to World War II, titanium was merely a curiosity to metallurgists, though it had the potential for great strength and light weight properties. Titanium in its natural form i.e. titanium oxide (rutile TiO_2) had limited applications, such as an additive to paint. It was only after the end of the Cold War that titanium expanded from military use to commercial applications, including artificial hips, golf clubs, tennis rackets, bicycles and wedding rings. Titanium is as strong as steel, yet it is 45% lighter and is twice as strong as aluminium and only 60% heavier. It is biologically inert, making it ideal for implants for the body. It also does not corrode in naturally corroding environments, therefore it may be used for sea submersibles, heat exchangers and a variety of chemical plant applications [**8**].

Titanium is difficult to obtain from its ore which commonly occurs as "black sand". Transforming this black sand into a usable material is a complicated and expensive process. William Kroll, a metallurgist developed the Kroll process whereby rutile titanium is converted to titanium tetrachloride and then reacts with magnesium or sodium to produce titanium [**8**].

2.1.2 Introduction to titanium and its alloys

Titanium is classified as a lightweight, corrosion resistant material. The material can be strengthened through alloying and heat treating. Titanium has the following properties:

- Good strength to weight ratio
- Low density
- Low coefficient of thermal expansion
- Good corrosion resistance
- Good toughness
- Good oxidation resistance at intermediate temperatures

Titanium is commonly used in the aerospace (for jet engines and airframe components) and marine industries due to the above properties and it is a representative material in modern turbine engines. Usage is also widespread in most

commercial and military aircraft. Its properties, as shown in Table 2.1 is what makes this metal highly versatile in industry [**9**].

Titanium alloys are determined by their alloying contents and heat treatments. Pure titanium has an "alpha" (α) structure up to 883°C and above this temperature it transforms to the "beta" (β) structure. This temperature is known as β-transus temperature [**10**]. These two phases exhibit different properties due to their different crystal structures. Table 2.1 lists some properties of CP Ti and Table 2.2 lists coefficients of thermal expansion at varying temperatures.

CP Ti exhibits a hcp crystal structure (See Figures 2.1a and b) and the coefficients of thermal expansion for the basal plane (along the a axis) will differ from the adjacent plane (along the c axis) (See Table 2.2) [**11**]. The difference in these coefficients of thermal expansion (COTE) values can be attributed to the fact that the binding between the neighbouring atoms in the basal plane is weaker than the adjacent planes, and hence atomic displacements due to temperature increase will be easier and larger along the a axis than along the c axis. Boyer et al. however, makes mention that the COTE values for the adjacent plane are reported to be 20% greater than that of the basal plane [**12**]. Hence, there is a discrepancy for the difference in COTE values in the basal and adjacent planes in the hcp crystal lattice. For the purpose of this research, only average COTE values along combined a and c axes were considered.

The addition of α stabilising elements such as (Al, Ga, Sn) increases the temperature of allotropic transformation and the addition of β stabilising elements such as (V, Nb and Ta) reduces the temperature of the allotropic transformation. Through various thermal treatments and the addition of alloying elements, various microstructures resulting in different mechanical properties may be obtained.

Alloying elements are either classified as α or β stabilizers

- α stabilizers increases the temperature at which the α phase is stable, e.g. Al, Ga, Ge, C, O_2, N_2, Sn, Zr
- β stabilisers decreases the temperature at which the β phase is stable, e.g. Mo, V, Ta, Fe, Cr, Si, Ni, Cu, H_2

Table 2.1: Selected properties of CP titanium [13]

Density (g/cm^3)	Poisson's ratio	Elastic modulus (GPa)	Tensile strength (MPa)	Yield strength (MPa)	Elongation (%)	Reduction in area (%)	Impact strength (J) (Charpy)	Hardness (HB)
4.51	0.34	104.1	310	172	25	70	20	265

Table 2.2: Reported Coefficients of thermal expansion at various temperature ranges for CP titanium [13]

T (°C)	Room T (along c axis)	Room T (along a axis)	20-100	20-315	20-540	20-650	20-815
Coefficient of thermal expansion (10^{-6}/°C)	5.6	9.5	8.6*	9.2*	9.7*	10.1*	10.1*

**Average COTE along combined a and c axes*

2.1.3 Alloying elements and classification of titanium alloys

Titanium is alloyed with other elements to improve its mechanical properties such as strength, toughness and hardness. There are three main types of titanium alloys based on the types and amounts of alloying elements, viz. α (hexagonal closed packed lattice structure), β (body centred cubic lattice structure) and α+β (two-phase) alloys.

a.) α (stabilised crystal structure being hexagonal close packed crystal structure) and near α-alloys. This is the low temperature allotrope of titanium and consists predominantly of the α phase which is non heat treatable and weldable. These alloys have medium strength and creep resistance at elevated temperatures [**14**].

b.) β (stabilised crystal structure being body centred cubic crystal structure). This alloy is capable of retaining 100% β when quenched from the β phase field. These alloys are heat treatable to very high strengths and are readily

formable. They also have a high density and low ductility. Due to these disadvantages they do not have much use at present [**14**].

c.) α+β alloys: Consists of mainly α-phase at room temperature, but they do have more of the β- phase than the α and near α alloys. Most of these alloys are heat treatable to a moderate increase in strength. These type of alloys have a medium to high strength level and have good forming properties [**14**].

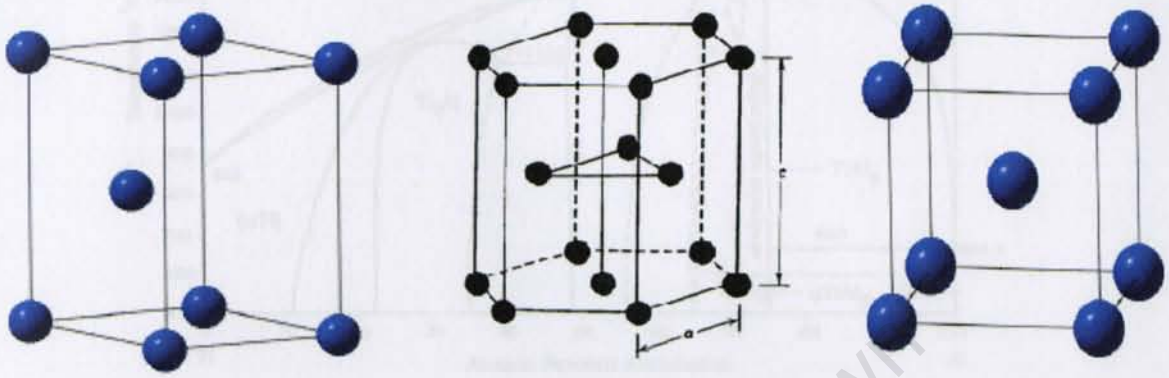

Figure 2.1: *Crystal structure of a) Primitive hexagonal close packed (hcp) [**15**] b) hexagonal type (hcp) showing lattice parameters a and c and c) body centred cubic (bcc) [**15**]*

2.1.4 The classification of Ti-6Al-4V alloy

The binary phase diagram for the Ti-Al system (See Figure 2.2) shows various intermetallic compounds with an increase in Al as well as α and β phases. The β-transus increases with an increase in Al, since Al is a α stabiliser.

For the Ti-V system as shown in Figure 2.3, the β-transus temperature decreases since V is a β stabiliser and hence lowers the temperature at which β-phase is stable.

Ti-6Al-4V is classified as a α+β alloy, since it is stable in this phase at room temperature as shown in Figure 2.4a by the dashed line. Figure 2.4a is a version of the Ti-6Al-4V pseudo-binary phase diagram derived from experimental technique and records the β transus to be 980°C [**16**].

The pseudo-binary phase diagram for Ti-6Al-4V was as predicted in Figure 2.4b using a software package ThermoCalc®. The software considered the influence of Ti, V, Al, Fe and O on the phase equilibria at nominal alloy composition. The vertical dotted line in Figure 2.4b indicates the composition of the alloy and shows that the amount of β-phase will increase during heating, completely transforming to β above 956°C i.e. the β-transus.

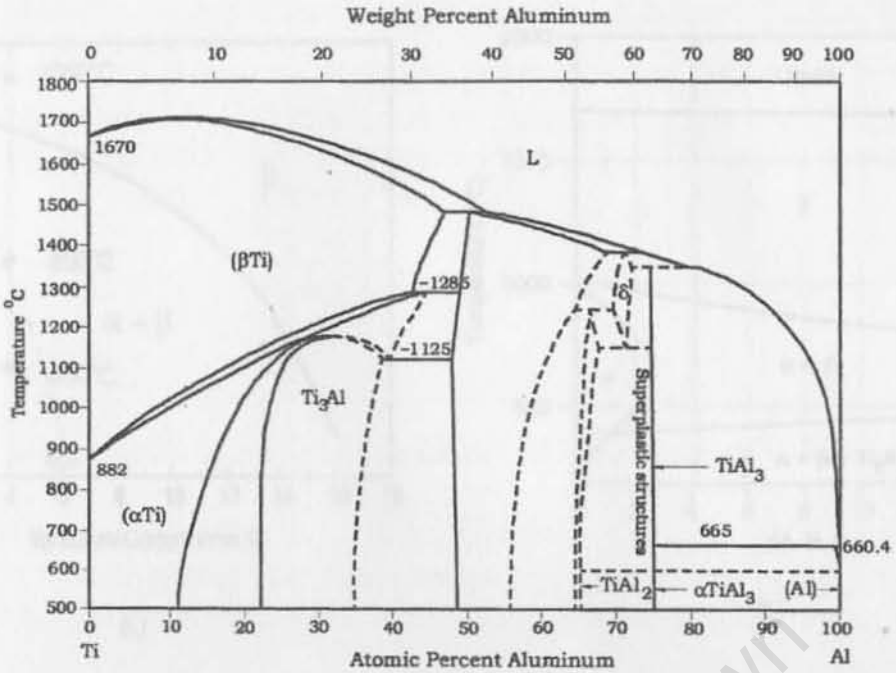

***Figure 2.2**: Phase diagram of Ti-Al system [17]*

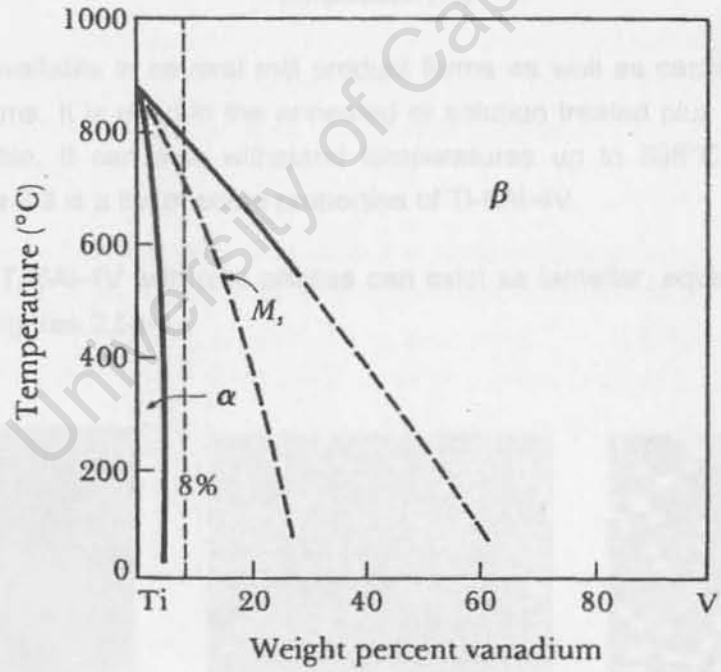

***Figure 2.3**: Phase diagram of Ti-V system [18]*

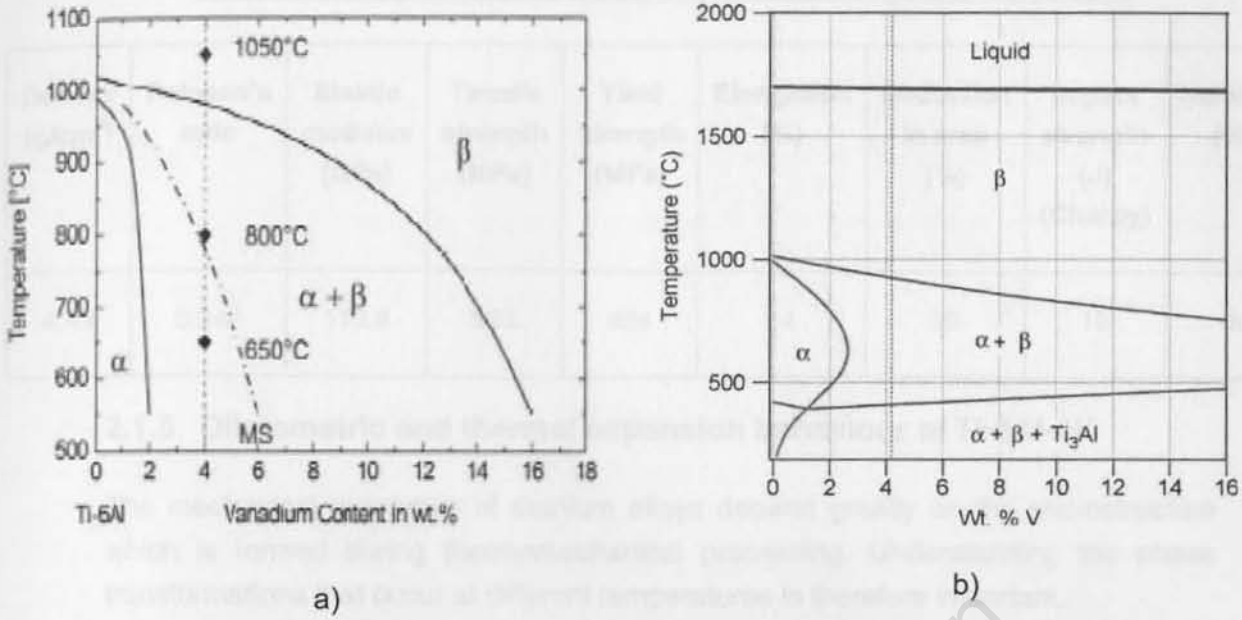

Figure 2.4: *Pseudo-binary Ti-6Al-4V phase diagram a) Experimentally calculated [**16**] b) Predicted using ThermoCalc® software showing the influence of vanadium content of the α-Ti and β-Ti phase. The vertical dashed line in both phase diagrams represents the nominal alloy composition [**19**]*

Ti-6Al-4V is available in several mill product forms as well as castings and powder metallurgy forms. It is used in the annealed or solution treated plus aged conditions and is weldable. It can also withstand temperatures up to 398°C without loss in ductility. Table 2.3 is a list of some properties of Ti-6Al-4V.

Furthermore, Ti-6Al-4V with α+β phases can exist as lamellar, equiaxed or bimodal as shown in Figures 2.5a-c.

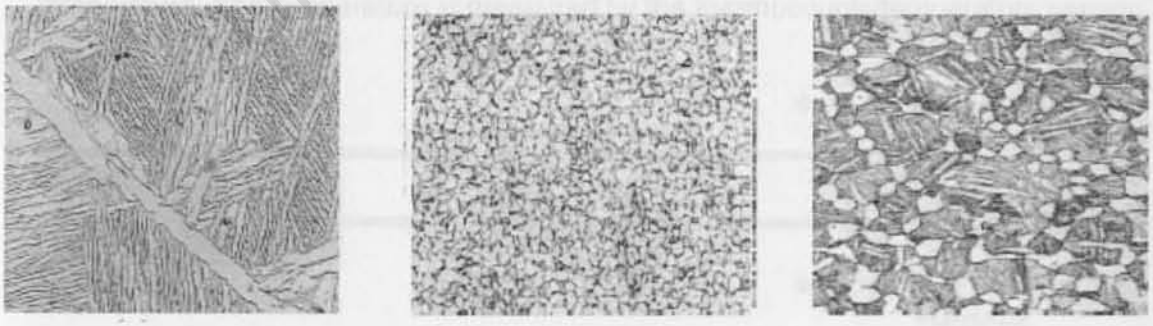

Figure 2.5: *Microstructure of Ti-6Al-4V a) lamellar structure b) equiaxed structure c) bimodal structure [**16**]*

Table 2.3: Mechanical and physical properties of wrought Ti-6Al-4V [20]

Density (g/cm^3)	Poisson's ratio	Elastic modulus (GPa)	Tensile strength (MPa)	Yield strength (MPa)	Elongation (%)	Reduction in area (%)	Impact strength (J) (Charpy)	Hardness (HB)
4.43	0.342	113.8	993	924	14	30	19	36

2.1.5 Dilatometric and thermal expansion behaviour of Ti-6Al-4V

The mechanical properties of titanium alloys depend greatly on the microstructure which is formed during thermomechanical processing. Understanding the phase transformations that occur at different temperatures is therefore important.

Dilatometry is one of the most useful techniques employed in the study of solid-solid phase transformations in metals. This technique permits the real-time monitoring of the evolution of transformations in terms of dimensional changes in length occurring in the specimen by application of a thermal cycle [**21**].

The applicability of this technique in monitoring phase transformations is due to the change in specific volume of a sample during cooling and heating of a specimen. A phase transformation will result in a volume expansion or contraction, which is observed as a change in length (Δl).

The functioning of a push-rod dilatometer is shown in Figure 2.6. The specimen is placed against a push-rod. During heating/cooling the specimen will expand/contract and will result in the displacement of the push-rod. The displacement causes the digital transducer to record the change in length of the specimen as a function with temperature. The temperature is measured by the thermocouple/temperature sensor.

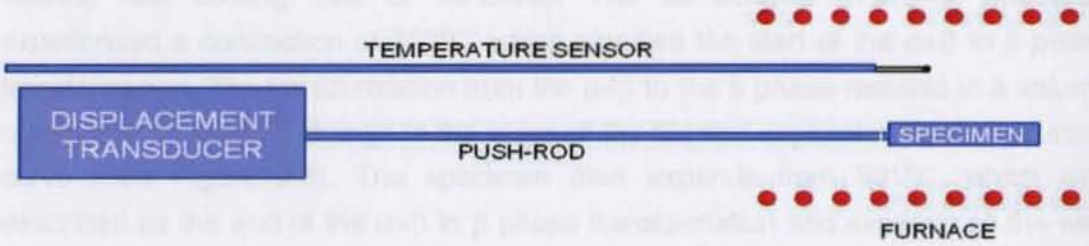

Figure 2.6: *Schematic of the functioning of a dilatometer*

From the Δl (change in length) data, strain can be calculated by the following relationship:

$$\text{Strain} = \frac{\Delta l}{l}, \text{ where } l \text{ is the initial length.}$$

Strain is then plotted as a function of temperature (See Figure 2.7). The coefficient of thermal expansion can be calculated from the slope of the strain vs. temperature curve. A marked change in slope of the strain ($\frac{\Delta l}{l}$) vs. temperature curve signifies a phase transformation [**21**].

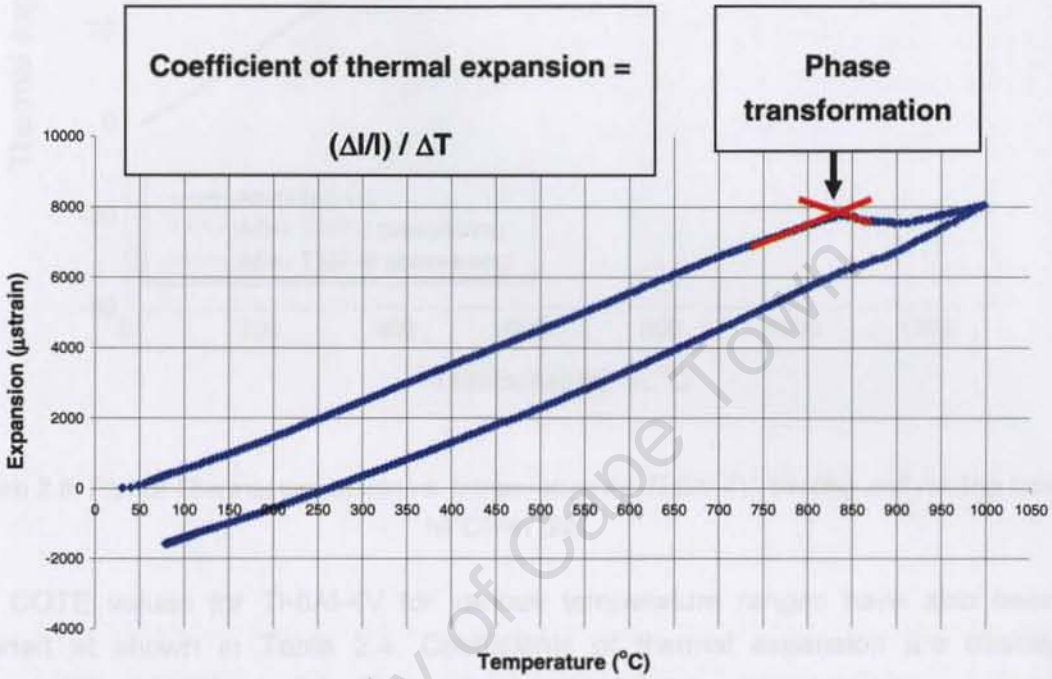

Figure 2.7: *Plot of Strain (µstrain) vs. temperature, slope of the graph equalling the coefficient of thermal expansion and change in slope signifying a phase transformation*

A Thermal expansion vs. temperature curves for Ti-6Al-4V (as received and thermomechanically treated by two methods) was reported by Motyka et al. as shown in Figure 2.7. The three specimens went through a heating and cooling cycle with a heating and cooling rate of 10°C/min. The as-received Ti-6Al-4V specimen experienced a contraction at 803°C, which signified the start of the α+β to β phase transformation. The transformation from the α+β to the β phase resulted in a volume contraction or marked change in the slope of the thermal expansion vs. temperature curve (See Figure 2.8). The specimen then expands from 991°C, which was described as the end of the α+β to β phase transformation and expands all the way up to 1200°C [**22**].

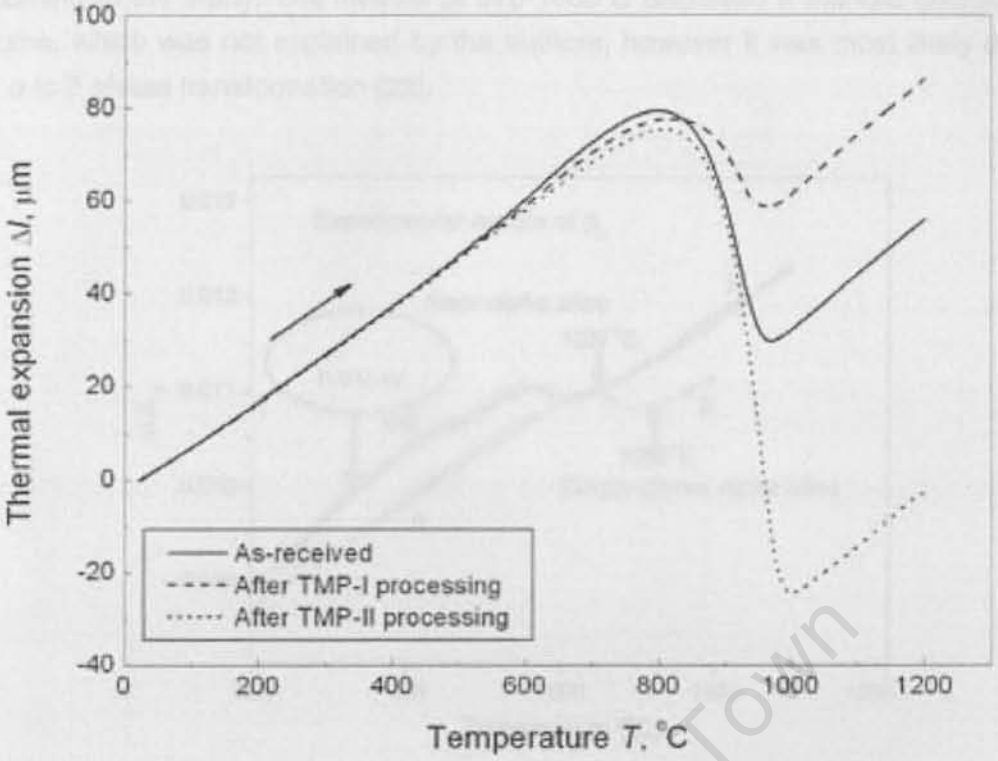

Figure 2.8: *Plot of Thermal expansion vs. temperature for Ti-6Al-4V, heating and cooling rate 10°C/min [22]*

The COTE values for Ti-6Al-4V for various temperature ranges have also been reported at shown in Table 2.4. Coefficients of thermal expansion are directly computed from the slope of the Thermal expansion vs. temperature curve.

*Table 2.4: Reported Coefficients of thermal expansion of Ti-6Al-4V at various temperature ranges [**20**]*

T (°C)	20-100	20-205	20-315	20-425	20-540	20-650
COTE X10^{-6}/°C	8.6	9.0	9.2	9.4	9.5	9.7

In a study by Reddy et al. the β-transus temperature was calculated using dilatometry as well as a feed forward neural network (FFNN) technique. The FNN technique works on the principle of using a back-propagation learning algorithm in order to predict the β-transus temperature. A plot of $\Delta L/L_o$ vs. temperature, as shown in Figure 2.9, showed that the volume changed from 994°C.The authors reported this temperature to be the β-transus. The estimated β-transus end point was 1037±5°C

according to the study. The interval of 970-1000°C displayed a marked decrease in volume, which was not explained by the authors, however it was most likely due to the α to β phase transformation [**23**].

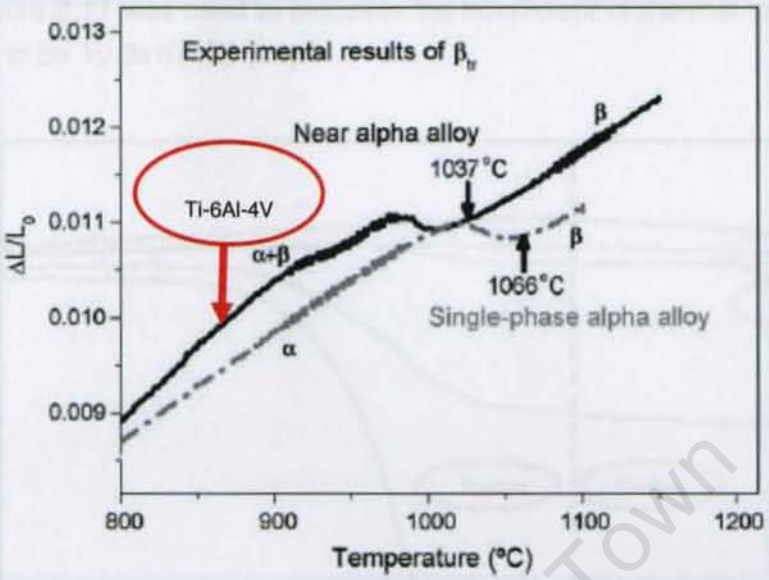

Figure 2.9: *Dilatometer plots used to determine the β-transus temperatures for the single-phase α and near α alloys. The arrows indicates the estimated β-transus end temperatures whereby the alloy is fully β above this temperature* ***[23]***

The FFNN technique predicted the β-transus to be at 1000°C and the experimental value using dilatometry was 994°C, as shown in Figure 2.9 and hence, the results were comparable.

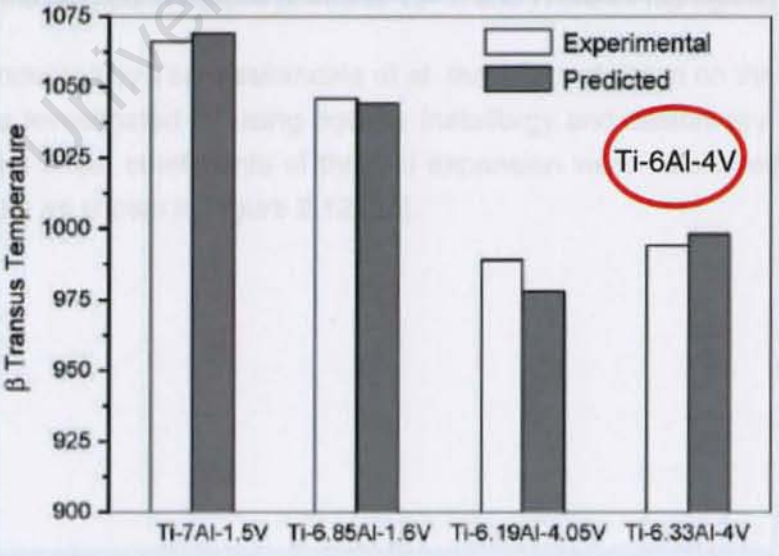

Figure 2.10: *Comparison of predicated and measured β-transus temperature for single phase α and near α alloys [23]*

Figure 2.11 showed the linear change (%) vs. temperature from 400°C onwards. A volume contraction was observed at 920°C for the CP Ti and Ti-6Al-4V, which signified the start of the α to β phase transformation. This study suggests that a volume contraction will occur during the α to β phase transformation. The cooling section of Figure 2.11 was used to calculate the coefficient of thermal expansion and was reported to be 10.3×10^{-6}/°C [**24**].

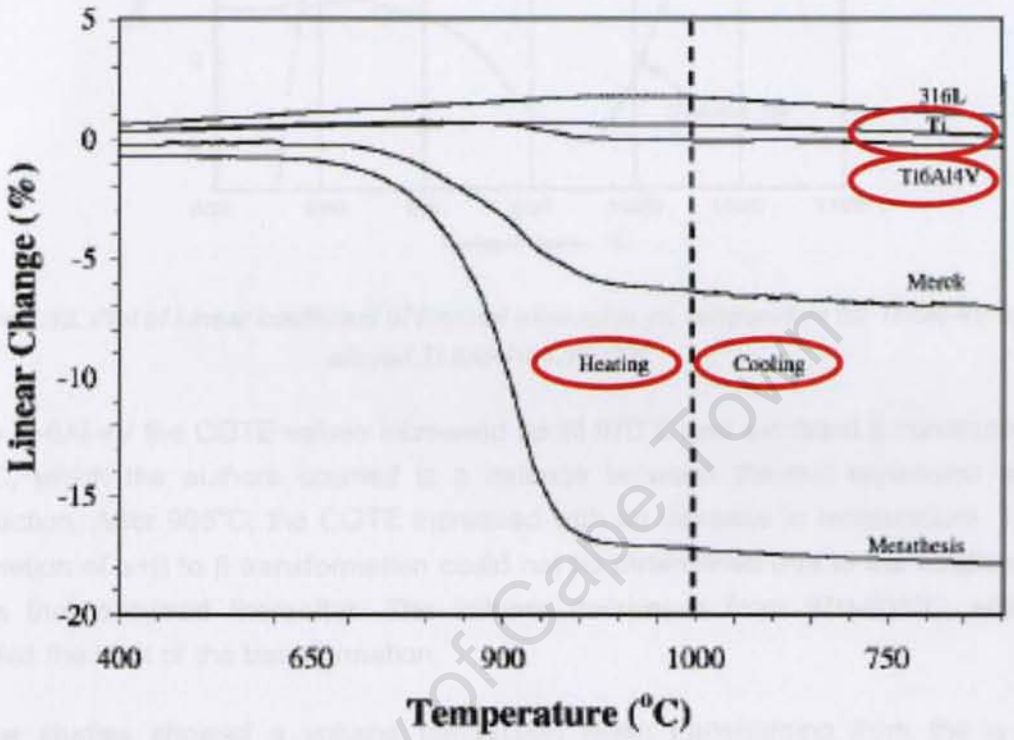

Figure 2.11: *Dilatometry plots for the three metals (CP Ti, Ti-6Al-4V, and 316L stainless steel), and the two hydroxyapatite powders). CP Ti and Ti-6Al-4V highlighted in red [**24**]*

In a study conducted by Tamirisakandala et al. the effect of boron on the β-transus of Ti-6Al-4V was investigated by using powder metallurgy and dilatometry curves were generated. The linear coefficients of thermal expansion were calculated and plotted vs. temperature as shown in Figure 2.12 [**25**].

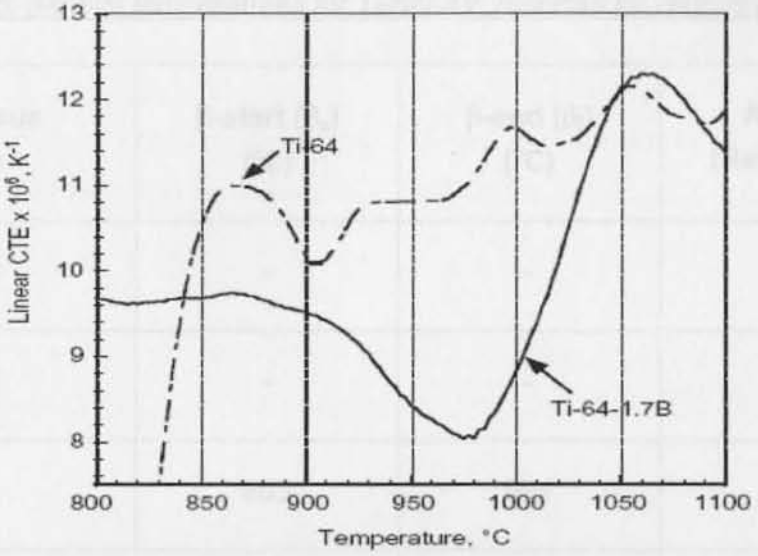

***Figure 2.12**: Plot of Linear coefficient of thermal expansion vs. temperature for Ti-6Al-4V and alloyed Ti-6Al-4V-1.7B [**25**]*

In the Ti-6Al-4V the COTE values increased up till 870°C and exhibited a minimum at 905°C, which the authors claimed is a balance between thermal expansion and contraction. After 905°C, the COTE increased with an increase in temperature. The completion of $\alpha+\beta$ to β transformation could not be determined due to the oscillatory peaks that occurred thereafter. The volume decreased from 870-905°C, which signified the start of the transformation.

All the studies showed a volume contraction when transforming from the α to β phase. Different β_s and β_f temperatures and actual β-transi temperatures have been reported by various authors. Table 2.5 is a summary of the various β transi temperatures reported by these authors. Some authors have reported the β-transus of Ti-6Al-4V to be a single temperature, whilst others have indicated a β_s and β_f temperatures. The latter is expected, since the rearrangement of atoms during the transformation of α to β and the effects of Al and V on the crystal lattice of Ti would cause the transformation to occur over a temperature range, rather than a single temperature.

Table 2.5: β-transi temperatures for Ti-6Al-4V, reported by various authors

β-transus (°C)	β-start (β_s) (°C)	β-end (β_f) (°C)	Author (Reference)
980	-	-	[16]
956	-	-	[19]
-	803	991	[22]
-	994	1037	[23]
-	820-865	970	[26]
1000	-	-	[27], [28]
890	-	-	[29]

2.1.6 The α to β phase transformation in Ti-6Al-4V during continuous heating

During heating of Ti-6Al-4V, equilibrium is rarely attained and hence the microstructures, which formed during heating, may be different than that predicted from the phase diagram. Predicting microstructural evolution is therefore not possible using only the phase diagram. Understanding the kinetics of the alloy is also required. Thermal cycling may also add complexity in predicting the microstructural evolution, since the microstructures formed during heating are altered during the phase transformations, which take place during cooling.

A study by Elmer et al. looked at the α+β to β phase transformation behaviour of alloy during heating to peak temperatures of 800, 900 and 1000°C. The amount of β-phase increases with increasing temperature, as shown in Figure 2.13a. A similar calculation was made by Semiatin et al., as shown in Figure 2.13b, which showed a similar result.

The α+β to β transformation is controlled by diffusion, hence only a small fraction of the β-phase formed will transform to the α-phase during the rapid air cooling of the

initial Ti-6Al-4V ingot. This results in a higher volume fraction of β-phase at room temperature than the predicted thermodynamics. During the heating cycle of the various samples, complete transformation to the β phase was not observed. This may be due to oxygen which can react with the alloy at elevated temperatures, which stabilised the α phase [**19**].

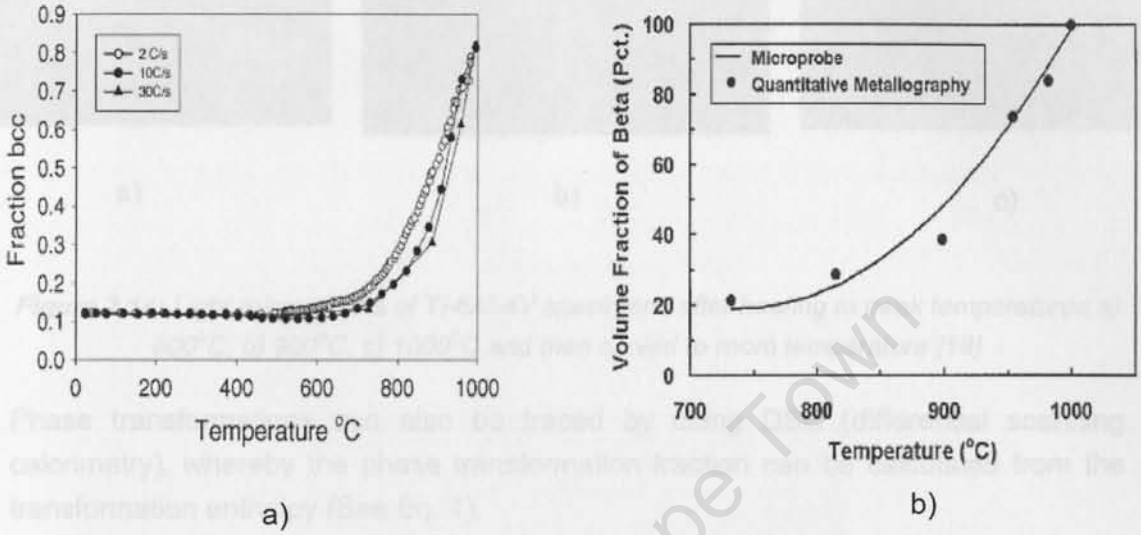

Figure 2.13: *a) Measured β-phase fraction Ti-6Al-4V during continuous heating a) of 2, 10 and 30°C/s thermodynamic prediction by Elmer et al. [**19**] and b) Calculated by Semiatin et al. [**30**]*

From Figure 2.14a it was observed that only a small fraction of the α-phase had transformed to the β-phase. The dark etching regions correspond to regions where the β phase was most concentrated. The regions appear diffuse in comparison to the base metal, indicating that some diffusion and transformation had taken place. In Figure 2.14b it appeared that 15% of the α-phase had transformed to the β-phase. The dark etching region in this micrograph of the base metal appeared to be gone, indicating increased transformation and diffusion at 900°C. At 1000°C, as shown in Figure 2.14c, complete or near completion of transformation to the β-phase occurred prior to cooling. This microstructure appeared different to the others and consisted mainly of acicular α-phase, which was formed during cooling from the large grained β structure.

From the Figures 2.13 and 2.14 it can clearly be seen that the β-phase increases with increasing temperature from 600°C and upwards. This is a critical temperature for hydrogen uptake, which will be discussed later.

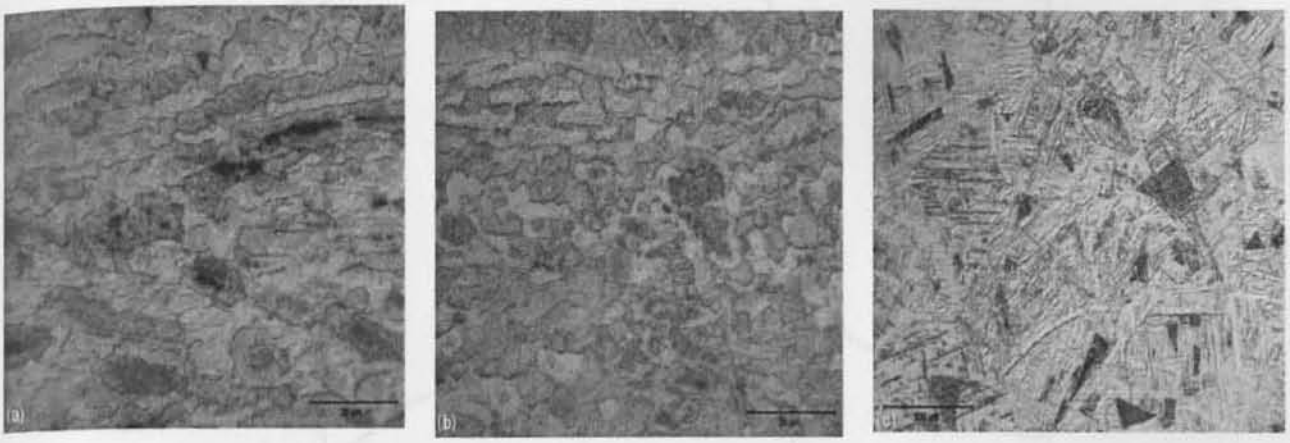

a) b) c)

Figure 2.14: *Light micrographs of Ti-6Al-4V specimens after heating to peak temperatures a) 800°C, b) 900°C, c) 1000°C and then cooled to room temperature [**19**]*

Phase transformations can also be traced by using DSC (differential scanning calorimetry), whereby the phase transformation fraction can be calculated from the transformation enthalpy (See Eq. 1).

$$V_f = \frac{P_f}{P_o} \times 100\% \quad (1)$$

V_f is the volume fraction of the new phase up to a defined temperature, P_f is the latent heat of consumption up to the defined temperature and P_o is the latent heat of the entire process [**31**].

A DSC curve was reported by Sha et al. as shown in Figure 2.15. The starting microstructure consisted of fine equiaxed α-phase with β-phase, as shown in Figure 2.16.

In Figure 2.15, endothermic peaks were observed at positions *1* and *2* and this was associated with the α+β to β phase transformation. Peak labelled *1* represented the transformation from α-phase in the transformed β-phase to the β-phase and peak labelled *2* the transformation from the primary α-phase to the β-phase [**31**]. The first transformation occurs at 925°C and the second at 980°C, as indicated by peaks labelled *1* and *2* respectively. The transformation was complete at 1100°C.

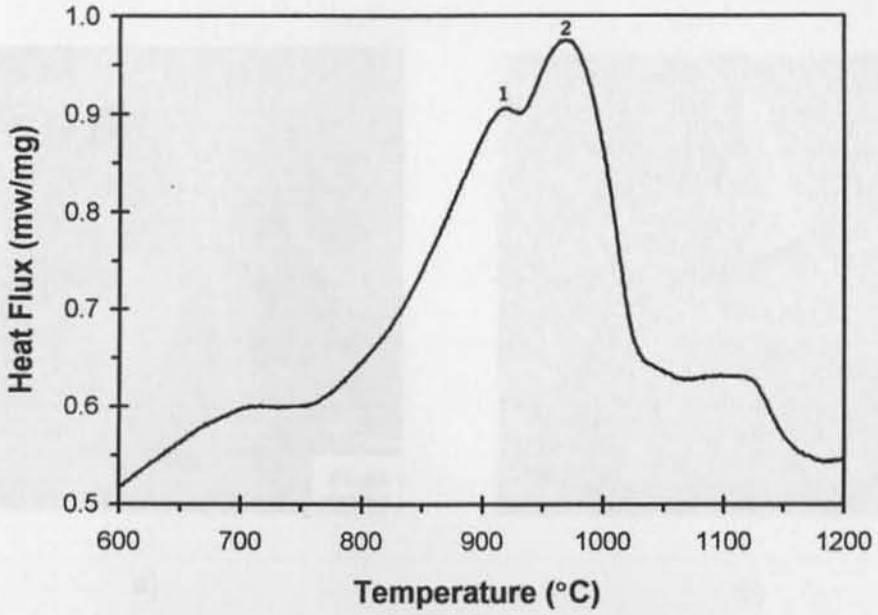

Figure 2.15: *DSC curve of Ti-6Al-4V, heating rate 50°C/min [**31**]*

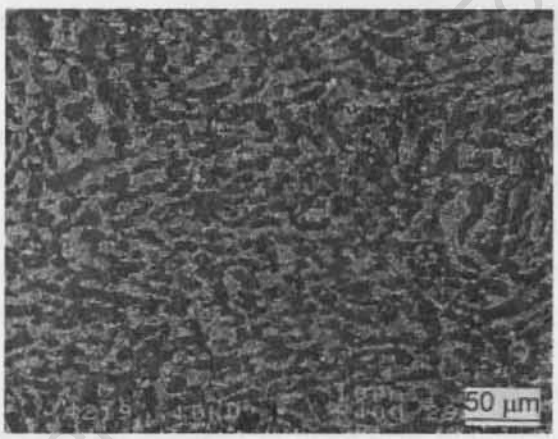

Figure 2.16: *Light micrograph of Ti-6Al-4V in the as-received condition [**31**]*

2.1.7 The β to α and β to α+β phase transformations in CP Ti and Ti-6Al-4V respectively during cooling

Based on heating and cooling rates various types of microstructures may arise i.e. α-phase lamellae in β matrix, α', α'' or a mixture of these various phases. Heating to the β-transus and slow cooling will result in an α-phase lamellae in a β matrix and fast cooling will lead to the distorted martensitic phases (α' and α''). Figures 2.17a and b shows that two types of microstructures may arise [**32**].

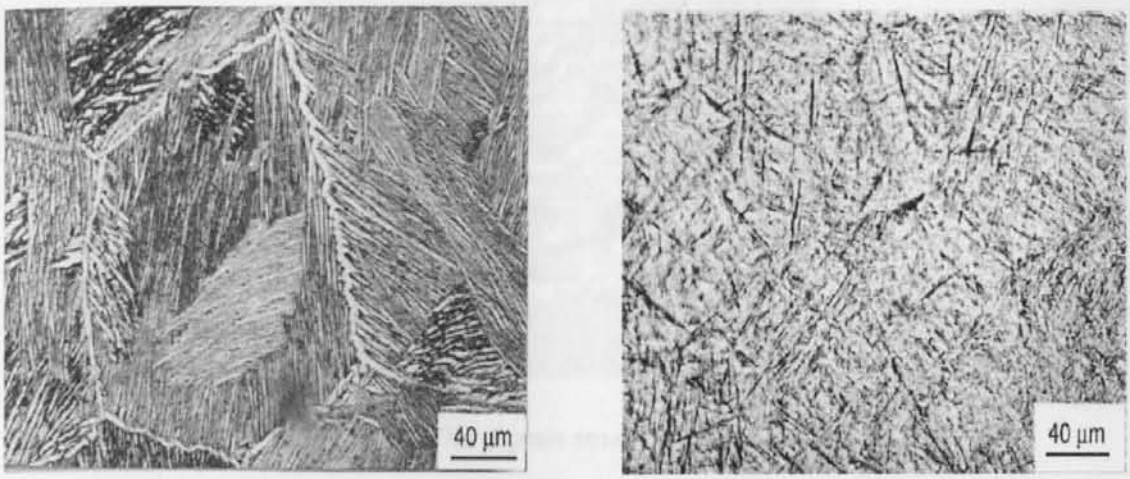

***Figure 2.17**: Light micrographs of Ti-6Al-4V a) After cooling in air (slow cooling), with α-phase in β matrix and b) After cooling in water (fast cooling) displaying the formation of α' and α" phases [32]*

In a study by Phelan et al. phase transformations were observed within CP Ti using a high temperature laser-scanning confocal microscope. The specimen passed the β-transus temperature and was heated to 1500°C and then cooled to room temperature. The *in-situ* microstructural evolution during cooling was observed for the β to α phase transformation [**33**].

At 1500°C the specimen was held isothermally for 5 minutes to encourage the formation of large β grains. An increase in grain size promotes the formation of the Widmanstätten morphology, as shown in Figure 2.18. The holding time at this temperature relieved surface roughness induced by the α to β transformation during heating. The grains were up to 1mm in diameter and the grain boundaries were sharp black lines. Some diffuse surface roughness could be observed on the β grains. Widmanstätten plates were formed during cooling, whereby the plates were formed by sympathetic nucleation on pre-existing allotriomorphs at the grain boundary [**33**].

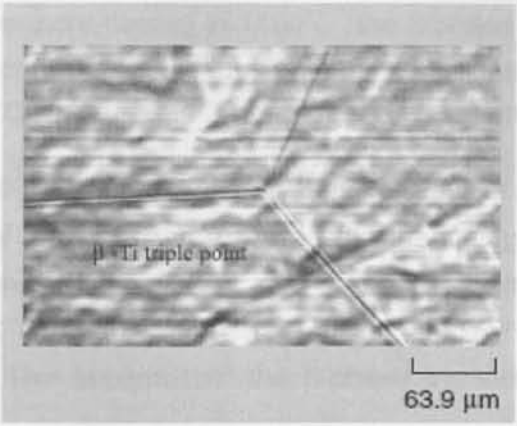

Figure 2.18: *The β grain structure at 1500°C [33]*

During cooling (unspecified cooling rate) a sequence of events occurred as shown in Figures 2.19a-d. A series of Widmanstätten plates propagate from or near the β grain boundary. These plates grew preferentially into one β grain and the other grains exhibited restricted growth, as shown in Figure 2.19a and b. As the transformation progressed the individual plates consumed the β-grains and further impinged on plates growing from other locations. At 845°C the transformation was complete [**33**].

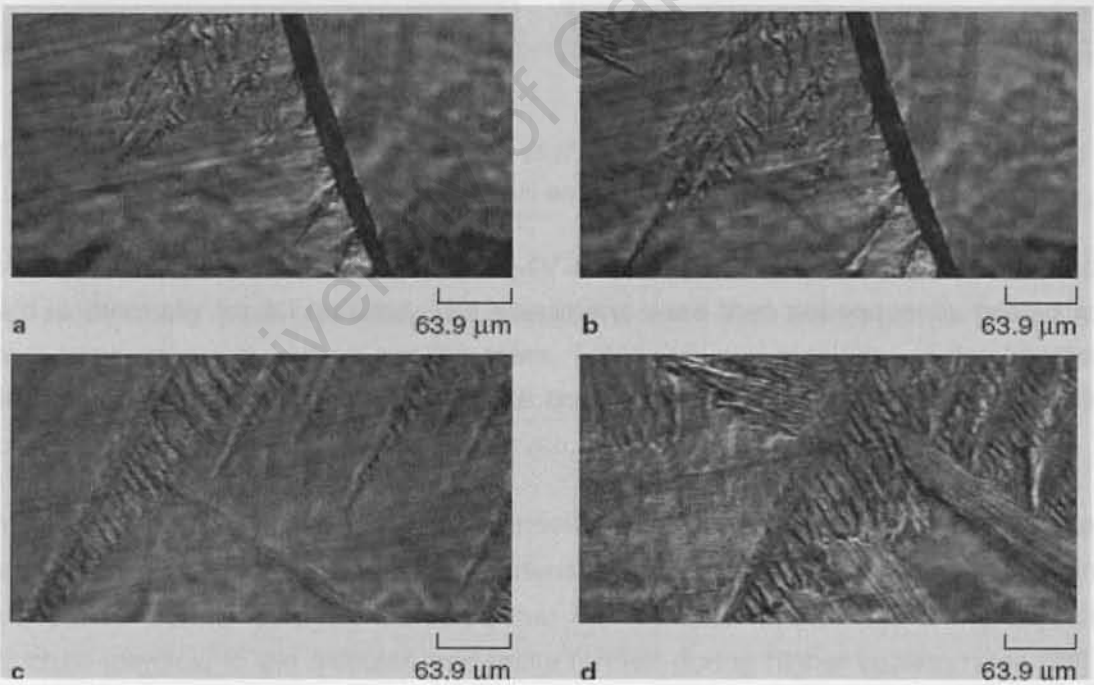

Figure 2.19: *The growth of α-Ti with Widmanstätten-type morphology at a) 863°C, b) 860°C, c) 849°C and d) 845°C [33]*

In a study by Malinov et al. differential scanning calorimetry (DSC) as well as computer modelling using the principles of the Johnson-Mehl-Avrami (JMA) theory was used to study the phase transformation behaviour of the β to α+β transformation

in Ti-6Al-4V. Specimens were heated to 1100°C (the β phase field) at a heating rate of 20°C/min, held isothermally for 20 minutes, then taken out of the furnace at 970°C, 940°C, 890°C and 860°C (cooling rate 20°C/min) and finally water quenched.

The microstructures of the quenched specimens displayed a mixture of the α+α' phases. The amount of α' decreased with a lower quenching temperature, implying that the β-phase transformation was incomplete. The microstructures of the specimens from 860°C and 750°C consisted of only acicular α-phase, as shown in Figures 2.20a and b. This implied that the β-phase transformation was complete above 800°C [**26**].

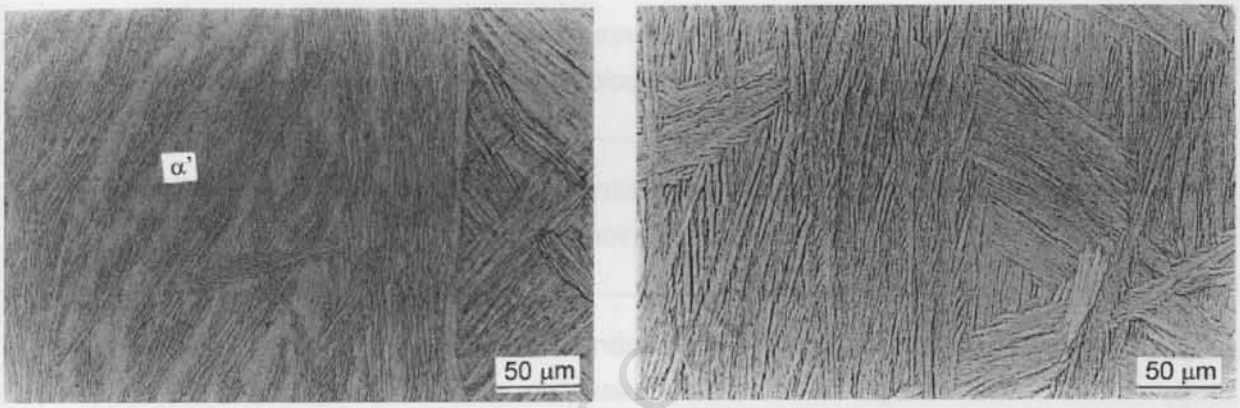

Figure 2.20: *Light micrographs of Ti-6Al-4V after continuous cooling (cooling rate 20°C/min) from a) 860°C/min and b) 750°C [**26**]*

In another study by Ahmed et al. Ti-6Al-4V specimens were heated to 1050°C and held isothermally for 30 minutes. The specimens were then subsequently cooled to room temperature at various cooling rates. Table 2.6 is a summary of the phases formed with different cooling rates. As the cooling rate decreases an increase in the volume fraction of the α-phase was observed.

Nucleation of the α-phase occurred progressively at prior β grain boundaries with a decrease in cooling rate and at martensite plates adjacent to prior β grain boundaries. Further analysis indicated that the α-phase formed had a hcp crystal structure identical to the acicular martensite formed during higher cooling rates [**34**]. The formation of α in this study is described as a massive transformation. This type of transformation is defined as a solid-solid phase transition in which the product phase has the same composition as the parent phase and the growth process is short range diffusional jump across disordered inter-phase boundaries. This type of transformation occurs at sufficiently low transformation temperatures. At high cooling rates α' was formed [**35**].

Table 2.6: Ti-6Al-4V heated to above the β-transus and cooled to room temperature at various cooling rates [34]

Cooling rate (°C/min) from 1050°C	Phases formed
31500	Hexagonal (α') martensite formed composed of long orthogonally orientated martensite plates with acicular morphology, as shown in Figure 2.21a
24600	Preferential grain boundary formation of secondary α morphology, as shown in Figure 2.21b
16500	Increase in preferential grain boundary formation of secondary α morphology, as shown in Figure 2.21c
10500	Increase in preferential grain boundary formation of secondary α morphology, as shown in Figure 2.21d
1200	Increase in preferential grain boundary formation of secondary α morphology, as shown in Figure 2.21e
900	Widmanstätten α formation, as shown in Figures 2.22a and b
90	Widmanstätten α formation , as shown in Figure 2.22c

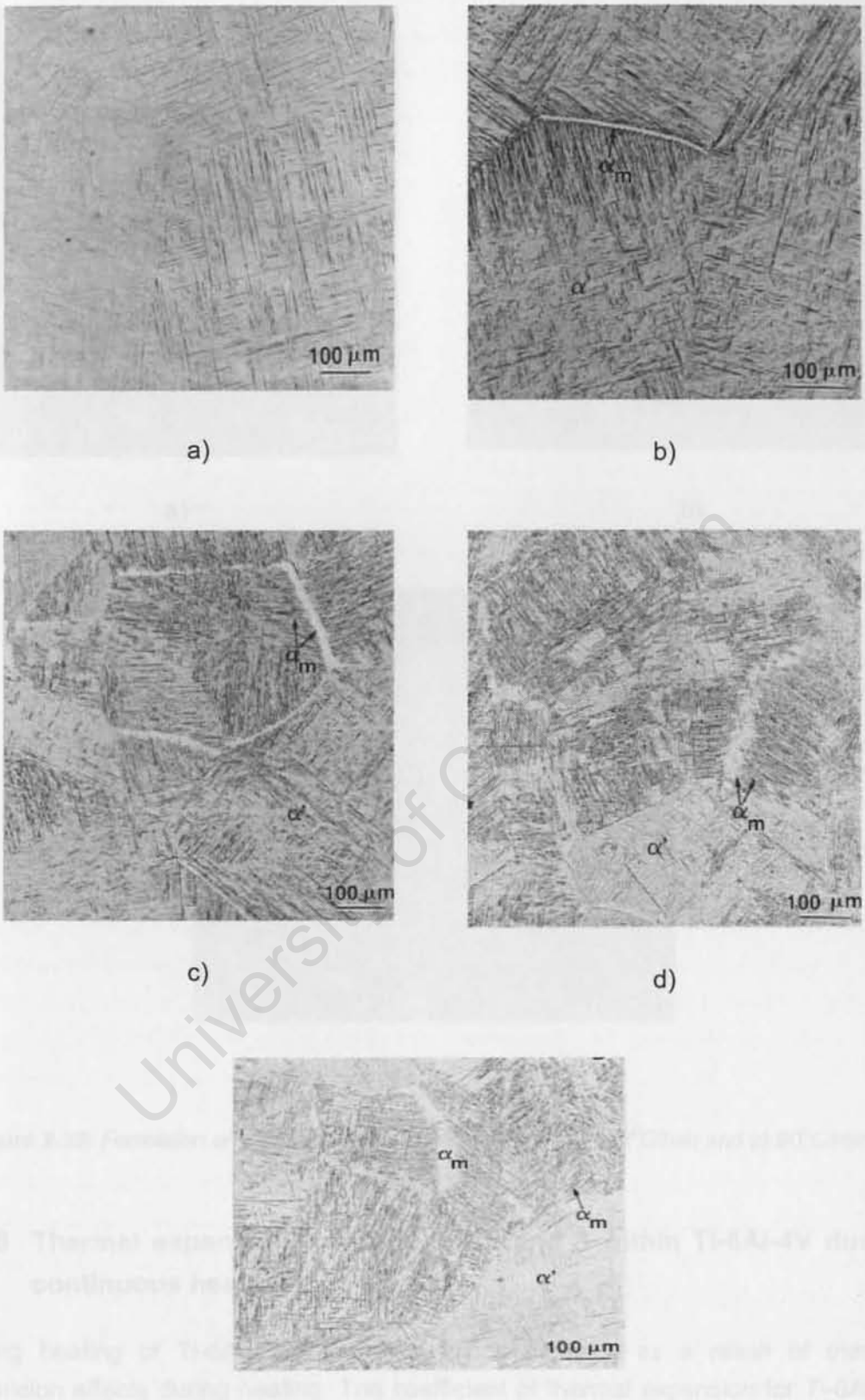

Figure 2.21: *Formation of α mixture of α' and α_m (α formed by massive transformation mechanism) cooling rate a) 31500, b) 24600, c) 16500, d) 10500 e) 1200°C/min in Ti-6Al-4V[**34**]*

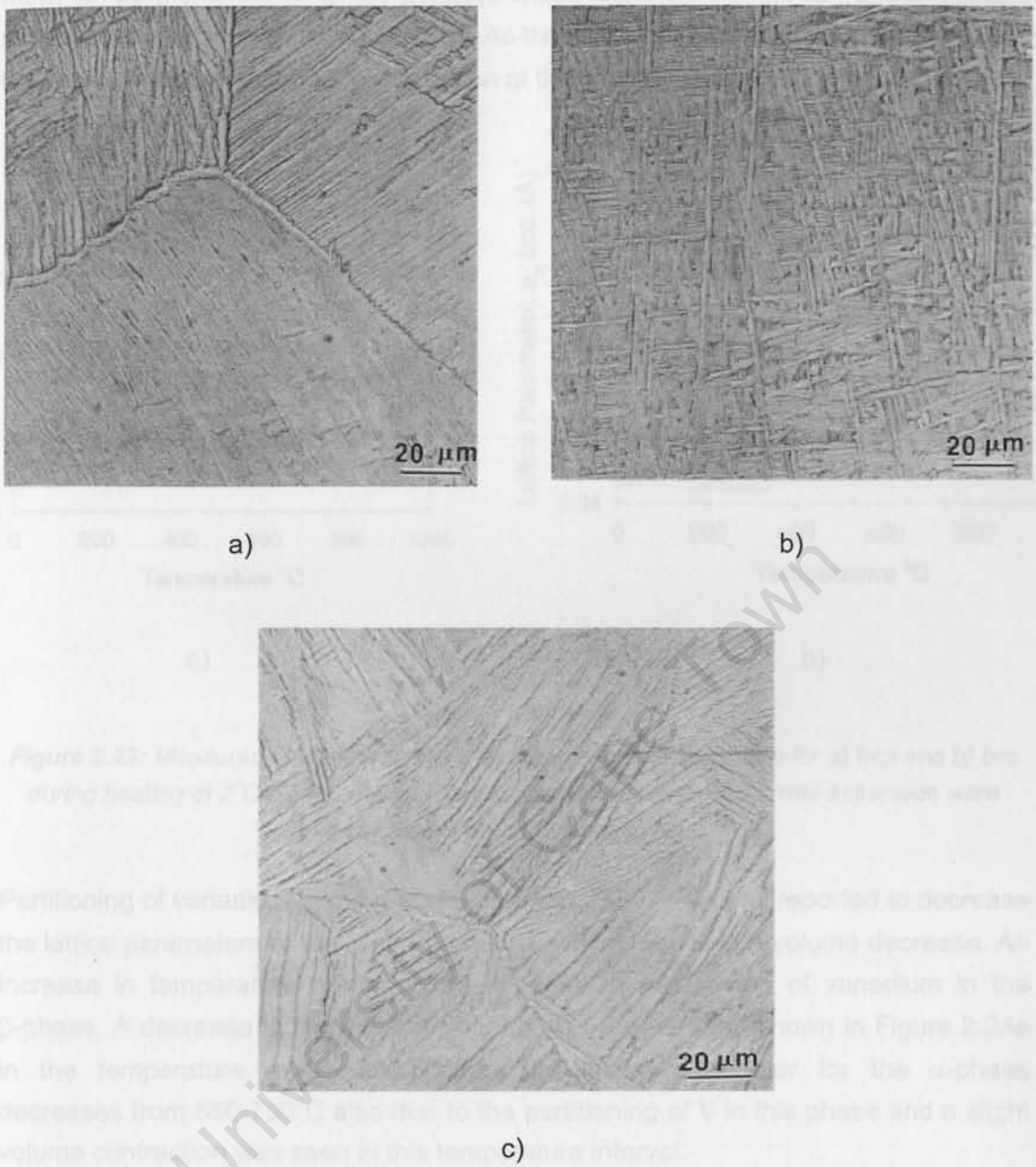

a) b)

c)

Figure 2.22: *Formation of Widmanstätten, cooling rate a), b) 900°C/min and c) 90°C/min in Ti-6Al-4V [**34**]*

2.1.8 Thermal expansion behaviour of α and β within Ti-6Al-4V during continuous heating

During heating of Ti-6Al-4V the crystal lattice expands as a result of thermal expansion effects during heating. The coefficient of thermal expansion for Ti-6Al-4V was reported to be between 8.5×10^{-6}/°C and 10×10^{-6}/°C near room temperature [**36**]. A study by Elmer et al. reported the thermal expansion coefficient for the α-phase to be 9.7×10^{-6}/°C, as shown in Figure 2.23a and 9.2×10^{-6}/°C for the β-phase, as shown in Figure 2.23b. Since the alloy consists mostly of the α-phase during heating from

room temperature, the weighted average lattice expansion of the two phase mixture should be closer to that of the α-phase. As the α+β to β phase transformation occurs, the β-phase increases and the expansion of this phase would then dominate. [**19**]

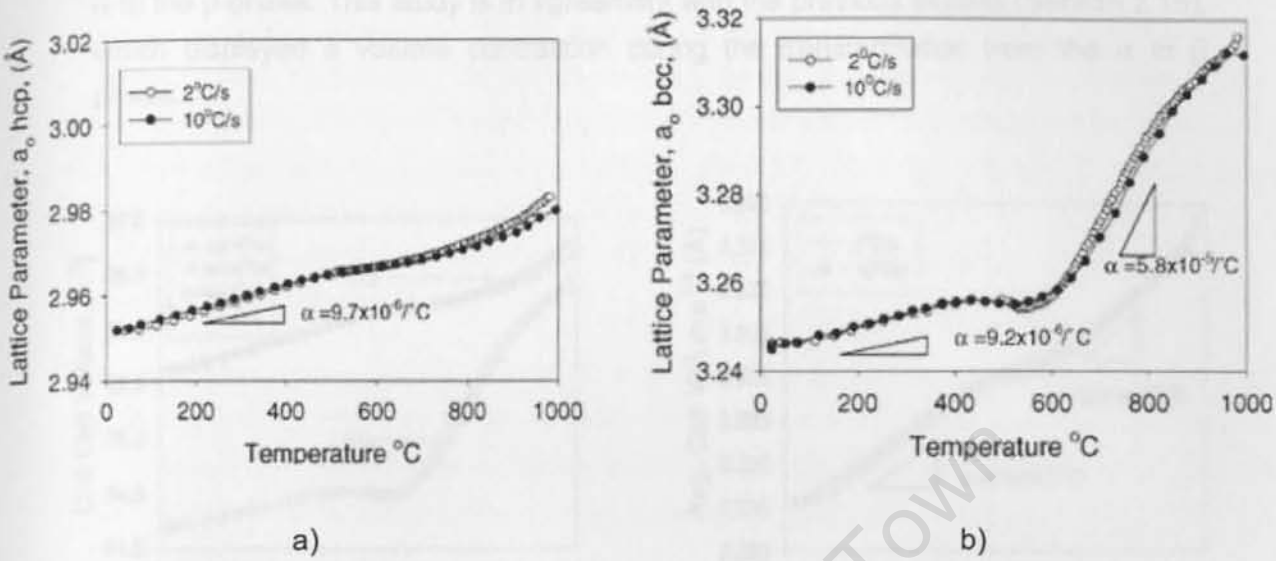

Figure 2.23: *Measured lattice parameters as a function of temperature for a) hcp and b) bcc during heating at 2°C/s and 10°C/s. The indicated coefficients of thermal expansion were calculated from the slopes [**19**]*

Partitioning of vanadium in the α and β phases in Ti-6Al-4V was reported to decrease the lattice parameters of the α and β phases, which results in a volume decrease. An increase in temperature results in an increase in partitioning of vanadium in the β-phase. A decrease in the unit cell volume was reported, as shown in Figure 2.24a in the temperature range 500-600°C. The lattice parameter for the α-phase decreases from 550-750°C also due to the partitioning of V in this phase and a slight volume contraction was seen in this temperature interval.

From the data in Figure 2.24a, the unit cell volume for each phase was multiplied by its respective volume fraction in the microstructure at each temperature. The sum of the two volumes represents the average volume of the α+β phases as a function of temperature. The cube root was then taken (Average cell volume)$^{1/3}$, which is the approximate average thermal dilation for the mixture of the α+β phase i.e. the alloy, as shown in Figure 2.24b. The thermal expansion coefficient of the α-phase was reported to be 9.5x10^{-6}/°C and 12.8x10^{-6}/°C for the β-phase, as shown in Figure 2.24b. A decrease in average dilation was seen in the temperature range 500-850°C, but once the α to α+β transformation was complete, the lattice expansion and lattice expansion rate increases [**19**].

From the above study it is evident that vanadium plays a role in the α to β phase transformation and was seen to decrease the volume of the respective phases when approaching the β-transus. The partitioning effects of vanadium is one of the factors that caused a volume contraction from 500-850°C during the transformation from the α to the β-phase. This study is in agreement with the previous studies (Section 2.15), which displayed a volume contraction during the transformation from the α to β phase.

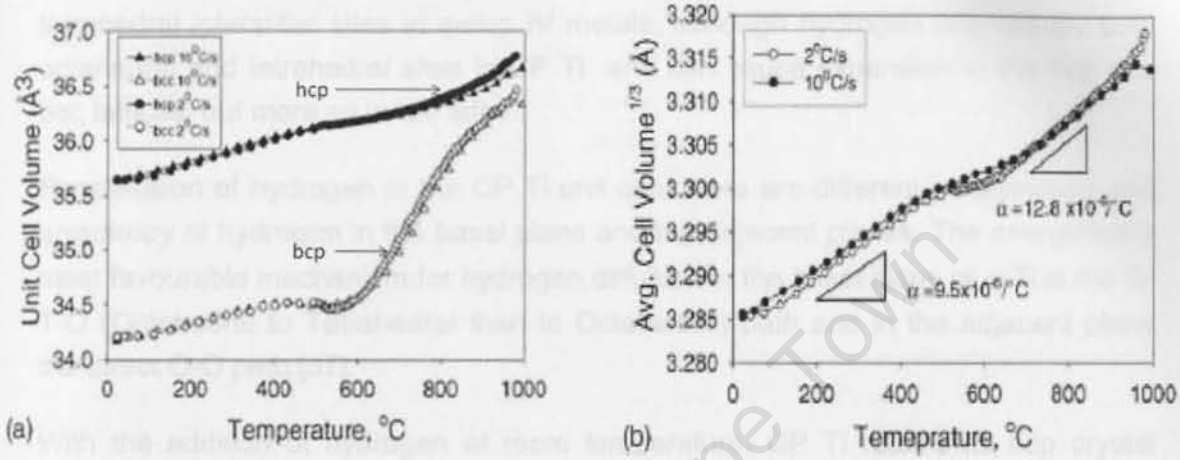

Figure 2.24: *a) Unit cell volume of hcp and bcc phases as a function of temperature and b) Average cell volume$^{1/3}$ (dilation) as function of temperature [**19**]*

2.2 Hydrogen as a temporary alloying element in Ti-6Al-4V

Hydrogen is used as a temporary alloying element since it can be easily added and removed without melting. Titanium and its alloys have a high affinity for hydrogen and are able to absorb up to 60% at 600°C [**1**].

If hydrogen is not used correctly during thermohydrogen processing, it can have deleterious effects on metals if trapped around structural defects and if local concentrations exceed a critical limit. The formation of hydrides can lead to hydrogen embrittlement, and hence hydride induced cracking.

Thermohydrogen processing makes use of hydrogen in order to enhance processing behaviour and final characteristics of titanium alloys. This is done by means of holding the metal at high temperatures in a hydrogen environment and heat treatment or thermomechanical processing. [**1**]

Hydrogen allows for titanium alloys to be mechanically processed at lower stresses and temperatures.

2.2.1 Effect of hydrogen on the crystal lattices of titanium alloys

Titanium has a strong affinity for hydrogen, but may lead to deterioration of mechanical properties. In α titanium alloys hydrogen embrittlement is as a result of hydrogen having a low solubility in the α phase in comparison to the β phase. The higher solubility of hydrogen in the β-phase is attributed to the relatively open body centred cubic (bcc) structure which consists of 12 tetrahedral and 6 octahedral interstices. The hexagonal closed packed (hcp) structure of the α phase exhibits only 4 tetrahedral and 2 octahedral interstitial sites [**9**]. Hydrogen tends to occupy tetrahedral interstitial sites in group IV metals, although hydrogen can occupy both octahedral and tetrahedral sites in CP Ti and can cause expansion in the hcp and bcc lattices, but more so in the latter.

For diffusion of hydrogen in the CP Ti unit cell, there are different mechanisms and anisotropy of hydrogen in the basal plane and the adjacent planes. The energetically most favourable mechanism for hydrogen diffusion in the basal plane of α-Ti is the O-T-O (Octahedral to Tetrahedral then to Octahedral) path and in the adjacent plane the direct O-O path [**37**].

With the addition of hydrogen at room temperature, CP Ti retains its hcp crystal structure. This would result in volume expansion in the tetrahedral and octahedral sites as shown in Figure 2.25, with the lattice expansion for the tetrahedral sites being bigger than the octahedral sites [**38**]. The sub-lattice of the tetrahedral interstitial sites of hydrogen can form a simple cubic lattice in the fcc α-hydride TiH_x phase.

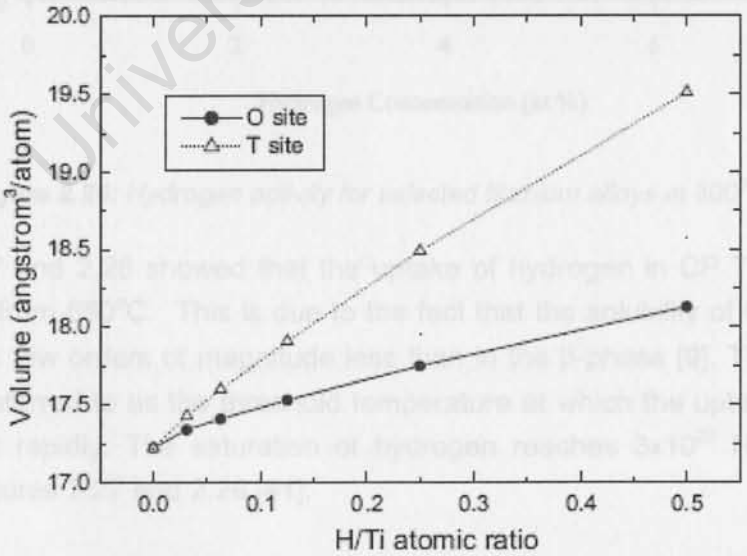

Figure 2.25: *Atomic volume of Ti-H phases as a function of H concentration [**38**]*

2.2.2 The solubility of hydrogen in titanium alloys

Figure 2.26 depicts the chemical activity of CP Ti and various titanium alloys. The material which has the lowest chemical activity will have the highest hydrogen solubility. The β titanium alloys has a higher activity than CP Ti, and hence the latter has higher hydrogen solubility than the β alloys. The activity of hydrogen in CP Ti is lower than the activity of hydrogen in Ti-6Al-4V at 800°C, as depicted in Figure 2.26. Hence, CP Ti has a higher solubility of hydrogen than Ti-6Al-4V [**39**].

Furthermore, the diffusivity of hydrogen in Ti-6Al-4V alloys with different starting microstructures also varies significantly. A β annealed alloy with a lamellar microstructure with continuous β has a higher diffusivity than duplex alloys. This is due to the fact that hydrogen has a greater absorption in the β phase; hence microstructure with more continuous β will tend to absorb more hydrogen [**40**].

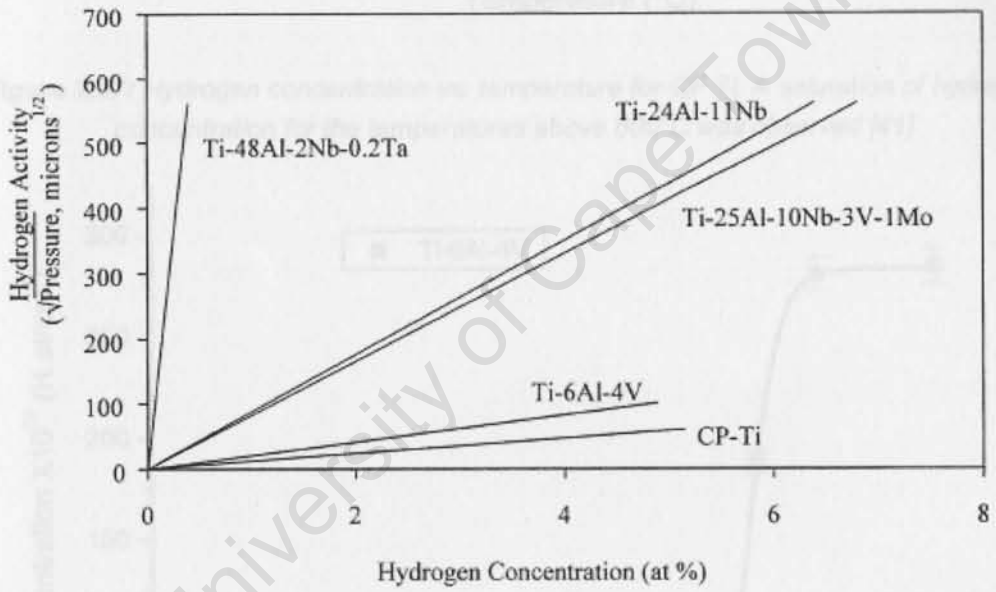

Figure 2.26: *Hydrogen activity for selected titanium alloys at 800°C [**39**]*

Figures 2.27 and 2.28 showed that the uptake of hydrogen in CP Ti and Ti-6Al-4V only occurs from 550°C. This is due to the fact that the solubility of hydrogen in the α phase is a few orders of magnitude less than in the β-phase [**9**]. This temperature (550°C) is referred to as the threshold temperature at which the uptake of hydrogen occurs most rapidly. The saturation of hydrogen reaches $3x10^{22}$ H atoms/cm^3 as shown in Figures 2.27 and 2.28 [**41**].

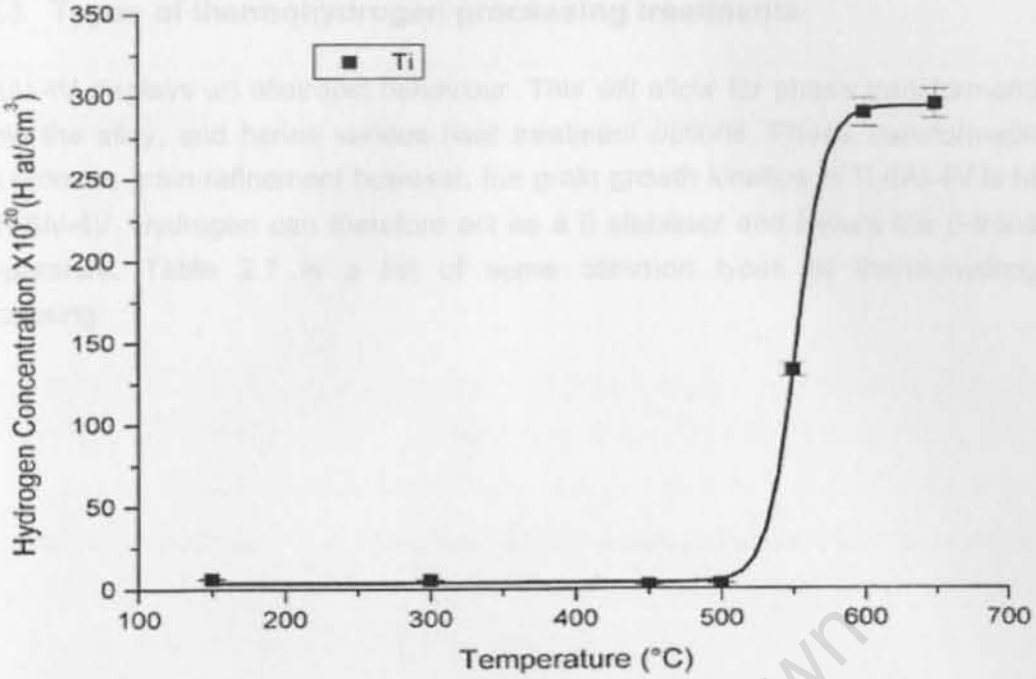

Figure 2.27: *Hydrogen concentration vs. temperature for CP Ti. A saturation of hydrogen concentration for the temperatures above 600°C was observed* ***[41]***

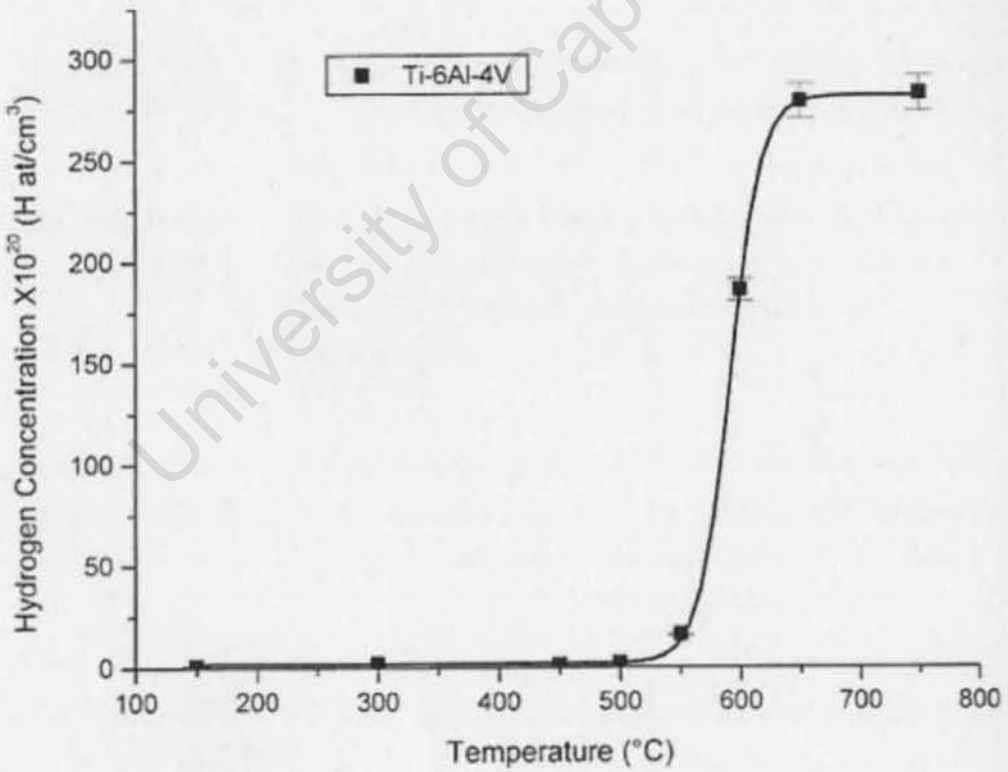

Figure 2.28: *Hydrogen concentration vs. temperature for Ti-6Al-4V. A saturation of hydrogen concentration for the temperatures above 650°C was observed* ***[41]***

2.2.3 Types of thermohydrogen processing treatments

Ti-6Al-4V displays an allotropic behaviour. This will allow for phase transformations within the alloy, and hence various heat treatment options. Phase transformations can promote grain refinement however, the grain growth kinetics in Ti-6Al-4V is high in Ti-6Al-4V. Hydrogen can therefore act as a β stabiliser and lowers the β-transus temperature. Table 2.7 is a list of some common types of thermohydrogen processing.

Table 2.7: Some types of thermohydrogen processing treatments [1]

Designation	Treatment
Hydrovac (HVC) [42]	The specimen is hydrogenated, β solution treated, water quenched, aged to form hydrides then dehydrogenated
Constitutional solution treatment (CST) [43]	Hydrogenate in β phase region, cool to below eutectoid temperature and then dehydrogenate
β quench and hydride-dehydride (BQ-HDH) [44]	β solution treated, water quenched, hydrogenate and dehydrogenated below eutectoid temperature
Hot isostatic pressing (HIP) of vacuum pressing (VHP) [45]	Hydrogenate, compact with hydrogen and dehydrogenate
High temperature hydrogenation (HTH) [46]	Hydrogenate in β phase field, cool to room temperature, dehydrogenate below normal eutectoid temperature
Below β(H) transus hydrogenation [47]	Hydrogenate just below β-transus, cool to below the eutectoid temperature, thermocycle to repeat the eutectoid β phase decomposition and finally dehydrogenate
Repeated eutectoid β-phase decomposition [48]	Hydrogenate above the β(H) transus, slow cool to below the eutectoid temperature, thermocycle to repeat the eutectoid β-phase decomposition and then dehydrogenate
Repeated martensitic β-phase decomposition [48]	Hydrogenate above the β(H) transus, quench to room temperature to produce α' martensite, thermocycle to repeat the martensite β phase decomposition and then dehydrogenate

2.2.4 Principles of thermohydrogen processing

The addition of hydrogen in Ti-6Al-4V is capable of destabilising the low temperature α-phase and stabilising the more ductile high temperature β-phase. Due to this the α-phase transforms partly into the β-phase above the eutectoid temperature. Furthermore, the temperature of transforming the α-phase to the β-phase phase is lowered and the temperature interval of the two phase (α+β) is increased when hydrogen is added.

The decrease in the temperature range of the α+β to β transformation (modified β transus) due to hydrogen addition leads to reduction in grain growth on heating into the modified β range. The hydrogen-induced increase in the temperature interval of the α+β range allows heat treatments to be performed, which would not otherwise have been possible without hydrogen addition [**1**]. This in turn leads to different microstructures in the conventional Ti-6Al-4V alloy and the opportunity to promote grain refinement in a manner similar to the practice of normalising steels.

2.2.5 Phase transformations within Ti-6Al-4V during hydrogenation

Phase diagrams were proposed by Kerr et al. [**28**] and Ilyin et al. [**27**], which displayed significant differences as shown in Figure 2.29. In Figure 2.29a, a hydride-phase formation was proposed by eutectoid transformation of the β-phase near 800°C. However, in Figure 2.29b, a phase diagram was proposed, which showed a hydride phase formation present only below 300°C and a wide α+β phase field above 300°C.

In a study by Qazi et al. cast Ti-6Al-4V was hydrogenated at 780°C and held isothermally for 24 hours by introducing varying levels of hydrogen within the alloy i.e. 10, 20, 30 at% H. This was done in order to establish the correct Ti-6Al-4V-H phase diagram.

Prior to hydrogenation a coarse α+β lamellar phase with an average prior grain size of 0.97mm and an average interlamellar a spacing of 5μm was observed, as shown in Figure 2.30a. An addition of 10at% H lead to the formation of α and martensite (α'), as shown in Figure 2.30b and the lamellar space decreased. The martensite regions were identified as a smooth etch resistant regions between α lamellae. The martensite volume fraction also increased from 30 to 80 vol%, as the hydrogen concentration increased from 10 to 30at%. The transformation of α-lamellae into fine chains of equiaxed particles was observed, as shown in Figures 2.30c and d. A hydride phase formation was detected in the specimens containing 20 and 30at% H, but not in the specimen containing 10at%H [**6**].

The specimen containing 30at% H was then annealed at 750°C and 800°C, 830°C and 850°C for 1 hour and then water quenched. Primary α particles and α' (martensite) phases were formed, with a volume fraction of α particles decreasing with an increase in temperature, as shown in Figures 2.31a and b. This indicated that both the specimens were annealed below the β-transus temperature. Annealing at 830°C and 850°C displayed only martensite, as shown in Figures 2.31c and d. This indicated that annealing was done above the β-transus temperature [**6**].

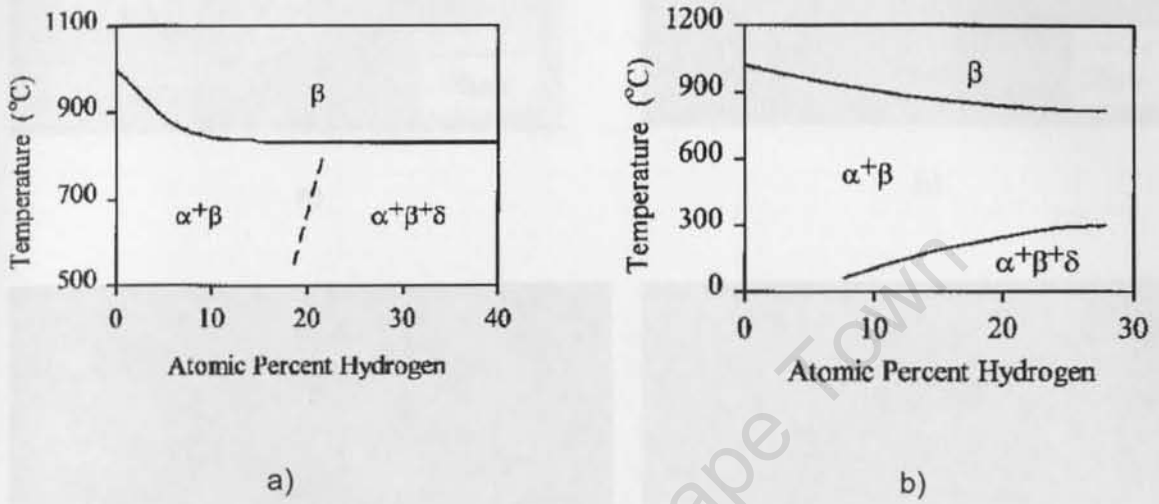

Figure 2.29: *Phase boundaries in Ti-6Al-4V-H system according to a) Kerr et al. [**28**] and b) Ilyin et al. [**27**]*

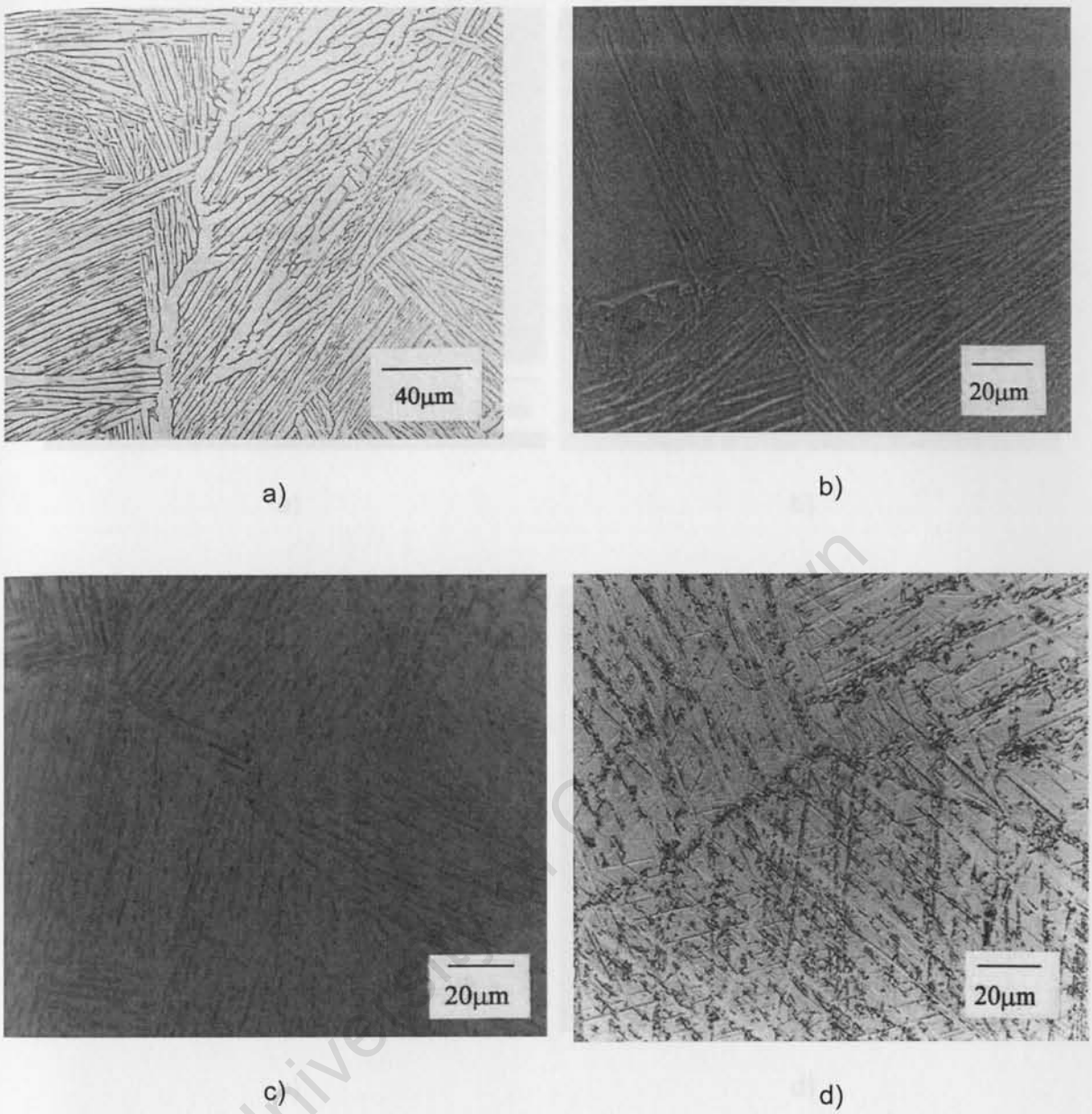

Figure 2.30: *Light micrographs of Ti-6Al-4V alloy a)As-cast, b) 10 at%H, c) 20 at%H, d) 30at%H all at 780°C for 24hours followed by air cooling* ***[6]***

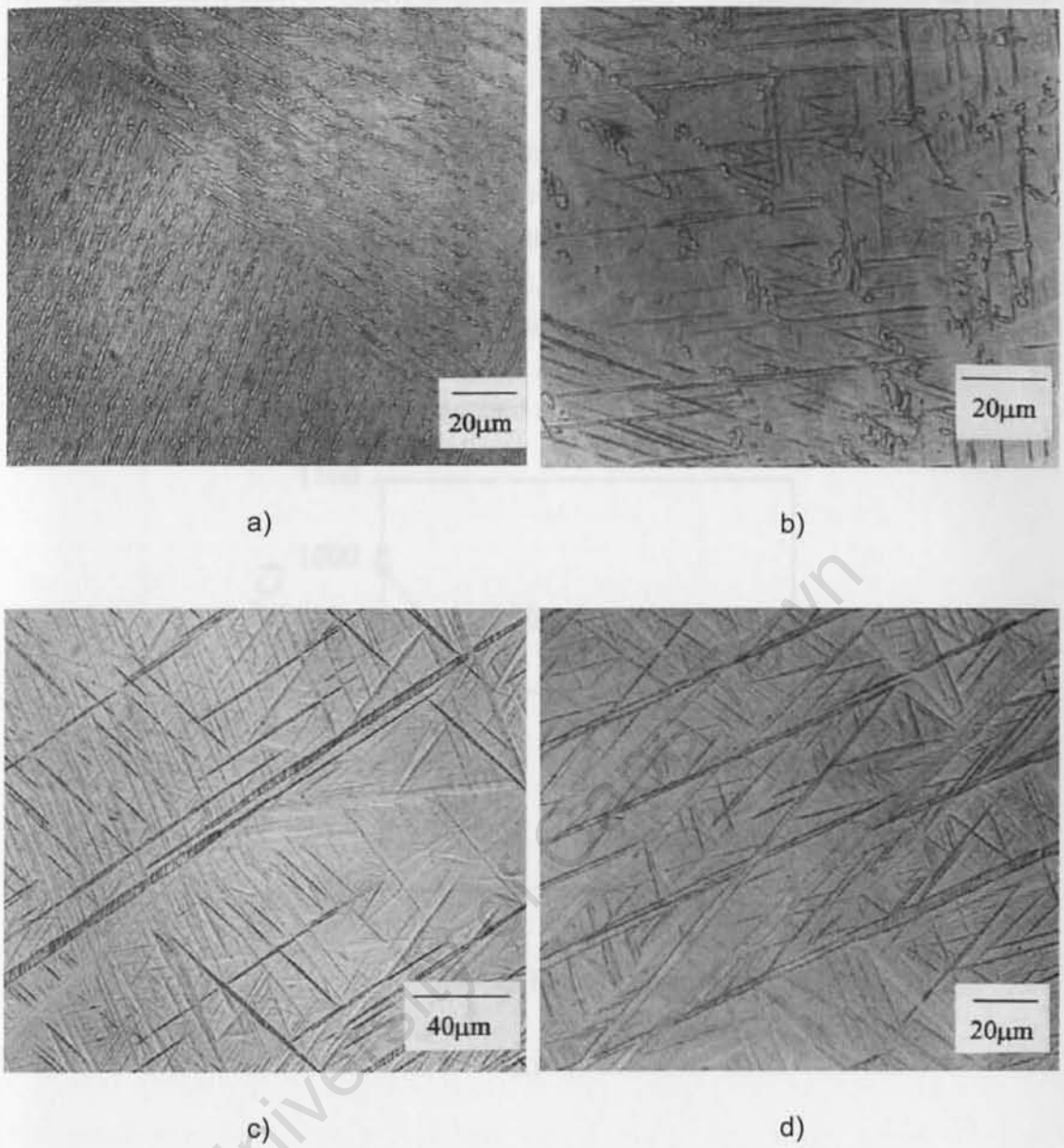

Figure 2.31: *Light micrographs of Ti-6Al-4V alloy containing 30at% H after heating at a) 750°C, b) 800°C, c) 830°C and d) 850°C for 1hour and water quenching thereafter [**6**]*

The phase diagram for Ti-6Al-4V-H was then established as shown in Figure 2.32a, which showed a decrease in the β-transus from 1005°C to 815°C, with an increase in hydrogen concentration from 0 to 30at%. From Figure 2.32a, it is seen that from a concentration of 0 to 10at%H no hydride phase was present from 20-1000°C. The hydrogen formed interstitial solid solutions in the α and β phases. The β-transus decreases rapidly with an increase in hydrogen concentration and the volume fraction of the β phase in the α+β phase field increases. This corresponds to the results by Kerr et al and Ilyin et al. At higher hydrogen concentrations Figure 2.32a disagrees with Figure 2.29b, but supports and expands Figure 2.29a. With a

hydrogen concentration of 15at% a hydride phase was detected and the three phase α+β+hydride field was present below the β-transus. A two phase β+hydride range was also detected above the β-transus.

Figure 2.32b shows the Ti-H phase diagram under ambient pressure obtained Wang et al. [**49**]. At 300°C, at approximately 40at%H the eutectoid reaction from the β-phase (with hydrogen in solid solution) to the α+ hydride phases occurs. Hence, the β-transus of CP Ti is lowered to 300°C, due to the addition of hydrogen. For temperatures above 800°C, with a hydrogen concentration >50at% βTi and hydrogen gas (G) exists, as shown in Figure 2.32b. Above 1600°C the melting point of CP Ti (with hydrogen in solid solution) is reached and the liquid phase (L) exists.

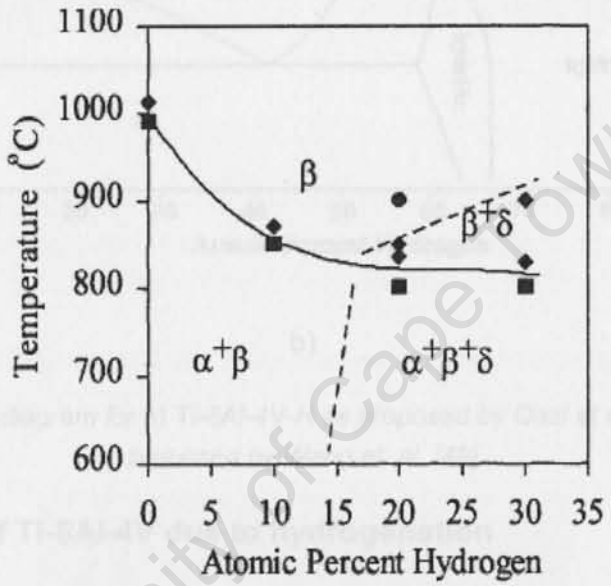

a)

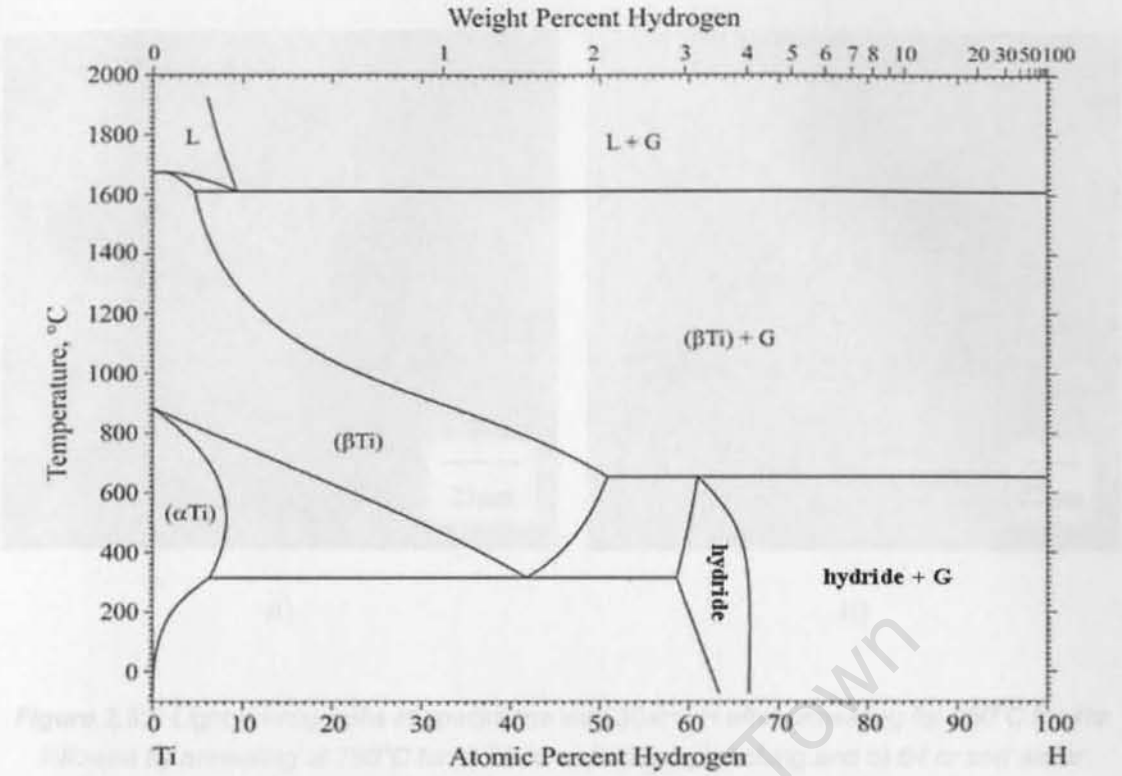

b)

Figure 2.32: *Phase diagram for a) Ti-6Al-4V-H as proposed by Qazi et al. [**6**] and b) Ti-H as proposed by Wang et. al. [**49**]*

2.2.6 Kinetics of Ti-6Al-4V due to hydrogenation

Qazi et al. extended their study from [**6**] to establish TTT (time, temperature, transformation) phase diagrams for specimens containing 10, 20 and 30at% H.

The specimens with 30at% H was annealed at 850°C for 1hour then annealed at 780°C for 16 hrs and 64hrs. The micrographs for the specimens as shown in Figure 2.33a showed that no decomposition of the β phase occurred after 16 hours of holding time and only martensite needles were seen. After 64 hours of holding time 12 vol% of α particles were detected along with martensite needles, which indicated that the start of β to α transformation occurred between 16-64 hours [**50**].

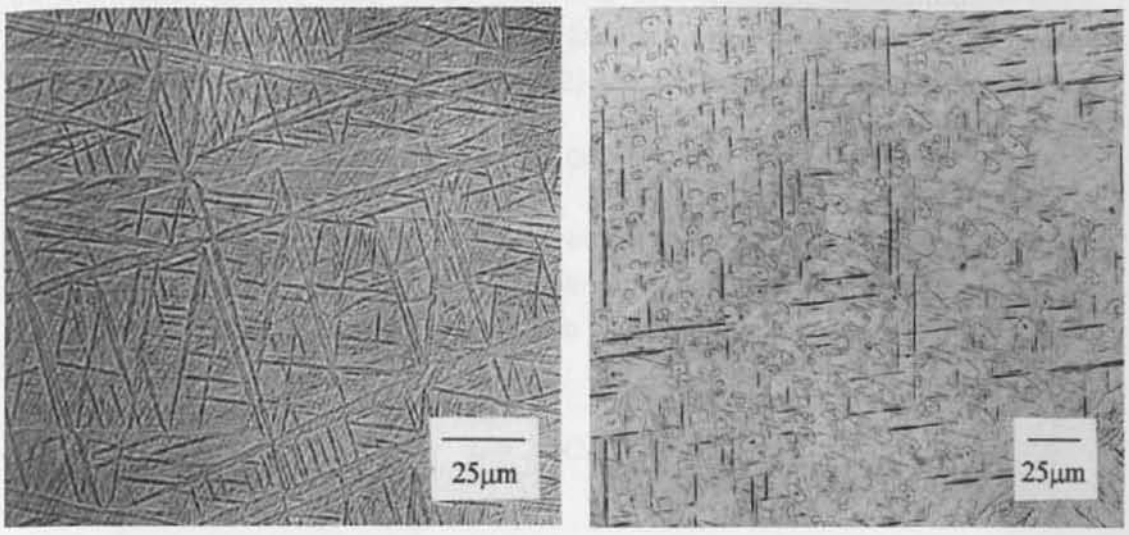

a) b)

Figure 2.33: *Light micrographs of specimens with 30at% H after annealing for 850°C for 1hr followed by annealing at 780°C for a) 16 hr and water quenching and b) 64 hr and water quenching showing 12vol% transformation* ***[50]***

For specimens with 20 and 30at%H TEM analysis indicated that a hydride phase was also present (See Figure 2.34) but not in the 10at % H specimens.

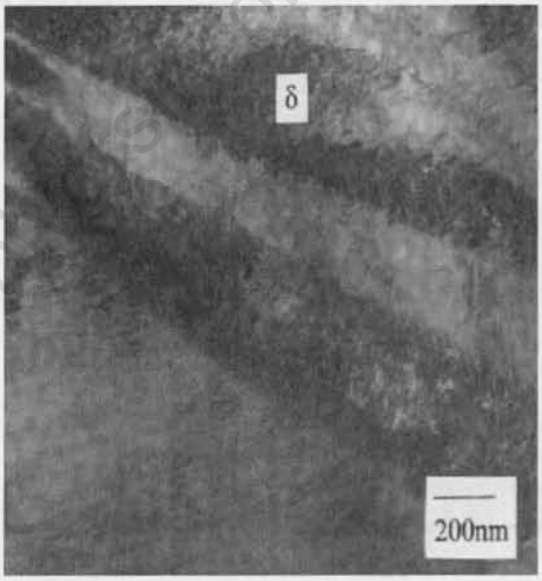

Figure 2.34: *TEM micrograph with 20at% H after annealing for 1h at 850°C and water quenching, BF showing titanium hydride laths* ***[50]***

TTT diagrams for the specimens containing 10, 20 and 30at% H are shown in Figure 2.35a-c. An increase in hydrogen concentration resulted in a decreased

transformation starting nose temperature and increased the transformation starting nose time. Nose temperature decreases linearly with increasing hydrogen content according to the following correlation (Eq. 2) and as shown in Figure 2.36a.

$$T_N = 731 - 5.0C_H \quad (2),$$

Where T_N is the nose temperature in degrees Celsius and C_H is the concentration of hydrogen in atomic percent. The nose-time (t_N) increased with an increase in hydrogen content as shown in Figure 2.36b and the relationship can be described by Eq. 3.

$$t_N = 2.8C_H^{\,2} \quad (3)$$

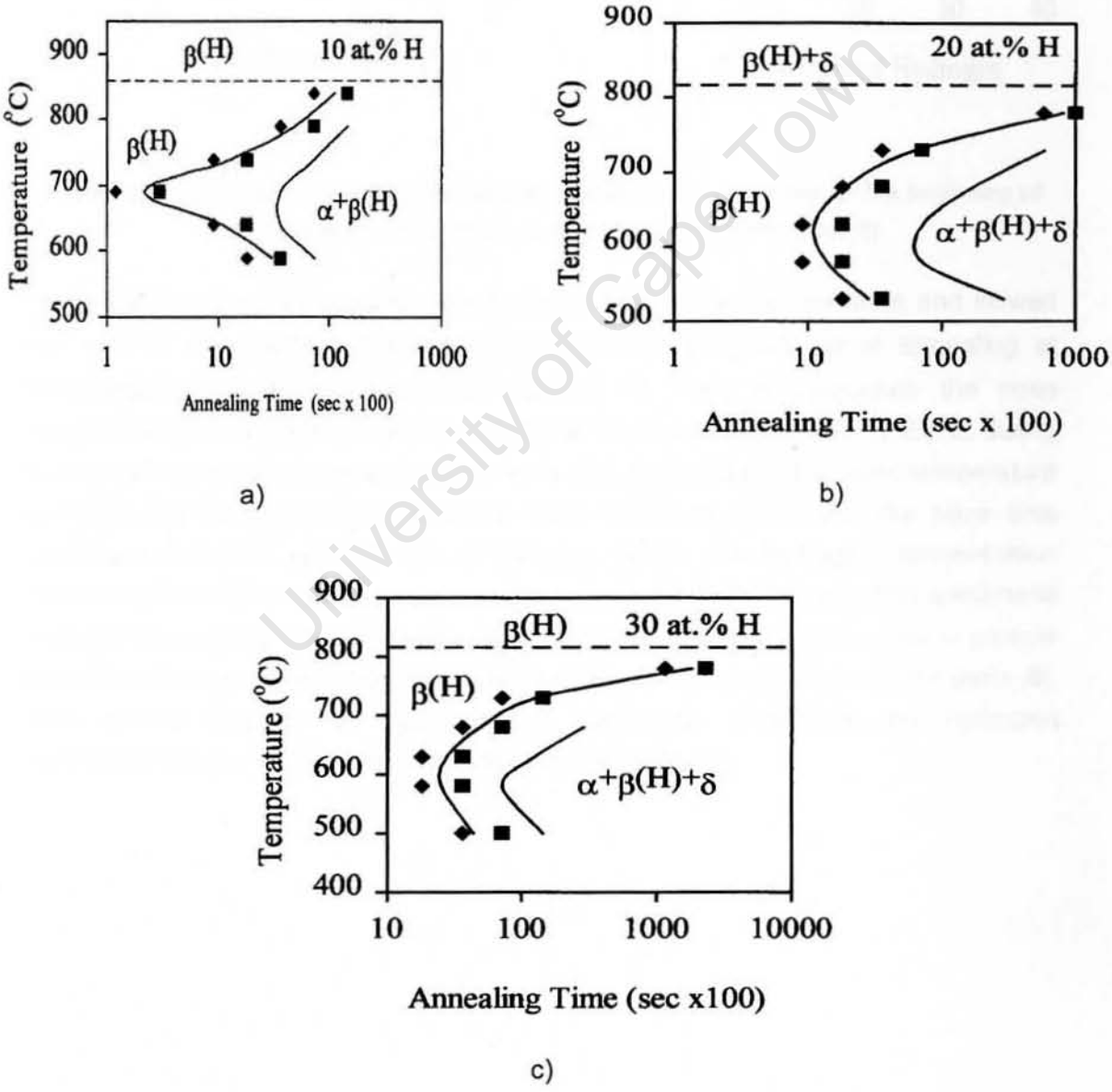

Figure 2.35: *TTT diagrams for b phase decomposition in Ti-6Al-4V specimens with a) 10at% H, b) 20at% H and c) 30at%H* ***[6]***

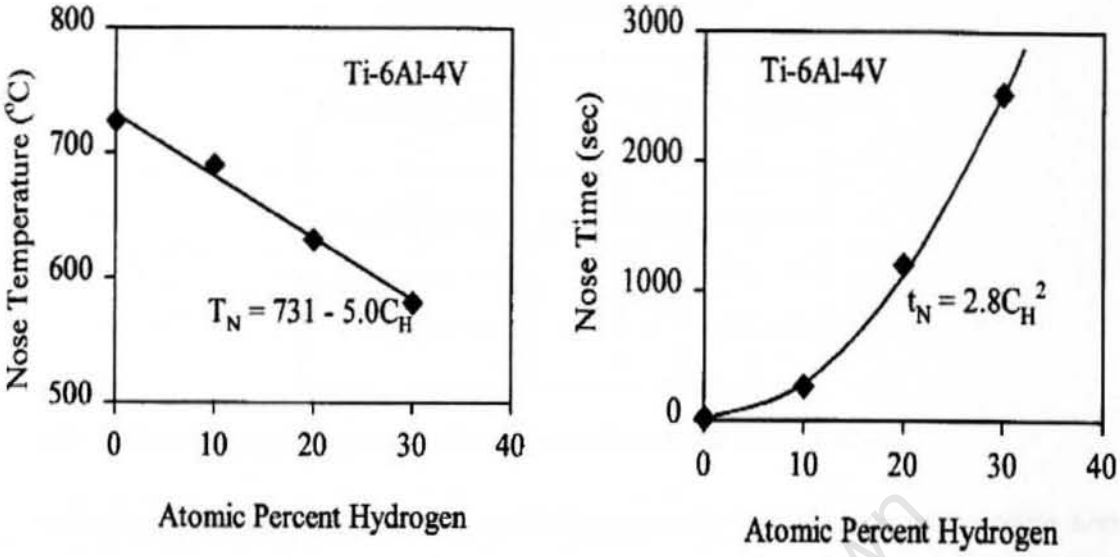

Figure 2.36: *Dependence of the a) nose temperature and b) nose time for the beginning of the β phase decomposition on the hydrogen concentration [**6**]*

Hydrogen acted as a β stabiliser decreasing the β-transus temperature and slowed the rate of the residual β-phase decomposition during isothermal annealing at temperatures below the β-transus. Addition of 1at% H decreases the nose temperature by 5°C and the time in non linear fashion as expressed by Eq. 2, during which the β-phase remains untransformed at this temperature. The nose temperature to begin the transformation decreases from 725°C to 580°C and the nose time increases from 12 seconds to 42 minutes, when the hydrogen concentration increased from 10 to 30at% H. Increasing hydrogen concentration within specimens lowered the cooling rates to obtain fully martensite structures and avoids α particle formation. Hence, a more homogenous structure can be obtained in thicker parts [**6**]. The overall kinetics of hydrogenated specimens depending on hydrogen concentration was altered and is summarised in Table 2.8.

*Table 2.8: The minimum critical cooling rate (V_m) to form 100% martensite and the maximum cooling rate V_d, below which no martenstite will form in Ti-6Al-4V with varying H concentrations [**6**]*

H content at%	0	10	20	30
V_m (°C/min)	1000	50	10	5.0
V_d (°C/min)	30	4	1.5	1.0

2.2.7 Effect of hydrogen on the microstructure of Ti-6Al-4V

Mechanical properties of (α+β) alloys are governed by the amount, size, shape and morphology of the α phase and the density of the α/β interfaces. Hydrogen as a temporary alloying element can refine the microstructure of the Ti-6Al-4V alloy and CP Ti and in turn improve the overall mechanical properties.

Hydrogen can alter the metastable phase transformations when the alloy is quenched from the β phase field. Specimens with varying amounts of hydrogen will exhibit different amounts of phase when heated to the β phase field and then quenched from this temperature. At low H concentrations (0-17.3at% H) hydrogen promotes the formation of α'' (orthorhombic martensite) and exhibits a mixture of α, α' and α'' when quenched from the β phase field (See Figures 2.37 a-c). With higher hydrogen content the amount of α'' decreases and the β phase is stabilised (See Figure 2.37d). This phenomenon is due to the fact that as the concentration of hydrogen increases the high temperature β-phase will be stabilized to room temperature rather than transforming into the α' phase [**51**].

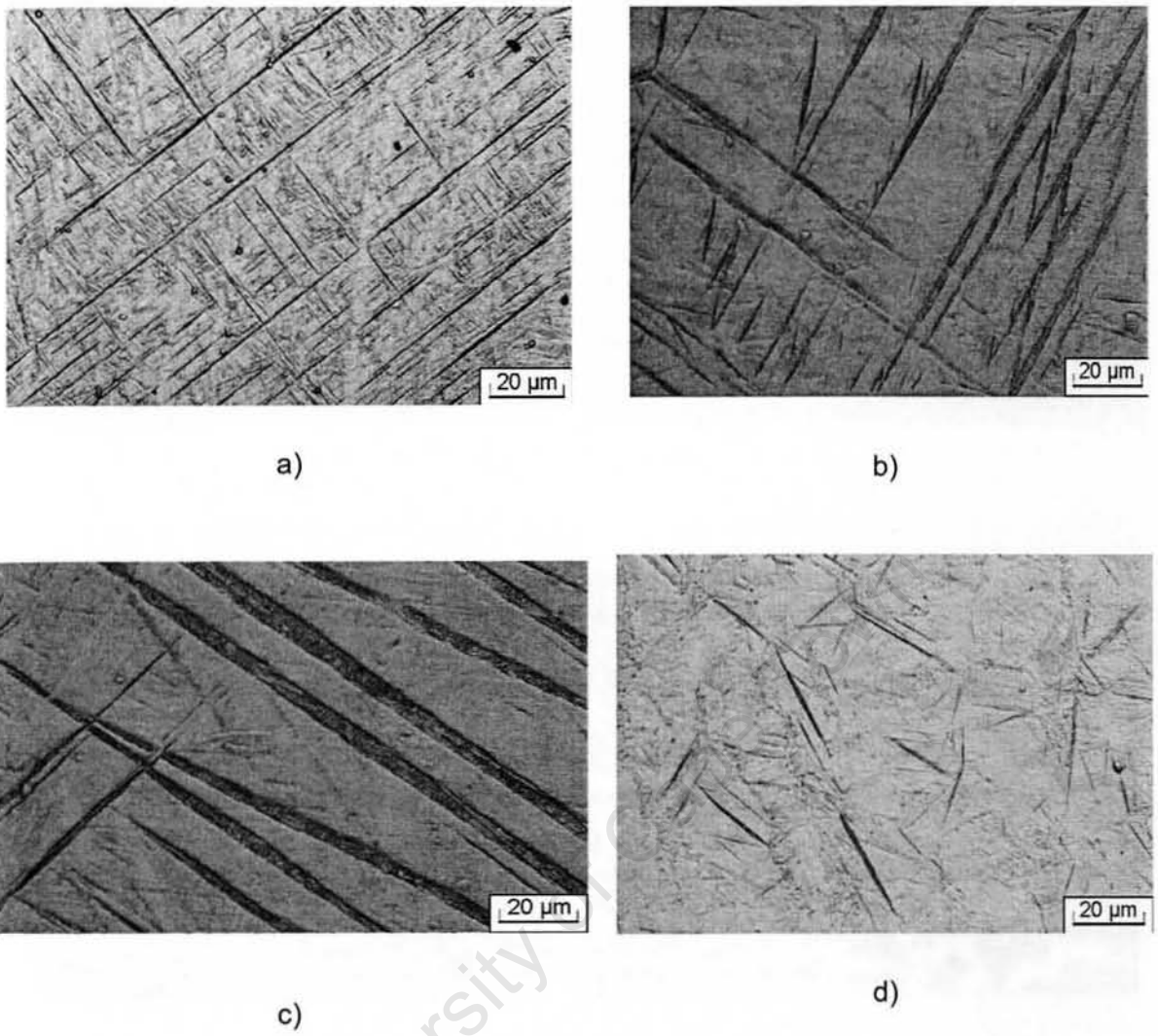

Figure 2.37: *Microstructures of Ti-6Al-4V containing a) 0at% H, b) 11.84at% H, c) 17.3at% H and d) 22.92at%H quenched from the β phase field* ***[51]***

The amount of hydrogen present will also affect the microstructrual evolution as shown in Figures 2.38a-d. Without hydrogen, a dual phase α+β was seen. The specimen with 4.71at%H was seen to have little effect on the microstructure, as shown in Figure 2.38b. Hydrogenating at 750°C, (below the β transus) with 4.71, 11.41 and 20.07at%H displayed α, β and α" phases during XRD analysis indicating that the β to α" phase transformation occurred during cooling. Microstructures with 11.41 and 20.07at% (Figure 2.36c and d) consists of α, β, α" and δ phases, indicating that the β_H to α+δ and β to α" phase transformations occurred during cooling **[52]**.

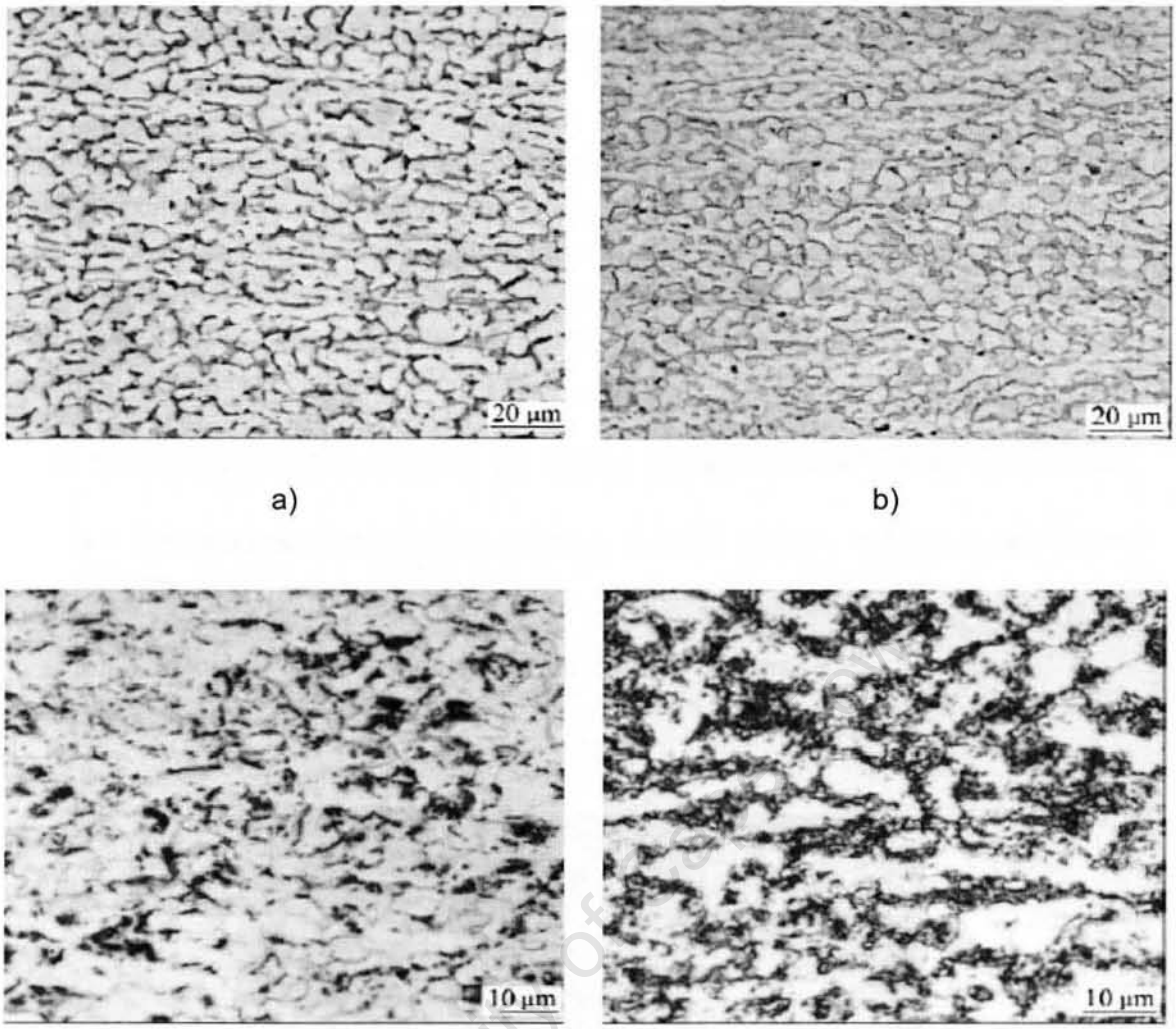

Figure 2.38**: Microstructure of Ti-6Al-4V hydrogenated at 750°C for 1hour followed by air cooling, samples containing, a) 0at% H, b) 4.71at% H, c) 11.41at% H and d) 20.07at% H **[52]

2.2.8 Hydrides in CP Ti and Ti-6Al-4V

Titanium hydrides exist in three known forms (δ, ε, γ) at room temperature. TiH_2 (δ) has a fcc crystal structure with the hydrogen atoms occupying the tetrahedral interstitial sites (CaF_2 type structure). Figure 2.39 is a micrograph of this hydride phase [**53**].

The presence of hydrogen in solid solution in both α and β phases results in lattice expansions. The β-phase is most affected with about 5.35% volume expansion. The transformation from α titanium to the hydride phase is followed by a volume expansion of 17.2% [**9**]. The lattice parameter of TiH_x with specific concentrations of hydrogen, also expand upon heating as shown in Figure 2.40. The diffusion of

hydrogen in the δ (hydride) phase is two orders of magnitude lower than the diffusion in α and β phases **[54]**. Hydrogen thus has a greater effect on the lattice parameters of the α and β phases than the δ phase.

The effect of hydrogen and hydride formation in the Ti-H and Ti-6Al-4V systems also differs considerably. The cell volume for $\delta_{Ti\text{-}6Al\text{-}4V}$ is 2.1% larger than the cell volume of δ_{Ti}. The expansion of the cell volume based on the same number of metal atoms for the transformation of α to β then to δ in the Ti-H system is 21.1%. For the Ti-6Al-4V-H system the transformation from α to δ is 26.6% and 32.3% for the β to δ phase transformation **[55]**.

The factors that would thus lead to the volume expansion in CP Ti and Ti-6Al-4V are:

- The absorption of hydrogen in the α, β and δ phases, with the β phase most affected
- The formation of hydrides from the α and β phases

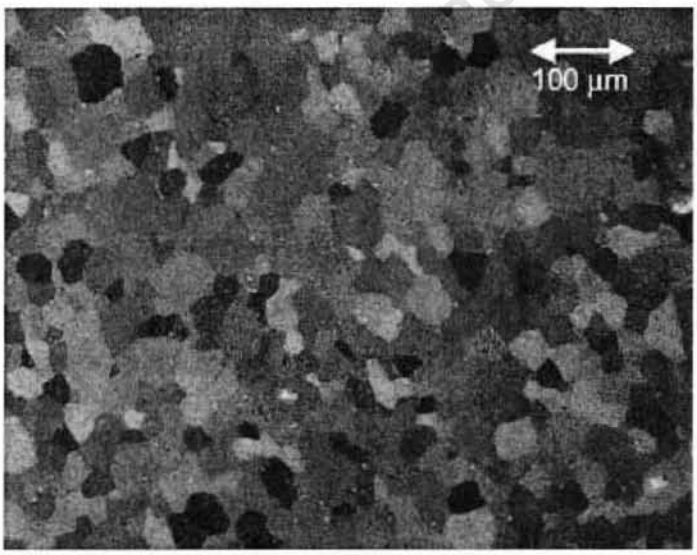

Figure 2.39: *Micrograph of bulk δ TiH_2* ***[56]***

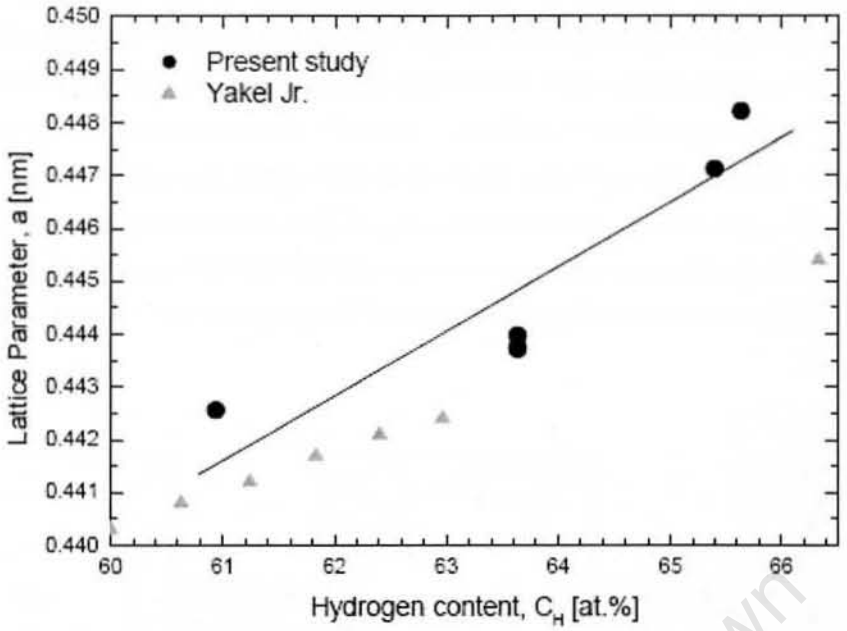

Figure 2.40: *Change in the lattice parameter a of δ TiH_2 with hydrogen concentration C_H* ***[56]***

Liangshun Luo et al. proposed a mechanism for hydride formation in Ti-6Al-4V specimens containing 0.1, 0.3 and 0.5 wt% hydrogen by considering the effects of hydrogen. The diffusion of hydrogen could not be ignored because of its considerable diffusivity D during the experiment which can be described by the following equations:

$$D_\alpha = 1.8 \times 10 - 6 \exp(-\frac{6230}{T}) \quad (4)$$

$$D_\beta = 1.95 \times 10 - 7 \exp(-\frac{3342}{T}) \quad (5)$$

Where D_α and D_β are the diffusitivities in the α and β phases respectively.

Figure 2.41 shows the mechanism of transformation of βH to α and δ (hydride phase). After hydrogenation of most of the α transformed into βH phase, according to the Ti-6Al-4V-H phase diagram (Fig 2.32a). The β to α reaction happened whilst cooling from the β phase to room temperature. The primary α precipitated along the βH grain boundaries as shown in Figure 2.41b and c. The δ phase did not precipitate directly from the β phase due to the large volume misfit going from bcc to fcc (8-11%). At the eutectoid temperature the βH (bcc) to α (hcp) + δ (fcc) transformation occurred, as shown in Figure 2.41d. The solubility of hydrogen in α is minimal and therefore a hydrogen rich zone emerged around the α (α^o), as shown in Figure 2.42. The hydrogen rich zone further promoted the precipitation of δ hydride. The δ hydride

precipitated along the primary α grain boundary because of high density defects. The δ hydride lamellar further grew from which hydrogen atoms supply which comes mostly from the βH phase. Hydride formation may also cause one zone lean in hydrogen which promotes the α phase formation. Coupled growth of δ hydride and the α phase occurred. After the eutectoid transformation, one eutectoid zone emerges whereby δ hydride and α are adjacent to each other as shown in Figures 2.41d and e. The eutectoid transformation was slow and occurred along the grain boundaries due to the clustering of hydrogen along the boundaries [**57**].

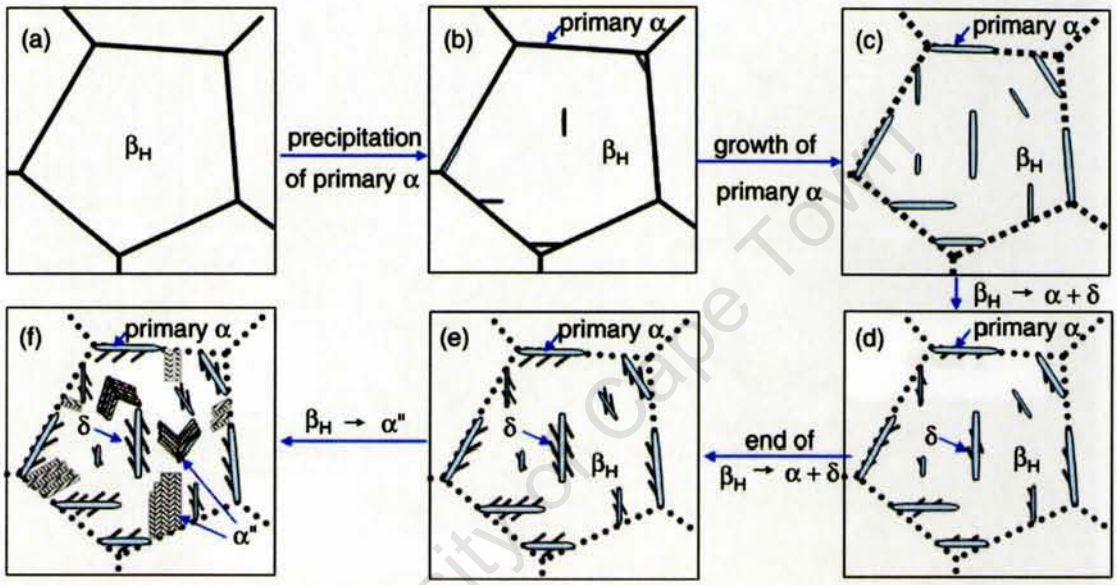

***Figure 2.41**: Schematic representation of eutectoid transformation mechanism from β_H to α and δ during cooling [**57**]*

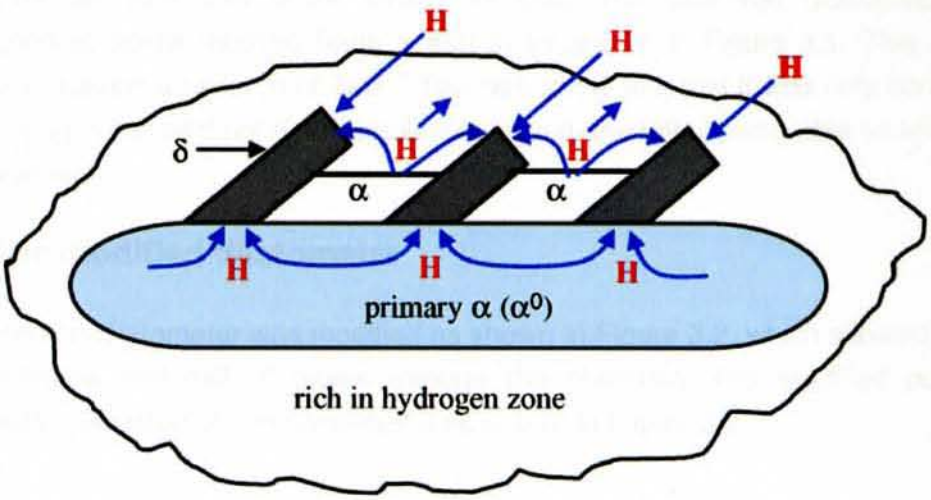

***Figure 2.42:** Hydrogen diffusion in the eutectoid β_H to α+ δ transformation [**57**]*

3 MODIFICATION OF TESTING EQUIPMENT

3.1 Testing requirements of dilatometer

The key requirement of the dilatometer was that it needed to act as a dual functioning hydrogen furnace and dilatometer. The redesign of the original push-rod dilatometer involved making it fit to comply with safety requirements. Gas needed to safely enter the system and after it was heated to temperatures of up to 1000°C and thereafter it needed to be cooled to in order to safely exit the system via a fume extraction hood.

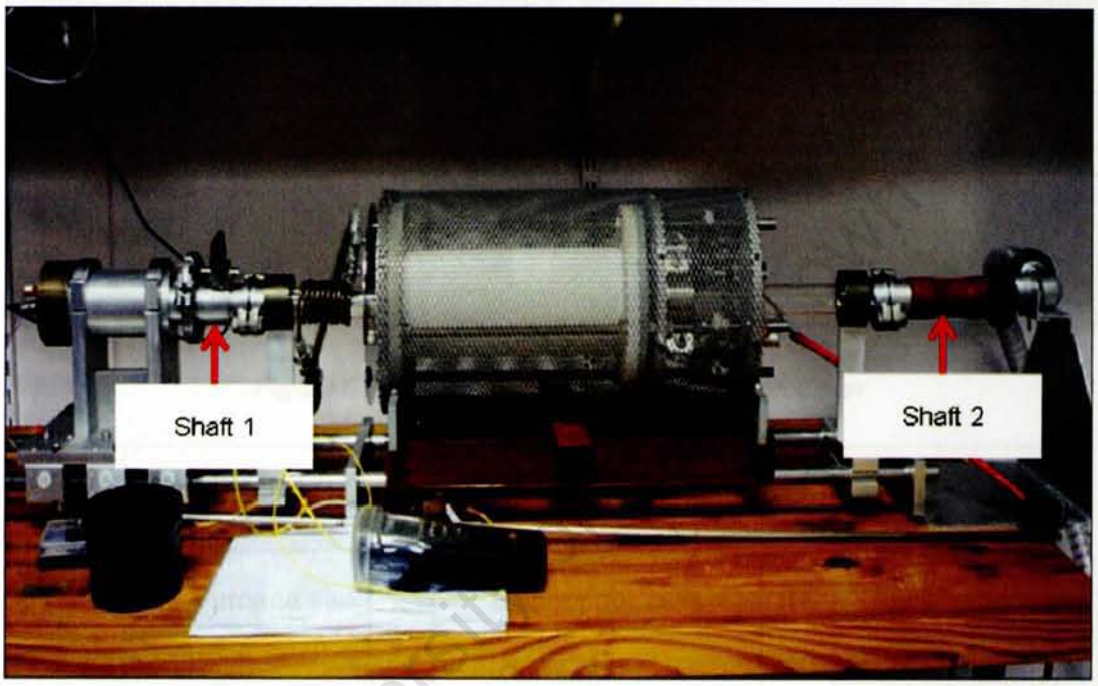

Figure 3.1: *Set up of original push-rod dilatometer*

Figure 3.1 shows the original set up of the push-rod dilatometer, which did not have valves for an inlet and outlet stream of gas. The push-rod dilatometer was redesigned at points labelled Shaft 1 and 2, as shown in Figure 3.1. This system could only sustain a vacuum of $1x10^{-2}$ Torr due to the fact that it was only connected to a backing pump and not a turbomolecular pump, the latter being able to achieve a better vacuum.

3.2 The modified dilatometer

The push-rod dilatometer was modified as shown in Figure 3.2, which allowed for the safe entrance and exit of gases through the chamber. The modified push-rod dilatometer consisted of components A-I as shown in Figure 3.2.

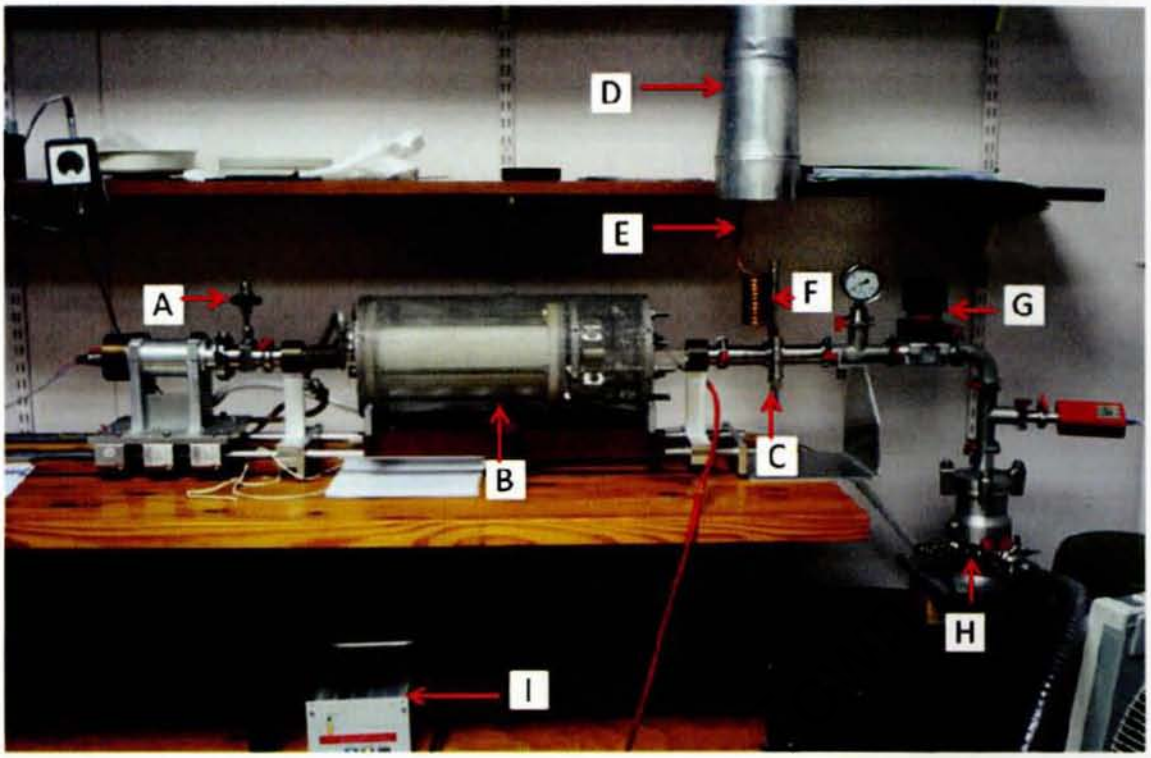

Figure 3.2: *Set up of modified push-rod dilatometer*

A	Inlet valve	D	Fume extraction hood	G	Speedi valve
B	Furnace	E	Exit copper coils	H	Turbo pump
C	Primary exit poppet check	F	Secondary poppet check valve	I	Turbo pump controller

The primary exit poppet check valve was set to open at 6KPa in order to allow the purging of gases in the system. The secondary safety poppet check valve was put in place in case the primary exit poppet check valve failed; the former and was set to "crack" at 15KPa in order to release the pressure in the system in the event of failure of the primary exit poppet check valve. The exit copper coils as shown in Figure 3.2, allows for the gas that is heated by the furnace to cool before exiting the fume extraction hood; this is critical for hydrogen since the gas is able to auto-ignite at temperatures greater than 500°C.

The turbo molecular pump is connected to a backing pump and collectively reaches a vacuum of $4X10^{-3}$ Torr. This vacuum ensures sufficient oxygen is removed from the chamber, in order to prevent extended oxidation of CP Ti and Ti-6Al-4V during the dilatometer thermal treatments.

4 EXPERIMENTAL PROCEDURE

4.1 Materials

4.1.1 CP Ti and Ti-6Al-4V

The materials under examination were commercially pure titanium (CP Ti, 99.6%) and Ti-6Al-4V obtained from *Goodfellow* in the annealed condition. Tables 4.1 and 4.2 show the elemental composition for the CP Ti and Ti-6Al-4V respectively.

Table 4.1: Chemical composition (ppm) of CP Ti (99.6%)

Al	Co	Cr	Cu	Fe	Mg	Mn	Ni	Si	Sn	Ta	V
<500	<2	<500	<200	<300	<20	<500	<500	<200	<200	<10	<500

Table 4.2: Chemical composition of Ti-6Al-4V

Al (%) (nominal composition)	V (%) (nominal composition)	Fe (ppm)	C (ppm)	H (ppm)	N (ppm)	O (ppm)
6	4	<300	<220	<100	<100	<650

4.1.2 Thermal history and preparation of materials

Specimens were cut from a 5mm diameter rod using a precision cutter to a length of 44mm, the required length for fitting into the sample holder of the push-rod dilatometer for both CP Ti and Ti-6Al-4V.

Prior to testing, both materials were vacuum annealed in the vertical furnace. This annealing treatment was performed to ensure that all the materials were in the same starting condition. For Ti-6Al-4V this was done to ensure that the alloy would contain near equilibrium α and β phase compositions (95%α and 5%β). Figure 4.1 outlines the annealing cycle. After vacuum annealing the oxide scale, which formed during the annealing process, was removed with 800μm SiC grit paper in order to avoid interaction with hydrogen during the experiments.

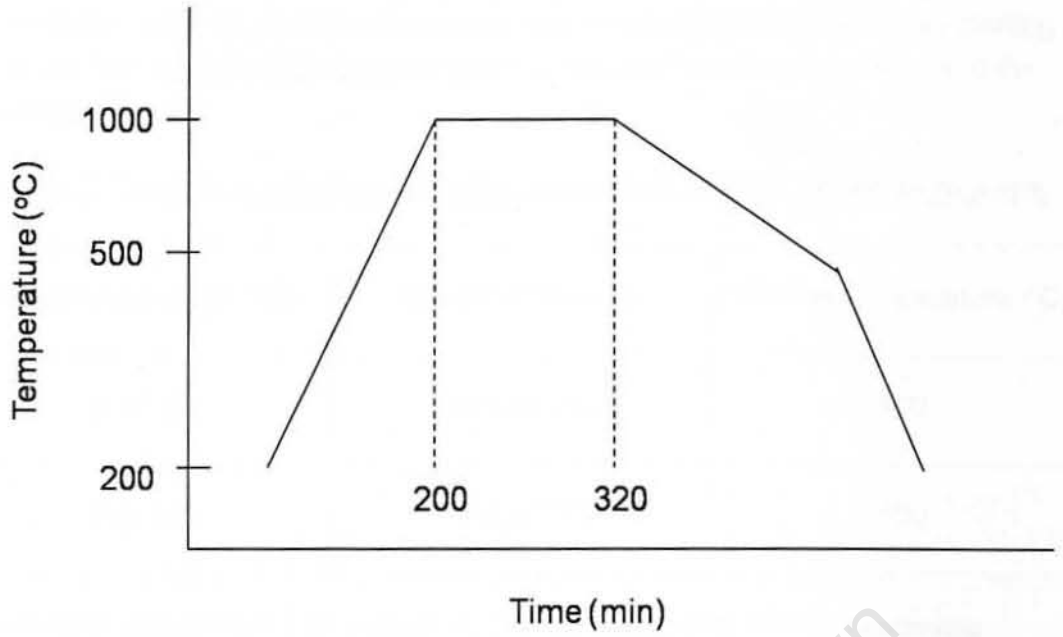

Figure 4.1: *Temperature profile of annealing procedure in vacuum*

4.2 Push-rod dilatometer

4.2.1 Set-up of dilatometer

The push-rod dilatometer was modified to act as a dual functioning hydrogen furnace and dilatometer (See Section 3.3). It consisted of software (*UCT Dilatometer V7*) for data acquisition, a furnace with built in fan (to prevent over heating of the furnace controller), *Gefran 800P* temperature controller, *Mahr Federal* digital transducer and a *Mahr Federal Maxum III* digital indicator. A quartz glass push-rod is seated in the glass quartz glass sample holder; the specimen length to be placed in the holder was 44mm in length and 5mm in diameter in order to produce a reading on the digital indicator. The *UCT Dilatometer V7* software allowed for temperature, heating/cooling rate inputs and recorded temperature and change in specimen length as a function of temperature.

Strain is then calculated by following relationship:

$$\text{Strain} = \frac{\Delta l}{l}$$

Where Δl is the change in length and l is the initial length.

The raw data was taken and averages for every five strain and temperatures values were computed using a *MATLAB* code (See Appendix). From this data strain vs. temperatures curves were plotted. The coefficient of thermal expansion (COTE) is defined as $\frac{1}{\Delta T} \times \frac{\Delta l}{l}$, which is the slope of the Strain vs. Temperature curve. The

slope of the Strain vs. Temperature curve was calculated for every 40°C, by plotting strain vs. temperature for every 40°C in *Excel* and adding a trend line to obtain the slope/COTE value.

Table 4.3: Example of data required to generate a COTE vs. Temperature curve.

Temperature range (°C)	Slope/COTE value	Median Temperature (°C)
80-120	$9.3X10^{-6}$/°C	100
100-140	$9.5X10^{-6}$/°C	120

The COTE values were then plotted vs. Temperature using the corresponding median temperatures (See Table 4.3 as an example). This was the best fit differential curve of the strain vs. Temperature curve.

4.2.2 Interpretation of dilatometric data

During heating the atoms within a material will move in the crystal lattice. As a result of this the material will experience a volume expansion in response to the increase in temperature. This is regarded as the normal thermal effects of the material during heating. The rate of expansion (COTE values) will increase slightly as a function of temperature. If however, the rate of expansion increases/decreases significantly, then this is attributed to a phase transformation. If the material experiences a volume contraction (negative COTE values) during heating, then this is also attributed to a phase transformation.

Figure 4.2 shows strain and COTE vs. temperature curves for CP Ti during heating from room temperature to 1000°C (as shown by the arrow). Heating from room temperature to 750°C, the strain curve is relatively linear and hence, the COTE values remains more or less constant. From 750-830°C, the slope of the strain curve becomes gentler and the COTE values decreases. This is described as a decrease in the rate of expansion. From 850-900°C, the slope of the strain curve becomes negative and hence the COTE values are negative. This is described as a volume contraction. The volume contraction is attributed to a phase transformation (from the α to β phase). The change in the COTE values from 800-940°C can thus be attributed to the complete transformation of the α to β phase. Once the phase transformation is complete (above 940°C) the specimen will continue to expand and the COTE values will increase (as seen in Figure 4.2).

During cooling the material will experience a volume contraction in response to the decrease in temperature. This is regarded as the normal thermal effects of the material during cooling. The rate of contraction (COTE values) will decrease slightly as a function of temperature. If however, the rate of contraction increases/decreases significantly, then this is attributed to a phase transformation. If the strain curve shows a volume expansion (negative COTE values) during cooling, then this is also attributed to a phase transformation.

Assuming perfect equilibrium, then the strain and COTE curves of CP Ti during cooling are then the same as the respective curves during heating. When cooling from 1000°C to 950°C (as shown by the arrow), the strain curve is relatively linear and hence, the COTE values remain more or less constant (See Figure 4.2). When cooling from 940°C to 910°C the slope of the strain curve becomes gentler and the COTE values decreases. This is described as a decrease in the rate of contraction. When cooling from 900°C to 850°C, the slope of the strain curve becomes negative and hence the COTE values are negative. This is described as a volume expansion during cooling. The volume expansion would be attributed to a phase transformation. The change in the COTE values cooling from 940°C to 800°C can thus be attributed to the complete reverse phase transformation of the β to α phase. Once the phase transformation is complete (below 800°C) the specimen will continue to contract and the COTE values will decrease due to the normal effects upon cooling.

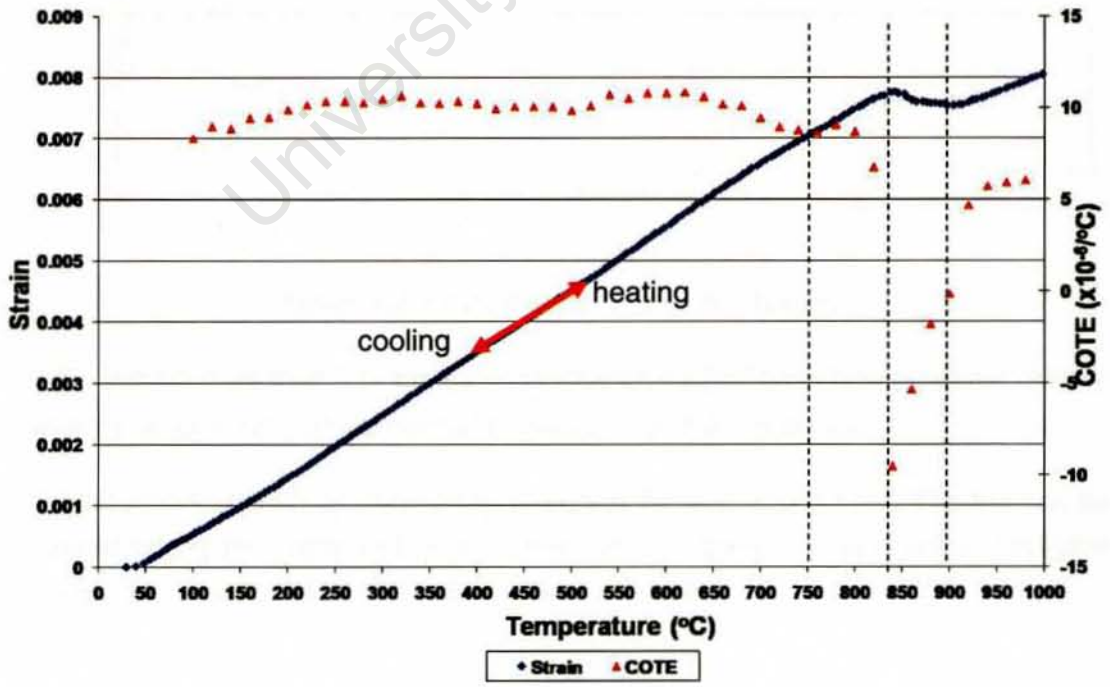

Figure 4.2: *Strain and COTE vs. temperature during heating and cooling of CP Ti, assuming perfect equilibrium*

4.2.3 Calibration of dilatometer using 0.1wt% carbon steel

In order to establish whether the dilatometer could produce reliable strain data, a low carbon steel specimen (0.1wt% C steel) was heated and cooled (heating and cooling rate 1°C/min). The expansion behaviour of iron and 0.1wt%C steel was modelled using the known data, such as lattice parameters and coefficients of thermal expansion. The purpose of modelling the strain based on known data was to compare and validate the experimental data, and hence the experimental set-up.

Iron exists in two crystal forms, i.e. ferrite (α) at room temperature, which transforms into austenite (γ) at 910°C as shown in Figure 4.3. The α to γ phase transformation is accompanied by an atomic volume change of approximately 1%. This is associated with a significant volume contraction in the strain vs. temperature curve during heating [**21**].

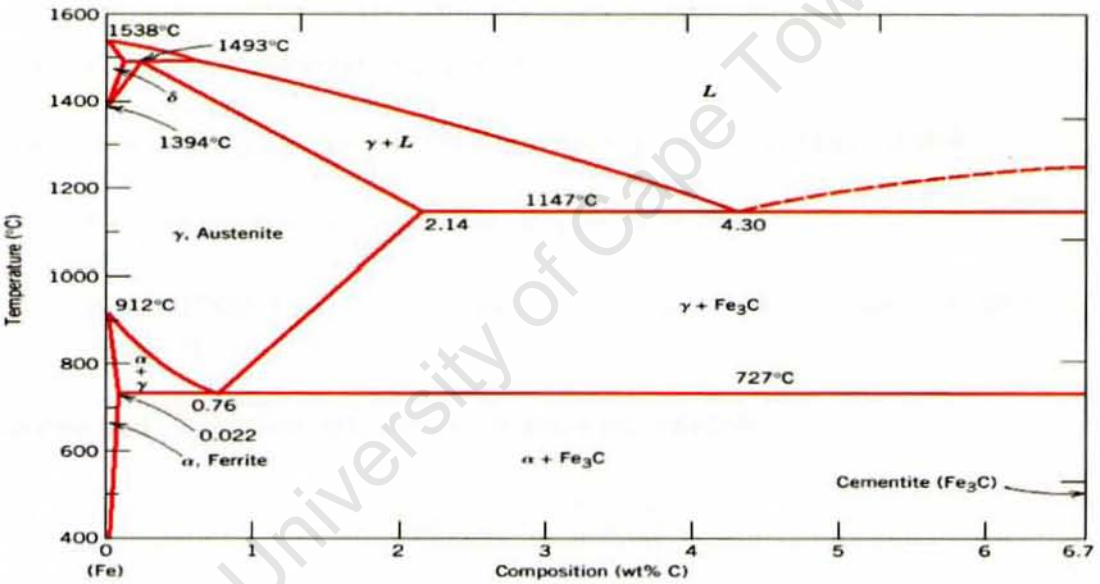

Figure 4.3: *Phase diagram of the Fe-C system*

For the transformation of α to the γ phase Bhadeshia [**58**] has shown that the relative change in length (Δl/l) can be related to the volume of the α phase.

The dilatometric (strain vs. temperature) curves for iron and 0.1wt% C steel can be modelled taking into account that the strain can be computed (assuming negligible density) by:

$$\frac{\Delta V}{V_o} \approx \frac{1}{3}\frac{\Delta l}{l} \quad (6),$$

Where V_o is the initial volume and l is the initial length of the specimen.

Volume and expansion calculation for the α (bcc) phase:

$$\text{From Eq. 6: } \frac{\Delta l}{l} = \frac{\Delta V}{3V_o} \quad (7)$$

$$\frac{\Delta V}{3V_o} = \frac{2V_\alpha - 2V_{ao}}{3 \times 2V_{ao}} \quad (8)$$

$$V_{a_o} = a_o{}^3 \quad (9)$$

$$V_\alpha = a_o[1 + \alpha_\alpha(T - 20)]^3 \quad (10)$$

The factor of 2 in the numerator of *Eq. 8* arises because the unit cell of the α (bcc) consists of two atoms whereas that of γ (fcc) consists of four.

- V_{ao} = initial volume of iron in the α phase
- V_α = volume of the ferrite (α) phase
- a_o = lattice parameter of iron at room temperature (α phase): 2.96Å
- T = temperature (increasing at increments of 10°C)
- α_α = coefficient of thermal expansion of α phase at room temperature: 15×10^{-6}/°C

Volume and expansion calculation for the γ (fcc) phase:

$$\text{From } \textit{Eq. 6}\text{: } \frac{\Delta l}{l} = \frac{\Delta V}{3V_o}$$

$$\frac{\Delta V}{3V_o} = \frac{V_\gamma - 2V_{ao}}{3 \times 2V_{ao}} \quad (11)$$

$$V_\gamma = b_o[1 + \alpha_\gamma(T - 20)]^3 \quad (12)$$

- V_γ = volume of the austenite (γ) phase
- b_o = lattice parameter of iron at room temperature (austenite): 3.27Å
- α_γ = coefficient of thermal expansion of γ phase at room temperature: 21.7×10^{-6}/°C

From the above relationships the strain vs. temperature curve for iron (ferrite and austenite) was modelled, taking into account the phase transformation of the α to γ

phase occurs at 910°C as shown in Figure 4.3. A volume contraction was experienced when ferrite transformed into austenite at 910°C. The unit cell volume for γ (fcc) is greater than the unit cell volume of α (bcc), however the volume per atom for the α (bcc) phase is greater than the volume per atom of the γ (fcc) phase. Due to this, a volume contraction was seen during the transformation from the α to the γ phase. Once the phase the α to γ phase transformation is complete, the metal expands from 910°C onwards.

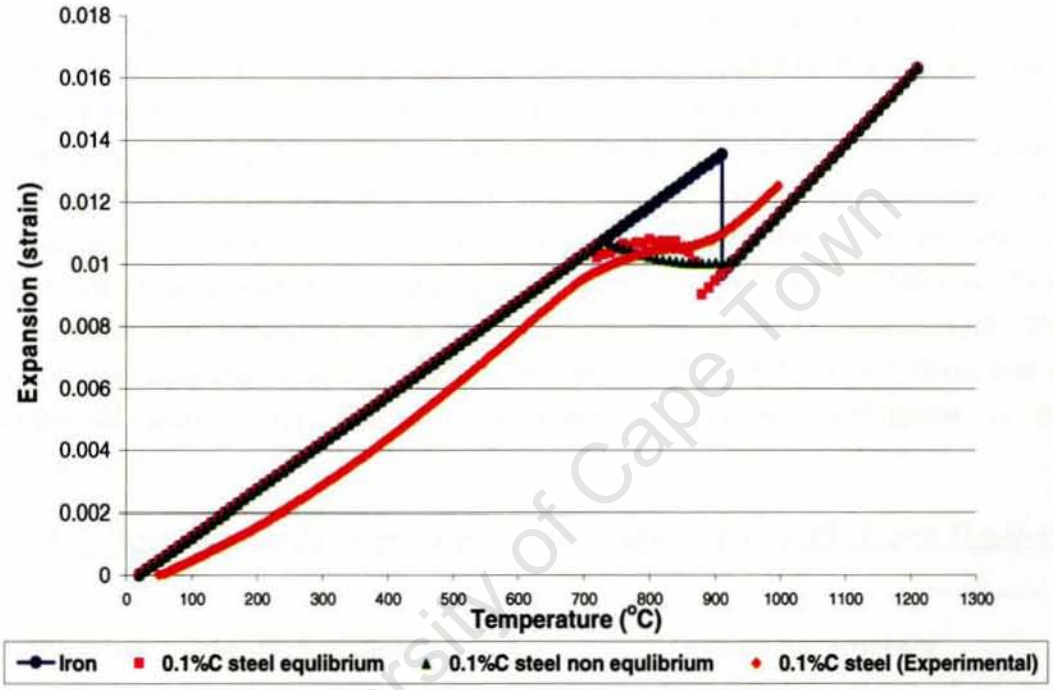

Figure 4.4: *Expansion behaviour of Iron, 0.1wt% steel at equilibrium and non equilibrium conditions (theoretical) and experimental*

The model for iron can further be extended to the addition of 0.1wt% C, assuming equilibrium conditions by using the phase diagram of Fe-C (Figure 4.3) to calculate incremental compositions of α and γ at 0.1wt% C, as shown in Figure 4.4. This graph shows a temperature range for the length/volume transition, which corresponds to the equivalent field in the equilibrium phase diagram.

A non-equilibrium case was modelled by assuming a linear increase of 0.005/°C in γ-phase from 723°C, as shown in Figure 4.4. Since one expects the departure from equilibrium during experiments, the latter curve gives some meaning to the inspection and interpretation of the experimental data.

The experimental result, which is for a 0.1wt% C steel heated to 1000°C (heating rate 1°C/min), is also shown in Figure 4.4.The expansion behavior approximates a similar

transformation temperature range depicted for the equilibrium and non-equilibrium cases, and thus reliably permits the transformation to be detected.

4.3 Testing procedure

4.3.1 Testing parameters of thermal cycles

In order to trace and compare the phase transformation behaviour of CP Ti and Ti-6Al-4V before, during and after hydrogenation, experiments in order to achieve this were formulated. Each thermal cycle signified a specific heat treatment with or without hydrogen. Cycle 0 was a dilatometry run is a neutral/vacuum environment. Cycles 1-4 were all were all performed on the same test specimen and followed each thermal cycle successively. The heating and cooling rate of 1°C/min was selected for all thermal cycles in order to obtain as much detail as possible in the dilatometric curves. An isothermal hold of 3 hours was selected for the hydrogenation and dehydrogenation steps to allow for maximum absorption and desorption of hydrogen respectively. The hydrogen used during experiments was a 15%H-85%Ar mix. Table 4.4 describes the various thermal cycles in vacuum or H_2/Ar environment. This sequence of experiments was performed on both CP Ti and Ti-6Al-4V. Note that all experiments were repeated thrice in order to establish confidence in the reproducibility.

Table 4.4: Thermal cycle designation and testing parameters for CP Ti and Ti-6Al-4V

Thermal cycle designation	Testing parameters
Cycle 0 Single step on annealed material	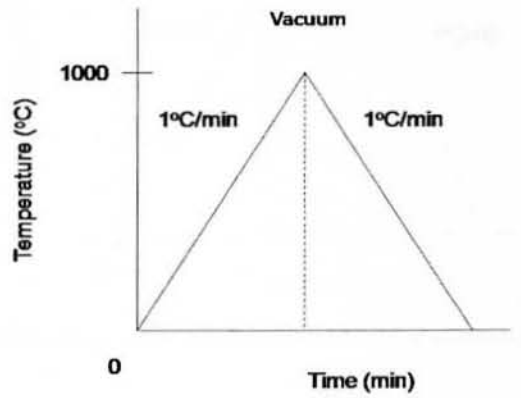

Cycle 1 Hydrogenation step	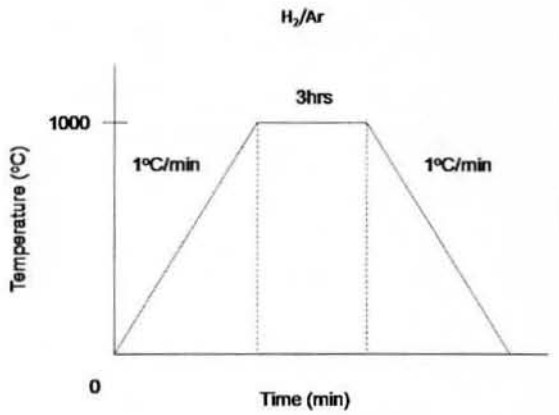
Cycle 2 (Post-hydrogenation step)	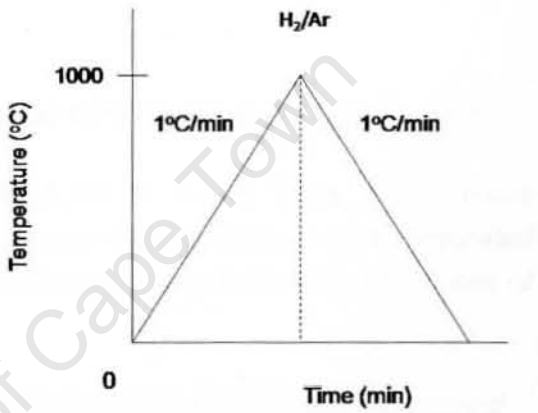
Cycle 3 (Dehydrogenation step)	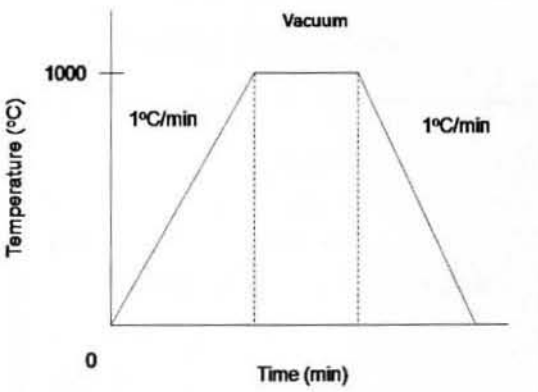

Cycle 4 (Post-dehydrogenation step)	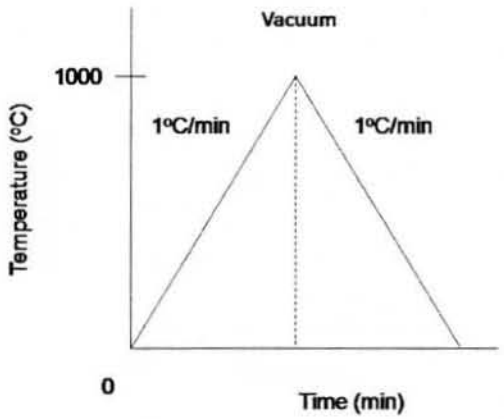

4.3.2 Additional quenched treatments for CP Titanium during Cycle 1

In order to monitor phase transformations of CP Ti during Cycle 1 at various temperatures during heating and cooling, water quench experiments were formulated and is described in Table 4.5, whereby Cycle 1 was interrupted at temperatures of interest and water quenched.

Table 4.5: Thermal cycle designation and testing parameters for CP Ti quenched experiments

Thermal cycle designation	Testing parameters
325°C quench at cooling	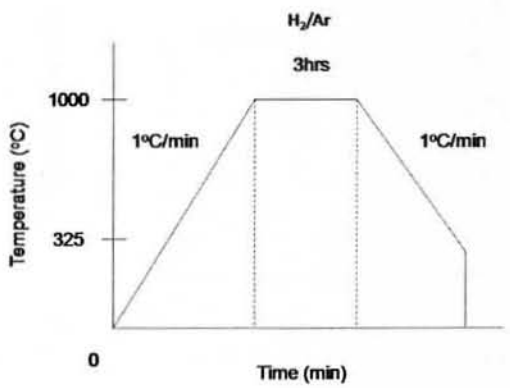

750°C quench	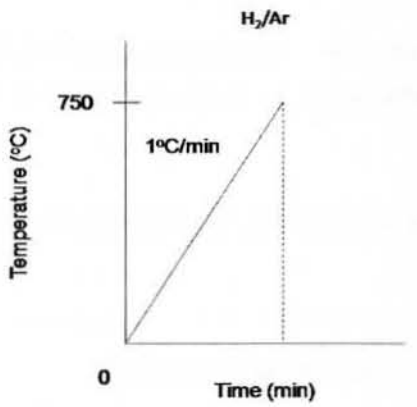
825°C quench	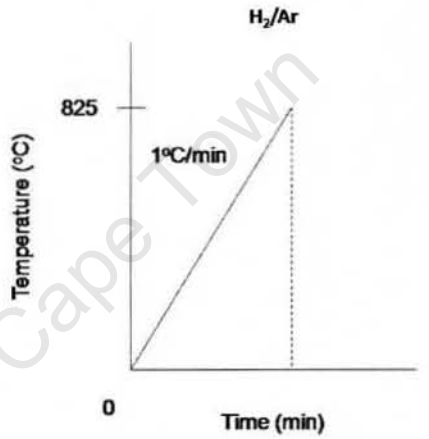
940°C quench	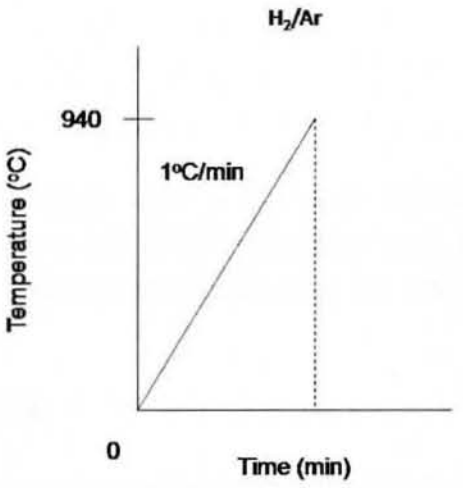

4.3.3 Additional quenched treatments for Ti-6Al-4V during Cycle 1

In order to monitor phase transformations of Ti-6Al-4V during Cycle 1, the specimen heated to 1000°C was water quenched at this temperature. Table 4.6 describes the testing parameters.

Table 4.6: Thermal cycle designation and testing parameters for Ti-6Al-4V quenched at 1000°C

Thermal cycle designation	Testing parameters
1000°C quench	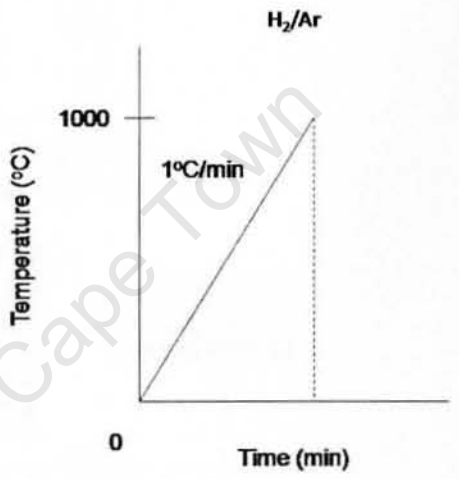

4.4 Microscopy analysis

4.4.1 Light microscopy

The microscope used for microstructural analysis was a *Reichert MeF3 A* microscope fitted with a *Leica DCF 320* camera and *Leica DCF* acquisition software. The bright field mode was used to examine the microstructures after the various thermal cycles.

4.4.2 Scanning electron microscopy (SEM)

The microstructures after specific thermal cycles were examined using the *FEI Nano FEGSEM 230* scanning electron microscope. The SEM was used to observe the morphology of the specimens. The region of interest was captured before and after EBSD scanning and an overlay of the SEM and EBSD images were obtained.

4.4.3 Electron Back Scatter Diffraction (EBSD)

Electron Back Scatter Diffraction (EBSD) is an application in the scanning electron microscope (SEM), which can be used to obtain crystallographic information and quantitative analysis of grain and sub grain structures [**59**]. In EBSD a stationary electron beam strikes the crystalline sample, which is tilted at 70° and the diffracted electrons form a pattern on a fluorescent (phosphor) screen as shown in Figure 4.5. This pattern, as shown in Figure 4.6 consists of Kikuchi bands, whereby the bands intersect each other. The sample has to be well prepared, free of surface damage (mirror shine) in order to achieve indexing of all points and accurate indexing, which is achieved by assigning indices to the Kikuchi bands [**60**].

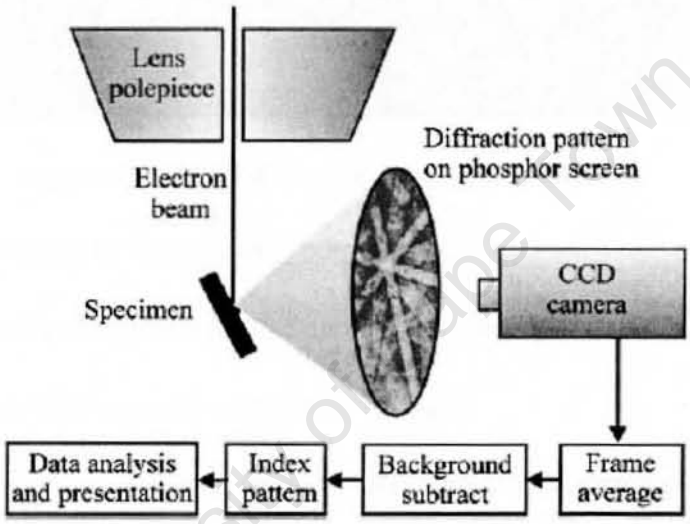

Figure 4.5: *Set up of an EBSD unit*

Each pattern is characteristic of the crystal structure and orientation of the sample region from which it was generated. The diffraction pattern can be used to measure the crystal orientation, measure grain boundary misorientations. When the beam is scanned in a grid across a polycrystalline sample and the crystal orientation measured at each point, the resulting map will reveal the constituent grain morphology, orientations, and boundaries. This data can also be used to show the preferred crystal orientations (texture) present in the material. A complete and quantitative representation of the sample microstructure can be established with EBSD [**60**]. For the purpose of this research EBSD was used for quantitative phase analysis, which was useful in tracing phase transformations during various thermal cycles.

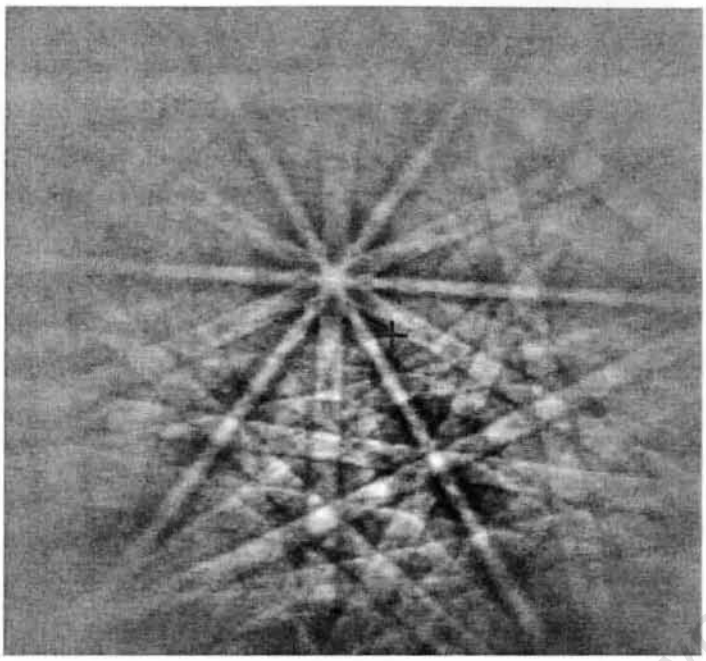

Figure 4.6: *An EBSD pattern showing Kikuchi bands*

The EBSD unit consists of the following components:

- *FEI Nova Nano FEGSEM 230* Scanning Electron Microscope
- Oxford Instruments solid state EBSD detector
- A camera used to view the diffraction pattern on the phosphor screen
- Hardware that controls the SEM, including the beam position, stage, focus, and magnification
- A computer with *Oxford HKL CHANNEL 5 Flamenco software*, for controlling of EBSD experiments, data acquisition and for analysing and solving diffraction patterns

Various regions in the test specimens were selected for EBSD analysis for qualitative and quantitative phase analysis. A beam intensity of 20kV was used with a working distance of 16mm. Maps were 250x250, 600x600 and 700x700μm in size depending on the area of interest. Step size ranged from 0.2-1μm to ensure a good quality and high resolution EBSD map.

4.4.4 Specimen preparation

After each cycle of treatment for both CP Ti and Ti-6Al-4V, the oxide scale was removed by using 800μm SiC grit paper. Thereafter cross sections of 5mm were cut from the 44mm rod test specimen using a precision cutting machine and then

mounted in carbon based hot mounting resin using a *Struers LaboPress-3* Hot Mounting machine. The specimens were then ground and polished, using a *Struers Rotopol-22* Automatic polisher, fitted with a *Struers RotoForce-4*, with samples inserted in the single sample holder. Table 4.7 outlines the grinding and polishing procedure to acquire a mirror shine finish for light microscopy, SEM and EBSD analysis.

EBSD is very sensitive to crystalline perfection and sample preparation may be needed to remove any surface damage. A well prepared sample is a prerequisite to obtaining a good diffraction pattern. Surfaces must be sufficiently smooth to avoid forming shadows on the diffraction pattern from other parts of the sample

Table 4.7: Polishing technique for CP Ti and Ti-6Al-4V

Grit/cloth	Lubricant	RPM	Force	Time (min)
800 SiC grit	Water	300	30	2:00
MD Dac 9μm	9μm lubricant and suspension in one	150	20	10:00
MD Nap	OP-Nap colloidal silica	150	20	10:00
MD Nap	Water and dishwashing detergent	150	20	10:00

For Ti-6Al-4V, Kroll's reagent (100ml distilled water, 4ml HNO_3 and 2ml HF) was used to etch the specimens for observation under the light microscope. For CP Ti Keller's reagent (95ml distilled water, 2.5ml HNO_3, 1ml HF and 1.5ml HCl) was used as the etching reagent. After etching, the specimens were thoroughly rinsed with distilled water in order to remove any traces of HF, which is detrimental to the lens of the optical microscope.

The 5mm discs were then mounted on an aluminium stub with conductive Ag-DAG and allowed to set for two hours before usage for EBSD analysis.

5 RESULTS AND DISCUSSION

This chapter deals with the results and discussion of the experiments that are described in Chapter 4. The results and discussion follows a similar format to the experimental procedure.

5.1 Expansion of α and β phases in CP titanium

The volume per atom for the α and β phases were modelled as a function of temperature and is shown in Figure 5.1a. From Figure 5.1a, it is seen that the volume per atom for the α–phase below 1050°C would always be greater than the volume per atom for the β–phase. This implies that the transformation from the α to β phase would always result in a volume contraction during heating up to 1050°C. Beyond 1050°C the volume per atom of the β-phase is greater than the volume per atom of the α-phase.

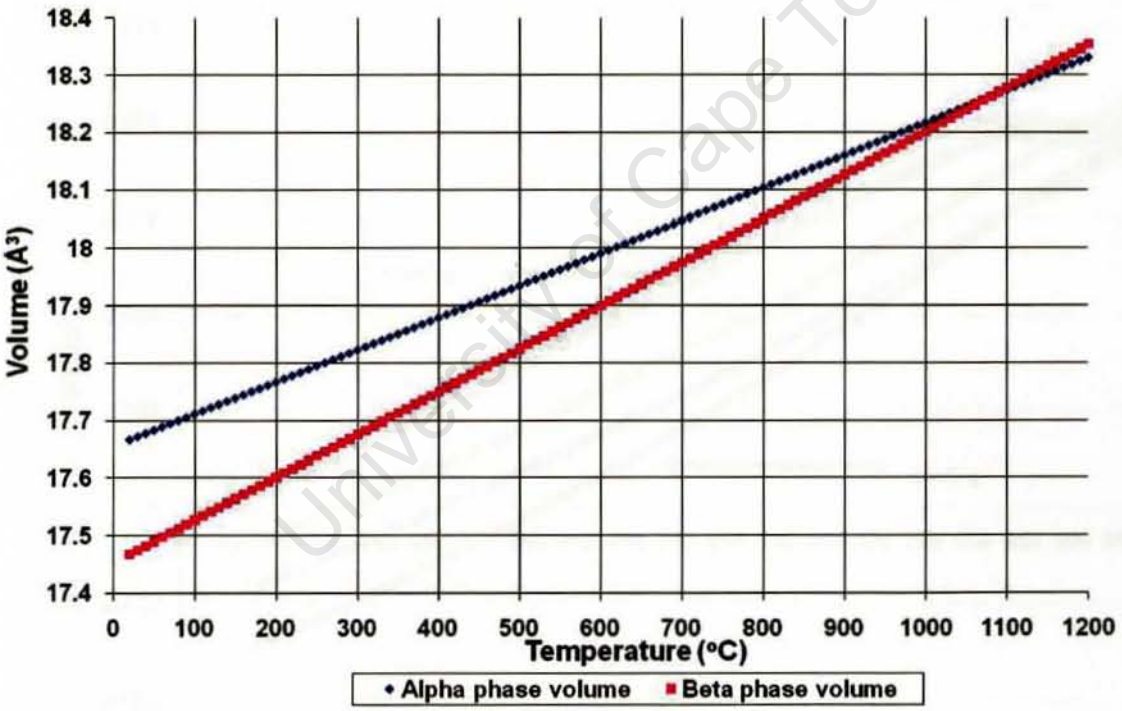

Figure 5.1: *a)Modelled volume of α and β phases (per atom) as a function of temperature for CP Ti*

5.2 CP Ti during heating and cooling

The strain and COTE vs. temperature curves for the following thermal cycles are plotted on the same set of axes: Cycles 0-2, Cycles 2-4 and Cycles 0 and 4. Comparisons between each thermal cycle during heating and cooling are made in

order to monitor the phase transformation behaviour of CP Ti before, during and after hydrogenation.

Cycle 0 is the heating and cooling of the metal in vacuum. Cycle 1 is the hydrogenation step, Cycle 2 the post-hydrogenation step (in hydrogen environment), Cycle 3 the dehydrogenation step and Cycle 4 the post-dehydrogenation step. Cycles 1-4 were performed consecutively (See Section 4.3).

The heating and cooling of CP Ti in vacuum experiment (Cycle 0) was repeated thrice in order to display confidence in the reproducibility of the data output from the dilatometer, as shown in Figure 5.2. The curves for Test 1, 2 and 3 in Figure 5.2 displays a similar shape and behaviour, with very little difference. The heating and cooling of CP Ti (Cycle 0) will be discussed further on. From Figure 5.2 it is clear that the push-rod dilatometer was able to output reliable data. All other experiments (for both CP Ti and Ti-6Al-4V) were also repeated thrice and a similar confidence in the reproducibility of the data output was also established.

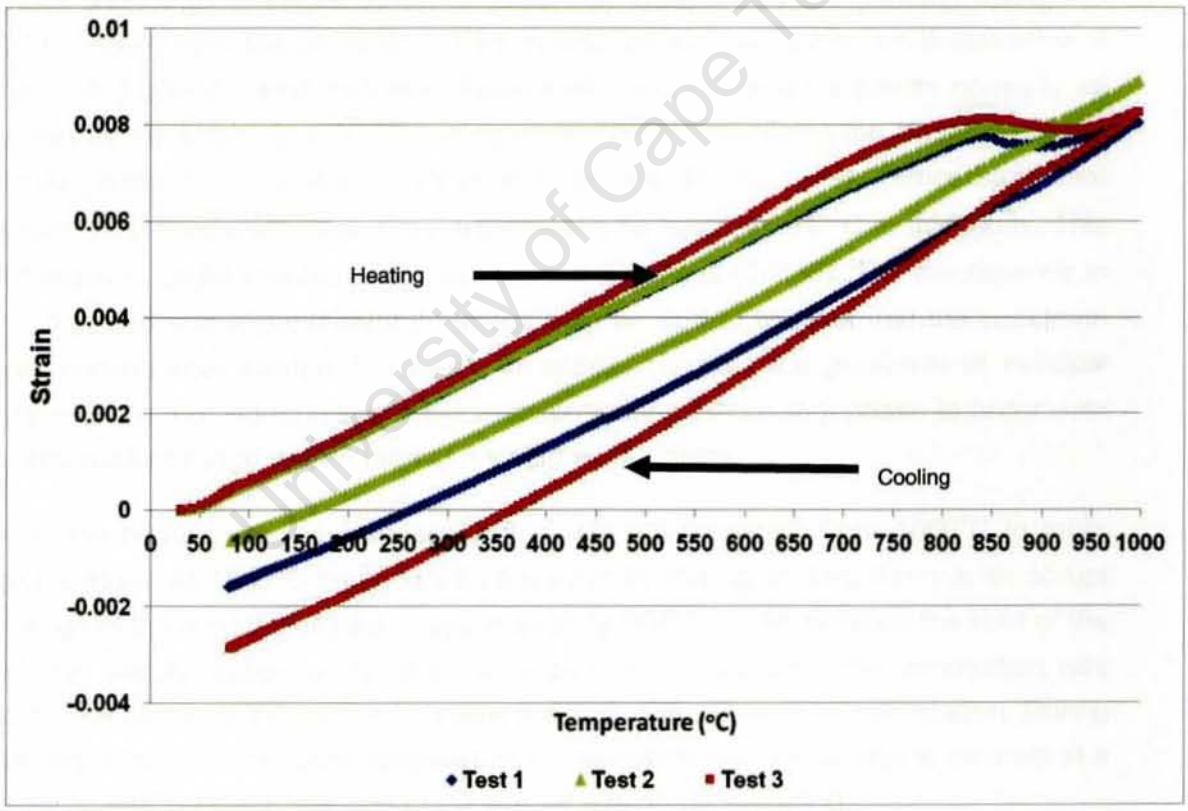

Figure 5.2: *CP Ti heated to 1000°C, heating and cooling rate 1°C/min, repeated thrice (Tests 1, 2 and 3) to illustrate reproducibility of the dilatometry technique.*

5.2.1 Cycles 0-2

This section refers to Figures 5.3 and 5.5, for the strain and COTE curves of Cycles 0, 1 and 2 during heating and cooling respectively.

The phase transformation behaviour for CP Ti is reported for the three conditions in this section, i.e. Cycle 0, 1 and 2. Cycle 0 aims to serve as a benchmark for Cycles 1-4, in order to monitor the influence of hydrogen on CP Ti.

The specimen in Cycle 0 expands from room temperature to 600°C at a constant rate of expansion due to the normal thermal effects during heating, which can be seen by the strain and COTE curves (See Figure 5.3). From 600-800°C, the specimen continues to expand, but at a slightly decreased rate of expansion as shown by the strain and COTE curves. This is not likely to coincide with a phase transformation, since early transformation from 600°C was unexpected. This is because an unalloyed metal i.e. CP Ti should display a single temperature below which everything should be α-phase and above this temperature everything should be β-phase viz. β-transus (883°C).

The α to β phase transformation is expected to accompany a volume contraction, since the volume per atom of the α phase is larger than the volume per atom of the β phase as shown in Figure 5.1. The specimen experienced a significant change in COTE values from the 800-940°C. This associated volume contraction is indicative of the α to β phase transformation. From 940°C the specimen expands normally as shown by the strain and COTE curves up to 1000°C, signifying the existence of the single phase β. Since the β-transus is described as the lowest temperature that maximum β-phase will exist, the β-transus can be taken as 940°C in this study. This β-transus is slightly higher than the reported β-transus (883°C). The discrepancy in the reported and experimental β-transus may be due to the fact that the specimen was continuously heated (1°C/min). In addition to this, the presence of residual elements i.e. Fe, would result in the transformation of the α to β phase to occur over a temperature range, rather than at a single temperature.

After the heating step, the specimen in Cycle 0 was cooled from 1000°C to room temperature. At 1000°C the single β-phase exists. During cooling, there is an abrupt change in the contraction rate at approximately 860°C, which signifies the start of the reverse transformation of the β to α-phase (See Figure 5.5). The contraction rate stabilizes below 780°C, which indicates the end of the reverse transformation. During cooling from 780°C to room temperature the specimen then continues to contract at a more or less constant rate due to the normal effects upon cooling.

Cycle 1 is the hydrogenation thermal cycle. This thermal cycle should consist of the α-phase at the start of Cycle 1. The specimen in Cycle 1 deviates slightly from Cycle 0 at 400°C. The solubility of hydrogen in the α-phase is relatively low in comparison to the solubility in the β-phase. However, hydrogen can increase the lattice parameter of the α-phase from 400°C onwards. From 400-550°C the rate of

expansion shows a slight increase as shown in Figure 5.3, which can thus be attributed to the increase in the lattice parameter of the α-phase [**61**].

The progression of the phase transformations in CP Ti with the addition of hydrogen, can be traced using the Ti-H phase diagram (See Figure 5.4), coupled with the use of dilatometry. The specimen in Cycle 1 deviates significantly from Cycle 0 at 550°C. At temperatures below 550°C, the uptake of hydrogen is relatively low, and above 550°C the uptake of hydrogen occurs more rapidly [**41**]. Hence, point *A* in Figure 5.4 signifies the start of hydrogen uptake. From 550-750°C, the specimen continues to expand, but the rate of expansion increases and then decreases after 750°C. This rise in the COTE values (See Figure 5.3) can be attributed to the increase in hydrogen uptake, whereby the solid solution of hydrogen occurs in the α-phase. The path along point *A* to *B*, in Figure 5.4 shows this increase in the hydrogen dissolution up to 750°C. From approximately 750°C, the specimen continues to expand but at a decreasing rate of expansion, which signals the α to β phase transformation. The rate of expansion increases thereafter. The path from point *B* to *C* in Figure 5.4 marks this transformation. It is difficult to identify the β-transus, since hydrogen will continue to dissolve and expand the β-phase. However, the β-transus should definitely be below the value for the vacuum cycle (Cycle 0) and is possibly in the vicinity of 875°C.

Above 875°C, the specimen is in the β-phase field. The specimen continues to expand but at an increasing rate and then the rate decreases above 940°C. The increase in the COTE values can be attributed to the absorption of hydrogen in the β-phase, which results in an increase in the lattice parameter of the β-phase. When heating from 940-1000°C, the decrease in expansion rate (as shown in the strain and COTE curves for Cycle 1) may be due to two reasons. One of the reasons may be that from point *D* (940°C) in the Figure 5.4, an increase in temperature results in the specimen moving along the (βTi)/(βTi)+G boundary, which would result in the loss of hydrogen gas from the specimen. The second reason may be that the increase in the rate of expansion (COTE values) caused by hydrogen absorption slows down as the rate of hydrogen absorption reaches saturation. Thus, there is an apparent decrease in the COTE values as the temperature rises.

Assuming that equilibrium was not achieved, the points plotted to form the curve extending from *A* to *E* in Figure 5.4, represents the maximum transformation temperatures. Hence, it is reasonable to indicate a shaded region (±50-75°C) below this curve (See Figure 5.3), which indicates the broader possible hydrogen uptake behaviour as a function of temperature and heating rate.

In Cycle 0 the α to β phase transformation occurred from 800-940°C, but the addition of hydrogen is known to lower the α to β transformation temperature. This lowering of

the transformation temperature can be seen from 750-875°C in Cycle 1, whereby the rate of expansion changes as shown by the strain and COTE curves signifying this phase transformation.

The proposed sequence of phase transformations for Cycle 1 during heating can be summarized as follows:

$$\alpha \rightarrow \alpha_H \rightarrow \alpha_H + \beta_H \rightarrow \beta_H \rightarrow \beta_H + (G)$$

Where α_H and β_H represent hydrogen in solid solution in the α and β phases respectively and G is hydrogen gas.

After the end of the heating step in Cycle 1, the specimen at 1000°C is in the β-phase field. During cooling from 1000°C to 750°C, the specimen in Cycle 1 experiences a continuous change in the COTE values, with the rate of contraction decreasing then increasing (See Figure 5.5). This change in the COTE values can be attributed to the increase in the uptake of hydrogen in the β-phase, and follows a path from point *A* to *B* as shown in Figure 5.6.

During cooling from 750°C to 300°C, the specimen in Cycle 1 exhibits a very gradual decrease in the contraction rate as shown by the strain and COTE curves. This suggests that no additional hydrogen uptake (or at least very little) occurred in this temperature interval. The progression from point *B* to *C* thus occurs, as shown in Figure 5.6, which indicates a relatively small change in hydrogen uptake during cooling over the relevant interval.

At 300°C, the specimen in Cycle 1 once again deviates from Cycle 0. During cooling from 300°C to 220°C a continuous change in the contraction rate is observed and a volume expansion is seen when cooling from 275°C to 250°C. These changes can be attributed to the eutectoid transformation of the β_H to α_H+hydride phase transformation, as shown by the path from point *C* to *D* in Figure 5.6. This eutectoid transformation occurs in the shaded region (40-44at%H), as shown in Figure 5.6. Hydrogen is able to lower the β–transus of CP Ti to ~300°C as seen by the Ti-H phase diagram. From 220°C to room temperature the COTE values remained more or less constant, signifying that the β to α+hydride phase transformation was complete. The final phases present after the completion of Cycle 1 (heating and cooling) was a mixture of the α+hydride phases.

The proposed sequence of phase transformations for Cycle 1 during cooling can be summarised as follows:

$$\beta_H \rightarrow \alpha_H + hydride$$

During heating, Cycle 2 does not exhibit the same trend as Cycle 1 (See Figure 5.3). At the start of Cycle 2 (after the completion of Cycle 1), the specimen contained both the α and hydride phases, as predicted by the Ti-H phase diagram and hydrogen in solid solution. The indications are that the rate of hydrogen dissolution in Cycle 2 is lower than in Cycle 1, since the strain curve of Cycle 2 is displaced below the strain curve of Cycle 1 (See Figure 5.3).

From 250-290°C the specimen continues to expand as shown by the strain curve, but at a decreased rate as shown by the COTE curve. From 300-350°C a volume contraction is seen. This change in the COTE values can be attributed to the α+hydride to β phase transformation. The same phase transformation was also seen during cooling in Cycle 1 (Figure 5.5). This eutectoid transformation occurs in the shaded region (40-44at%H), as shown in Figure 5.7, and follows the path from point *A* to *B* as shown in Figure 5.6. According to Figure 5.7, hydrogen is able to lower the β-transus to 300°C. Once this hydrogen induced phase transformation is complete, from 350-750°C the trend is similar to that of Cycles 0 and 1, whereby the specimen continues to expand at a more or less constant rate. This is due to little or no additional uptake of hydrogen as shown in Figure 5.7 (the path followed from point *B* to *C*).

From 750-850°C, the specimen continues to expand and the rate of expansion increases and reaches a maximum at 850°C. This change in the COTE values can be attributed to an increase in the uptake of hydrogen, as shown in Figure 5.7, from point *C* to *D*. Beyond 850°C the specimen continues to expand but the rate of expansion decreases. This decrease in the rate of expansion is associated with the loss of hydrogen from the specimen, which is indicated by the path from point *D* to *E* in Figure 5.7. At the end of the heating step, the specimen contains approximately 40at%H.

The proposed phase transformation sequence for Cycle 2 during heating can be summarised as follows:

$$\alpha_{II} + hydride \rightarrow \beta_{II} \rightarrow \beta_{II} + (G)$$

After heating in Cycle 2, the specimen at 1000°C is in the β-phase field. When cooling from 1000°C to 700°C, the specimen experiences a continuous change in the COTE values, with the rate of contraction decreasing and then increasing. This change in COTE values can be attributed to the increase in the uptake of hydrogen in the β-phase and follows a path from point *A* to *B*, as shown in Figure 5.8.

During cooling from 700°C to 300°C, a very gradual decrease in the contraction rate is observed as shown in Figure 5.8. This suggests that no additional hydrogen (or at least very little) occurred in this temperature interval. The progression from point *B* to

C thus occurs as shown in Figure 5.8, which indicates a small change in hydrogen uptake during cooling over the relevant interval.

During cooling from 300°C to 220°C in Cycle 2, a continuous change in the contraction rate is observed and a volume contraction is seen cooling from 275°C to 250°C. These changes can be attributed due to the β to α+hydride phase transformation, as shown in Figure 5.8 (path followed from point *C* to *D*). Hydrogen thus lowered the β–transus to this temperature. From 220°C to room temperature the COTE values remained more or less constant signifying that the β to α+hydride phase transformation was complete. The final phases present after the completion of Cycle 2 (heating and cooling) was a mixture of the α+hydride phases.

The proposed phase transformation sequence for Cycle 2 during cooling can be summarised as follows:

$$\beta_{II} \rightarrow \alpha_{II} + hydride$$

The strain curve for the Cycle 2 during cooling is displaced below the strain curve of Cycle 1 during cooling as shown in Figure 5.5. This is as a result of the different initial lengths l_o of the specimens values for each thermal cycle (See Figure 5.5). For Cycle 1 the final length l_f is greater than l_o. This suggests that the rate of hydrogen absorption in Cycle 1 was greater than that of Cycle 2. This was due to the prior existence of hydrogen at the start of Cycle 2.

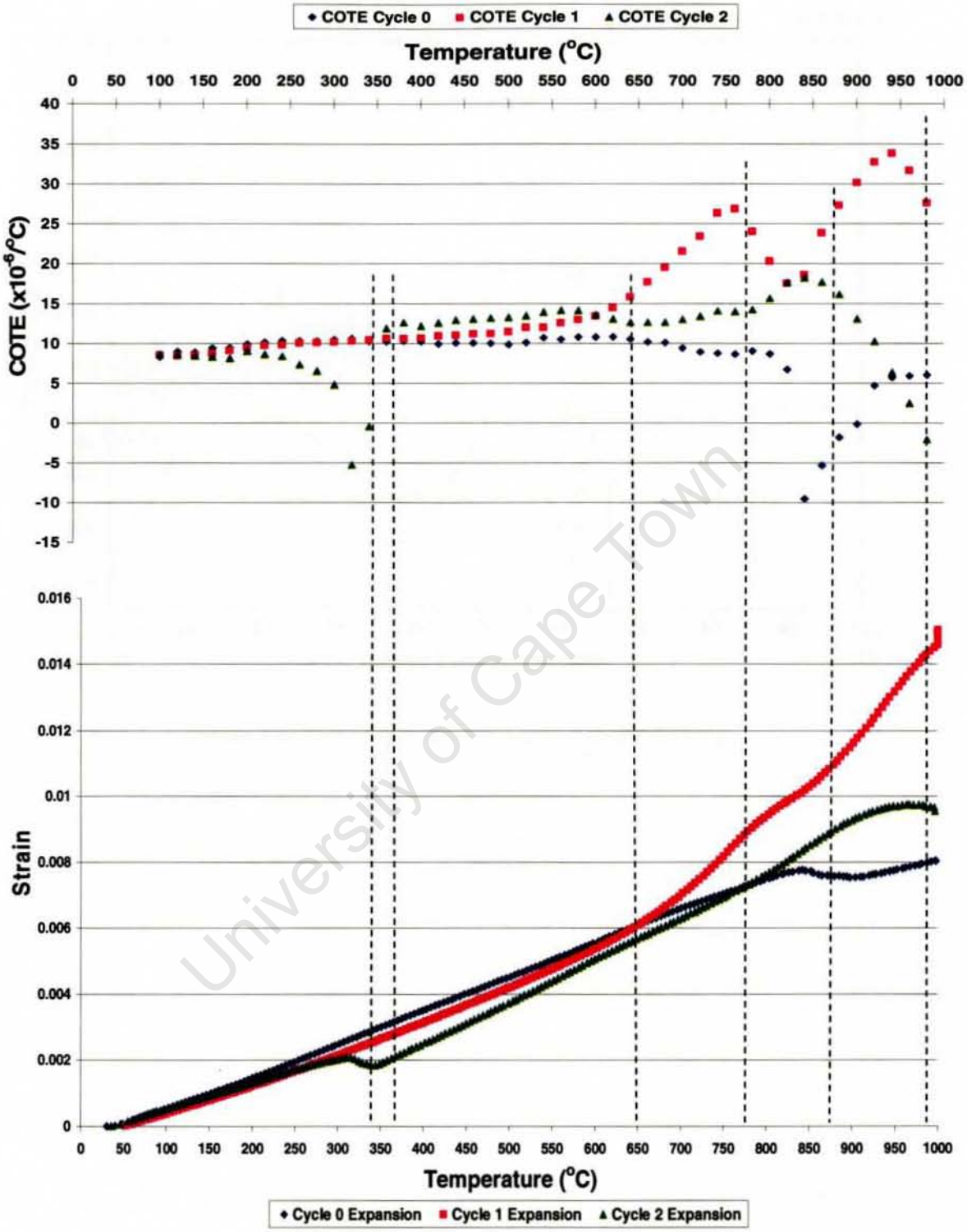

Figure 5.3: *Plot of Strain and COTE vs. temperature, Cycles 0-2, during heating of CP Ti*

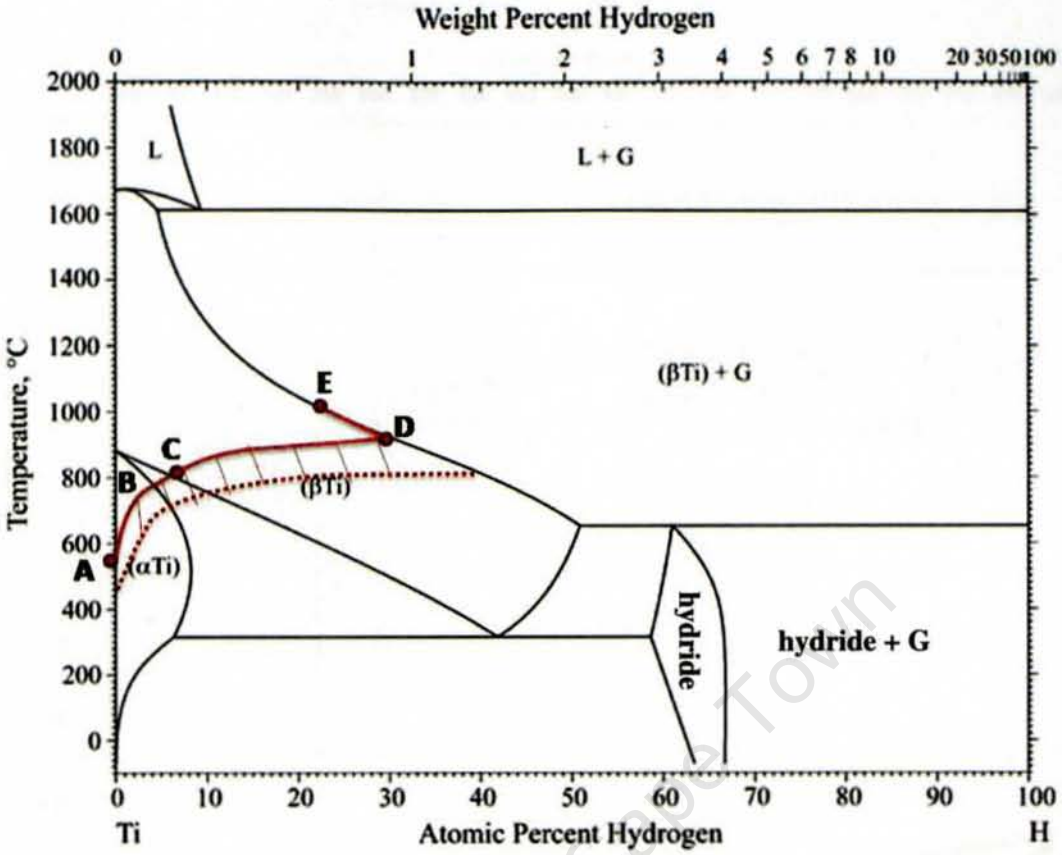

Figure 5.4: *Ti-H phase diagram: Cycle 1 during heating*

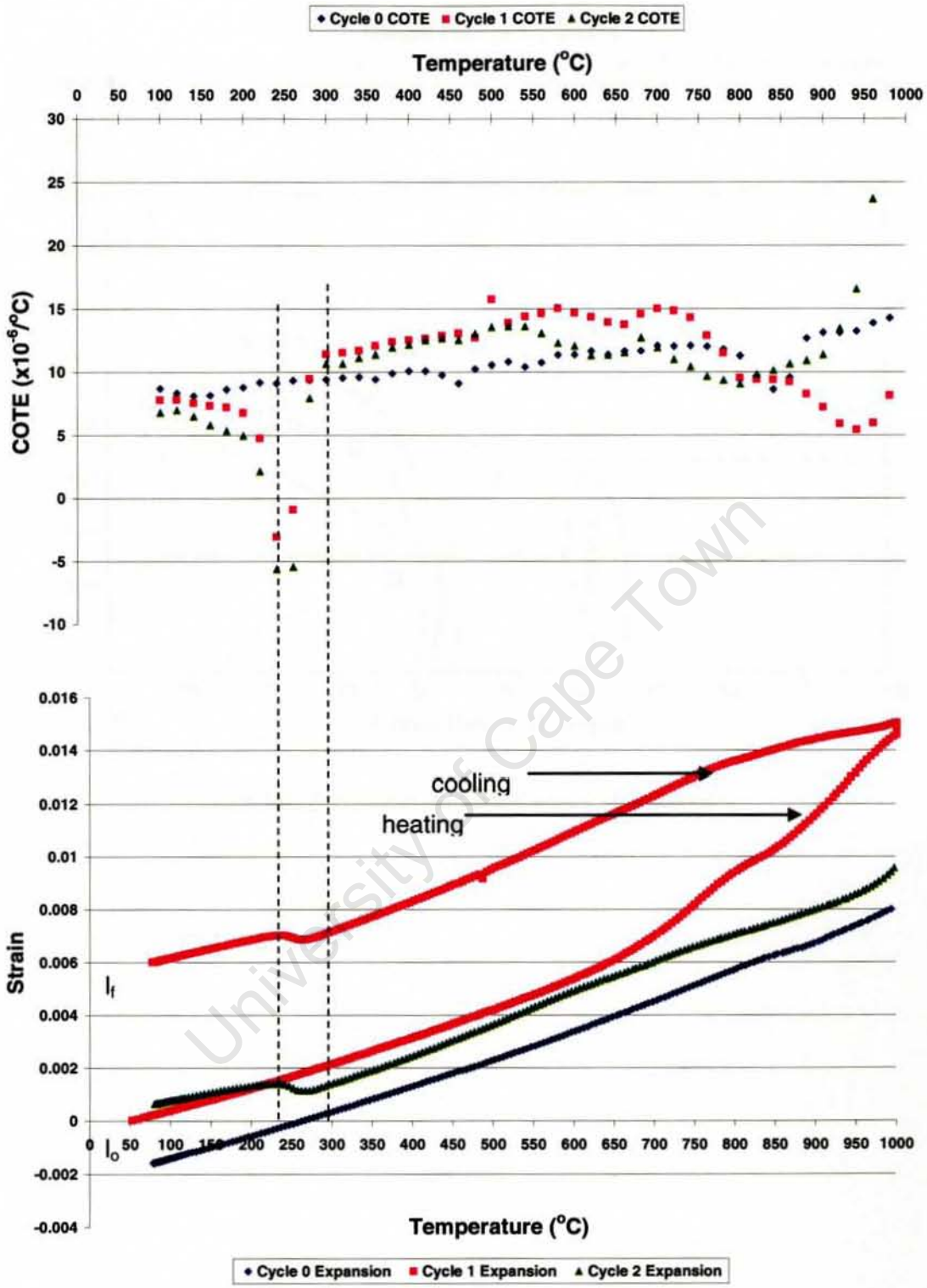

Figure 5.5: *Plot of Strain and COTE vs. temperature, Cycle 0, 1 and 2 during cooling of CP Ti*

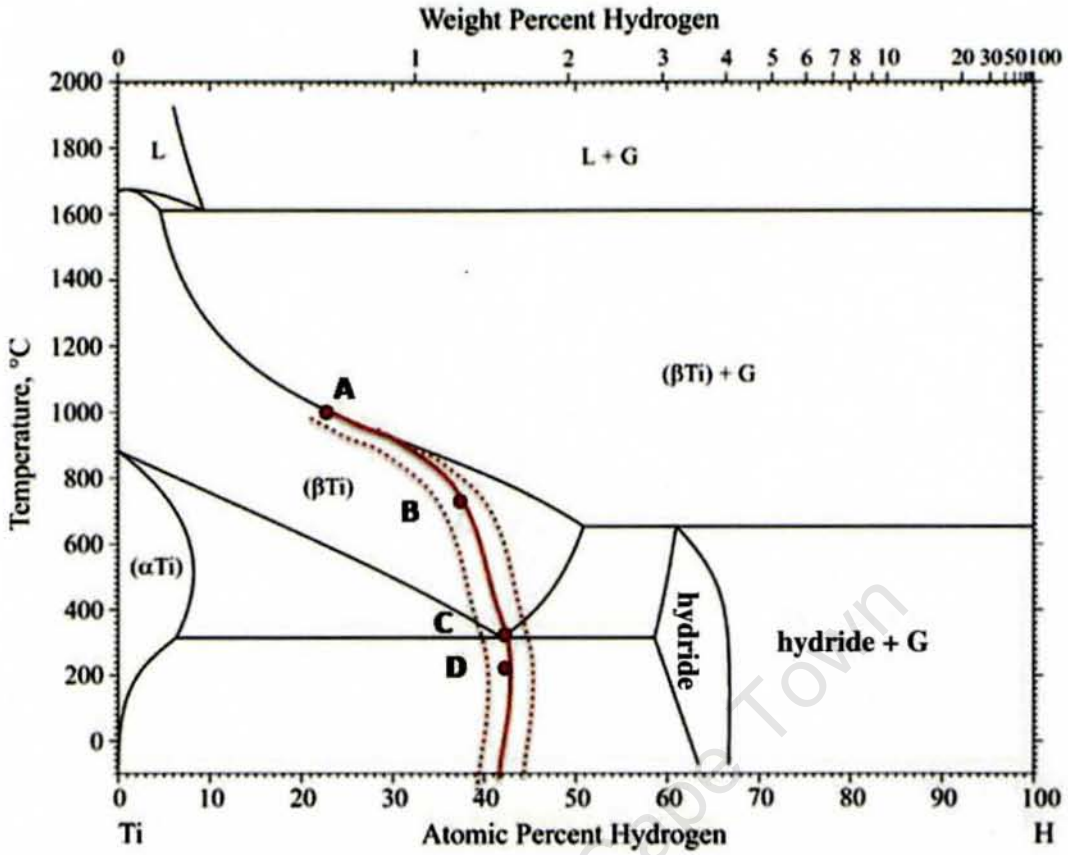

Figure 5.6: *Ti-H phase diagram: Cycle 1 during cooling*

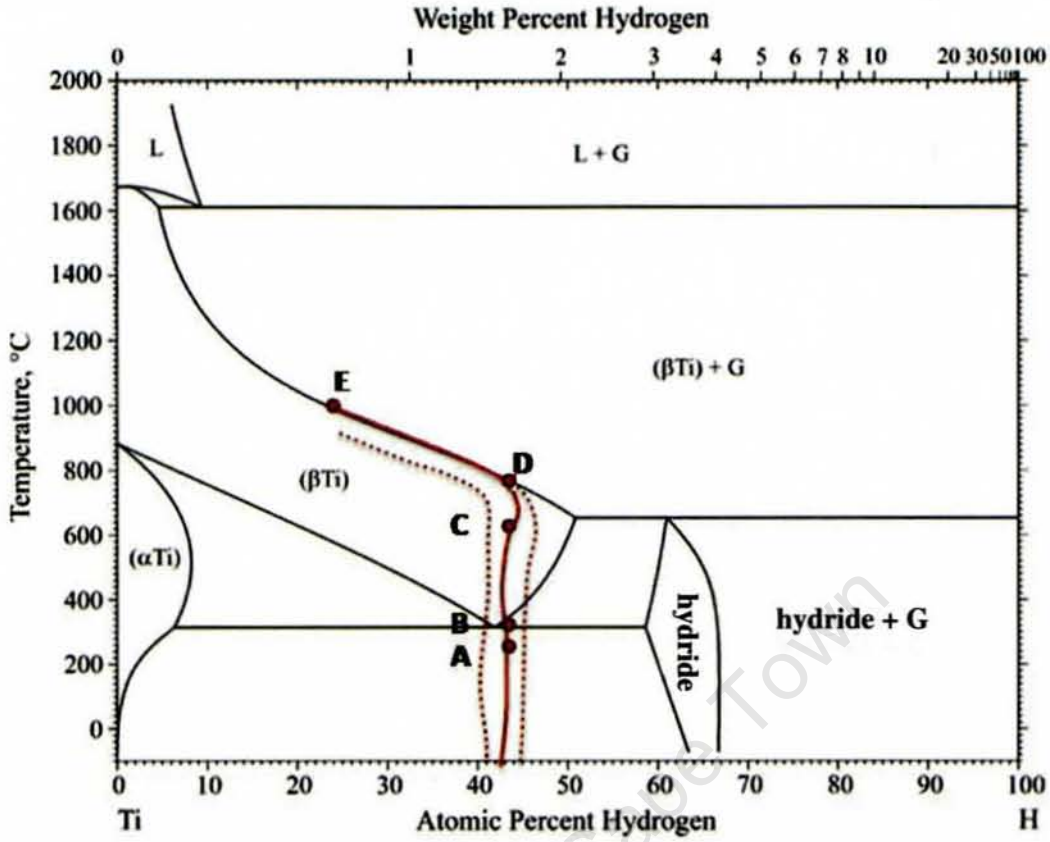

Figure 5.7: *Ti-H phase diagram: Cycle 2 during heating*

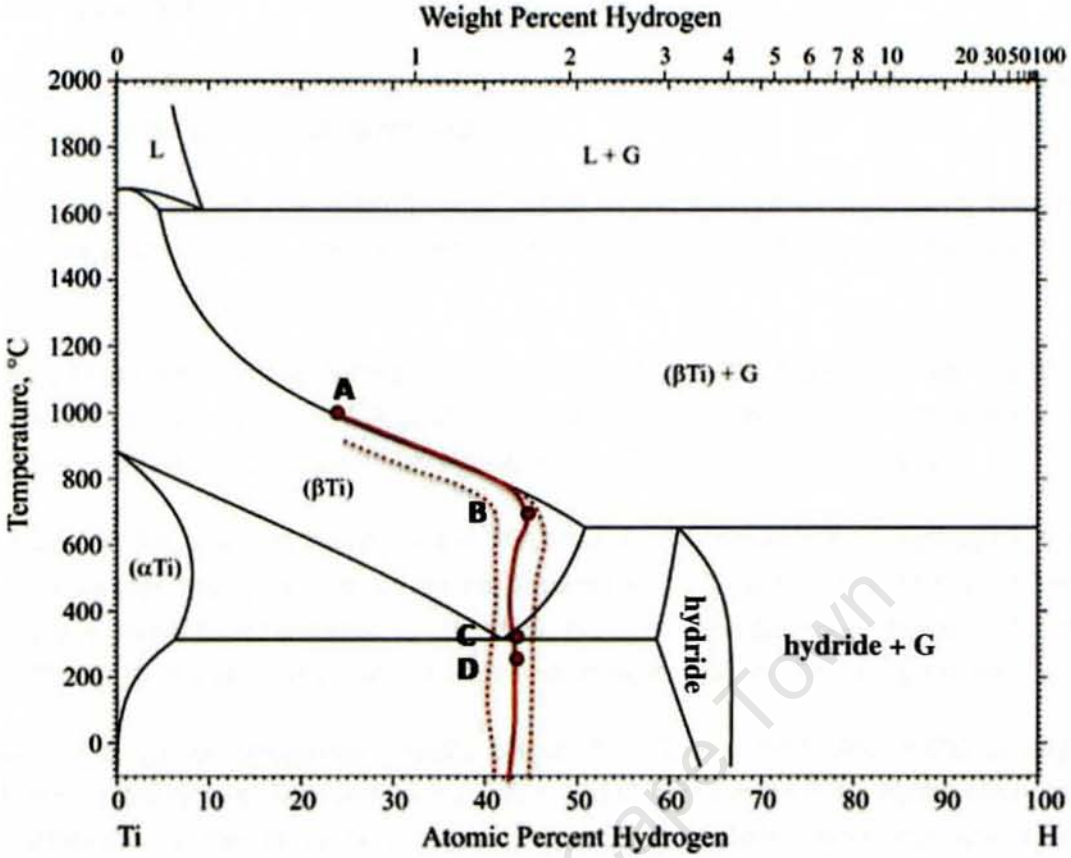

Figure 5.8: *Ti-H phase diagram: Cycle 2 during cooling*

5.2.2 Cycles 2-4

This section refers to Figures 5.9 and 5.10, for the strain and COTE curves of Cycles 2-4 during heating and cooling respectively.

Cycle 3 is the dehydrogenation thermal cycle. At the start of Cycle 3 (after heating and cooling in Cycle 2), the phases present are α and hydrides, with hydrogen in solid solution in the α-phase.

During heating from room temperature to 650°C, Cycle 3 exhibits a similar trend to Cycle 2, as shown in Figure 5.9 for the strain and COTE curves. This is not surprising since both thermal cycles start with similar a mix of α_H and hydride phases.

In spite of the vacuum environment in Cycle 3, the presence of hydrogen and hydrides within the specimen lowers the β-transus to 300°C (as seen in Figure 5.4). Once this phase transformation is complete, the specimen continues to expand from 350-600°C at an almost constant rate, as shown by the strain and COTE curves.

The COTE values decreases rapidly above 750°C, and from 800-900°C a large volume contraction is indicated by the strain and COTE curves. This observation can be attributed to the large of amount of hydrogen escaping from the specimen, bearing in mind that after the completion of Cycle 2 the specimen contained ±40at%H. The levelling off of the COTE values at approximately 960°C, suggests that most of the hydrogen has been expelled by this stage.

The proposed phase transformation sequence for Cycle 3 during heating can be summarised as follows:

$$\alpha_H + hydride \rightarrow \beta_H \rightarrow \beta$$

After heating to 1000°C in Cycle 3, the specimen is in the β-phase field. At this stage, it is unclear as to whether all the hydrogen was removed or not during the heating step in Cycle 3. The specimen experienced a slight decrease in the contraction rate after cooling from 1000°C to 900°C. It is unclear whether or not this change can be attributed to the reverse β to α phase transformation, since the change is relatively minimal. If Cycle 3 is compared to Cycle 0, then this temperature range is very high for the β-phase decomposition reaction. Below 900°C, the specimen then gradually contracts and the contraction rate increases cooling from 880°C to approximately 750°C, as shown by the COTE curves due to normal contraction effects upon cooling.

Cycle 4 is the post dehydrogenation step. Cycle 4 should contain the α-phase and possibly residual hydrogen, with no hydride phases after the completion of Cycle 3.

Since a substantial amount of hydrogen was removed in Cycle 3, Cycle 4 does not display the early, hydrogen induced β-transus at 300°C, as seen in Cycles 2 and 3. From 250-840°C, the specimen continues to expand. The strain curve appears linear in this temperature interval, the rate of expansion being constant as shown by the strain and COTE curves. This suggests that no phase transformation occurs in this temperature interval. From 850-900°C, the specimen continues to expand, but the rate of expansion decreases slightly as shown by the COTE curve. It is unclear as to whether this can be attributed to the α to β phase transformation, since the change is very minor. The rate of expansion (COTE curve) remained relatively constant when heating from room temperature to 1000°C.

The trend of Cycle 4 is dissimilar to Cycles 2 and 3. In Cycle 3, hydride decomposition and the removal of hydrogen occurred in the 650-900°C temperature interval and if this occurred effectively, then little or no hydrogen or hydrides should be present at the start of Cycle 4. The deviation of Cycle 4 from Cycles 2 and 3 can be attributed to the absence of hydrides and the presence of far less hydrogen than in Cycles 2 and 3. If however, residual hydrogen remained after the completion of Cycle 3, then during heating of Cycle 4, hydrogen will continue to be expelled from the specimen. This may be the case in this study, which is preventing the identification of the $\alpha \rightarrow \beta \rightarrow \alpha$ transformation from the dilatometry data.

After heating to 1000°C in Cycle 4, the specimen should be in the β-phase field if no residual hydrogen was present. During cooling in Cycle 4, the rate of contraction does not change significantly as shown by the strain and COTE curves (See Figure 5.10). Hence, the β-transus could not be determined. It appears as if little or no phase transformation occurred during this thermal cycle. During the cooling step Cycle 4, exhibits a similar trend as Cycle 3 (cooling).

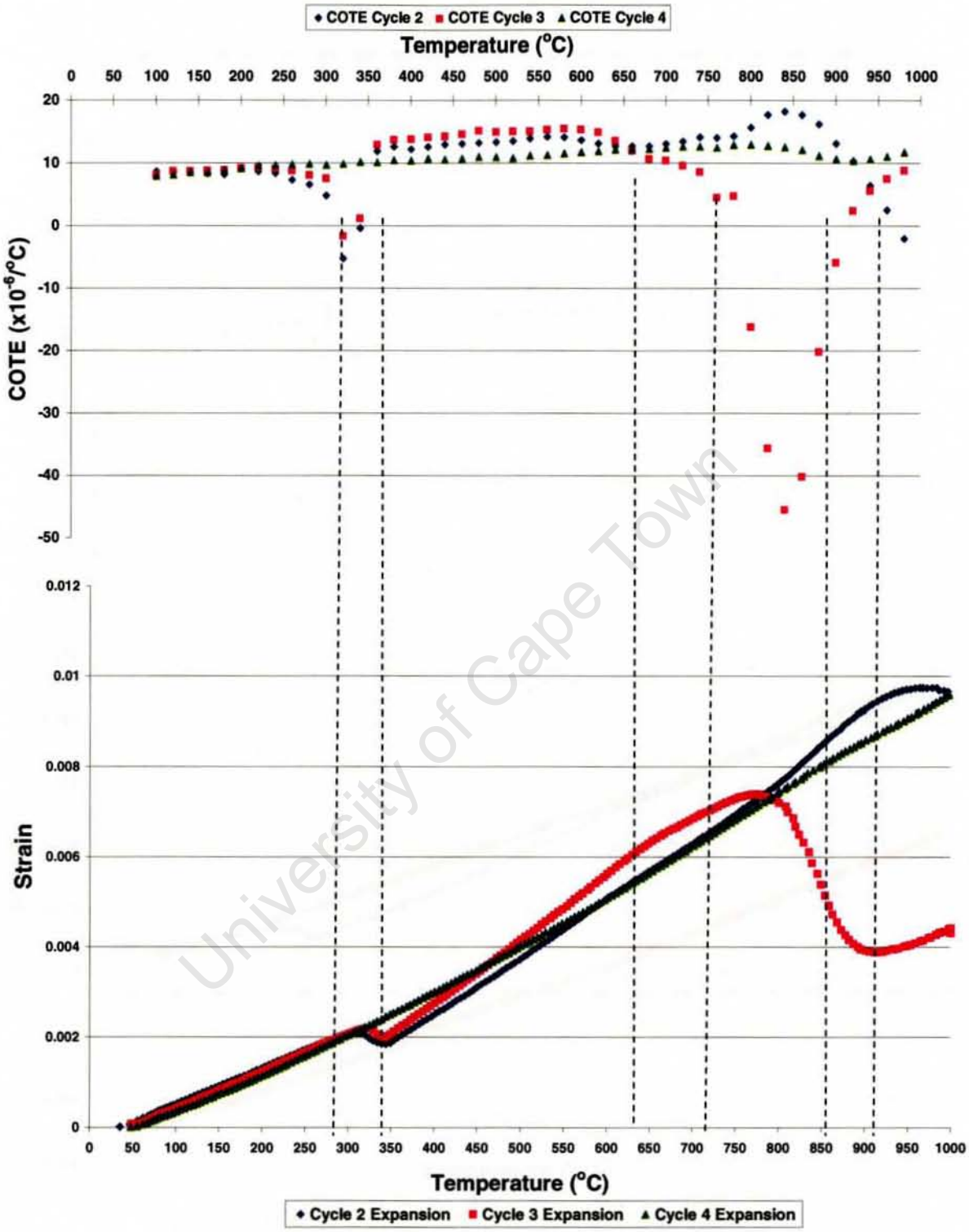

Figure 5.9: *Plot of Strain and COTE vs. temperature, Cycles 2-4, during heating of CP Ti*

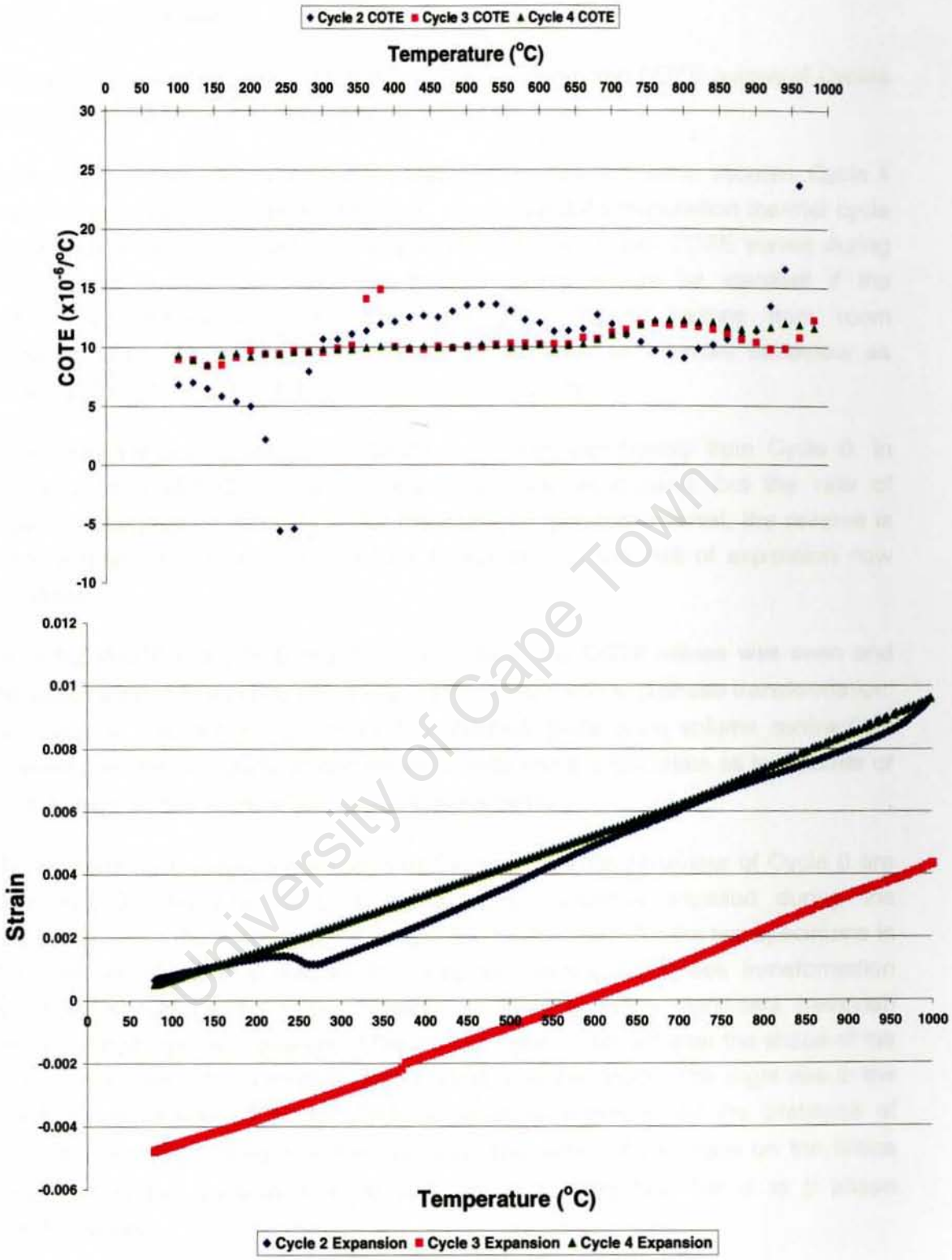

Figure 5.10: *Plot of Strain and COTE vs. temperature, Cycles 2-4 during cooling of CP Ti*

5.2.3 Cycles 0 and 4

This section refers to Figure 5.11 and 5.12, for the strain and COTE curves of Cycles 0 and 4 during heating and cooling respectively.

Cycle 0 is hydrogen-free since the thermal cycle was performed in vacuum. Cycle 4 should contain little or no hydrogen either, due to the dehydrogenation thermal cycle (Cycle 3) that was performed on the specimen. The strain and COTE curves during heating and cooling for these two thermal cycles should be identical if the hydrogenation-dehydrogenation cycle is complete. During heating from room temperature to 600°C, the two thermal cycles exhibit a very similar behaviour as shown by the strain and COTE curves (See Figure 5.11).

From temperatures above 600°C, Cycle 4 deviates significantly from Cycle 0. In Cycle 0, from 600-800°C the specimen continues to expand, but the rate of expansion decreases. In Cycle 4, for the same temperature interval, the reverse is seen, whereby the specimen continues to expand but the rate of expansion now increases.

From 800-940°C in Cycle 0, significant change in the COTE values was seen and this associated volume contraction was attributed to the α to β phase transformation. For Cycle 4, over the same temperature interval, there is no volume contraction; however the rate of expansion decreases slightly and it is uncertain as to whether or not this may be due to the α to β phase transformation.

The reasons for the above deviations of Cycle 4 from the behaviour of Cycle 0 are uncertain. On the one hand, if hydrogen is completely expelled during the dehydrogenation thermal cycle (Cycle 3), then the chemistry for the two specimens in Cycle 0 and Cycle 4 should be identical, and hence the phase transformation behaviour should be the same. However, if there is still a significant (residual) amount of hydrogen was present at the start of Cycle 4, this will alter the shape of the strain curve. The latter is most likely the situation in this study. The slight rise in the COTE values above 600°C for Cycle 4 could be explained by the presence of residual interstitial hydrogen in the α-phase. The effect of hydrogen on the lattice parameter of the α-phase may be sufficient to partially hide the α to β phase transformation.

The behaviour of Cycle 4 during cooling is also similar to the behaviour of Cycle 0 during cooling (See Figure 5.12). However, the only difference is that in Cycle 0, the reverse β to α phase transformation can be seen (by the change in COTE values cooling from 1000°C to 800°C), whereas this reaction is not easily identified in Cycle 4 for the same reasons described above.

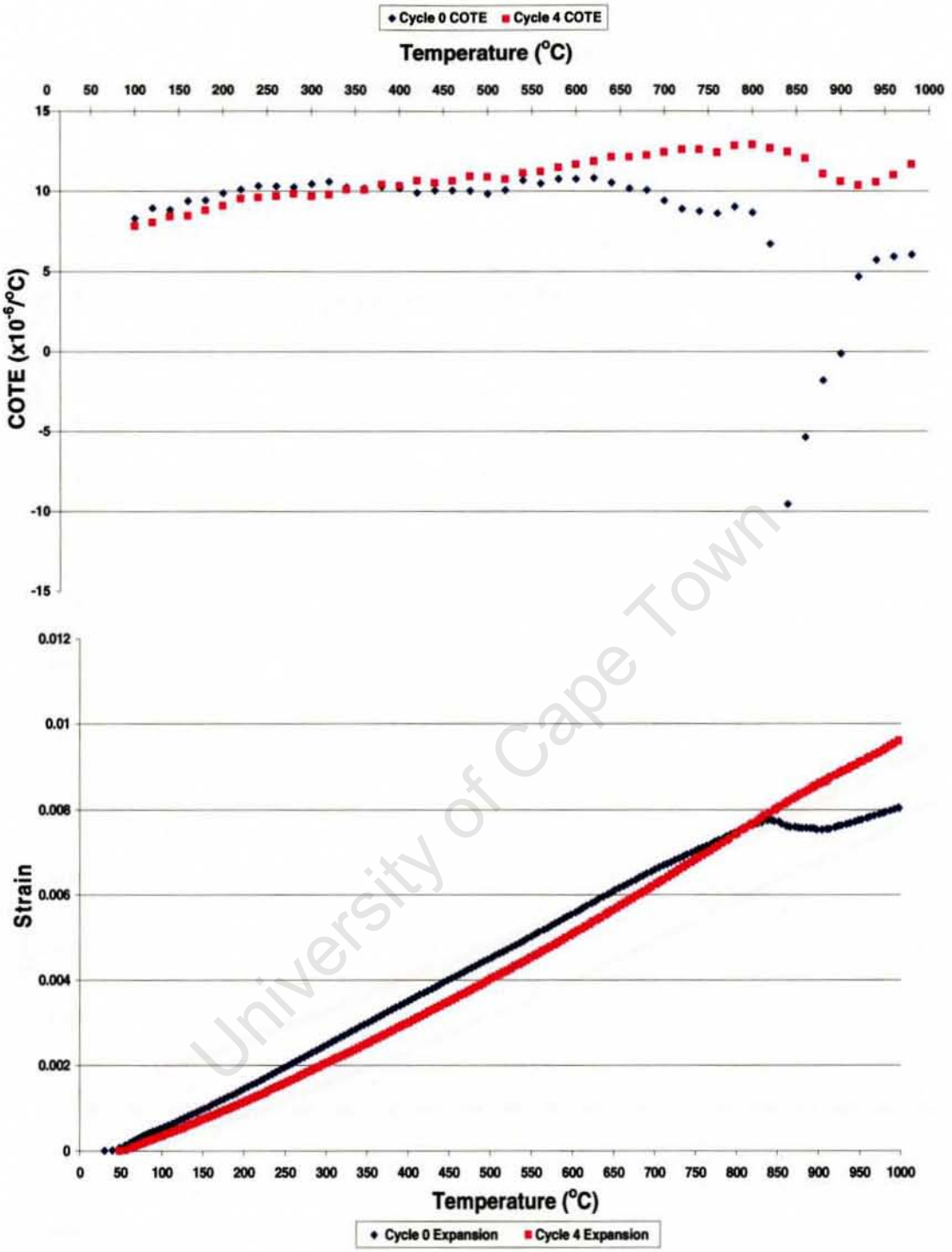

Figure 5.11: *Plot of Strain and COTE vs. temperature, Cycles 0 & 4, during heating of CP Ti*

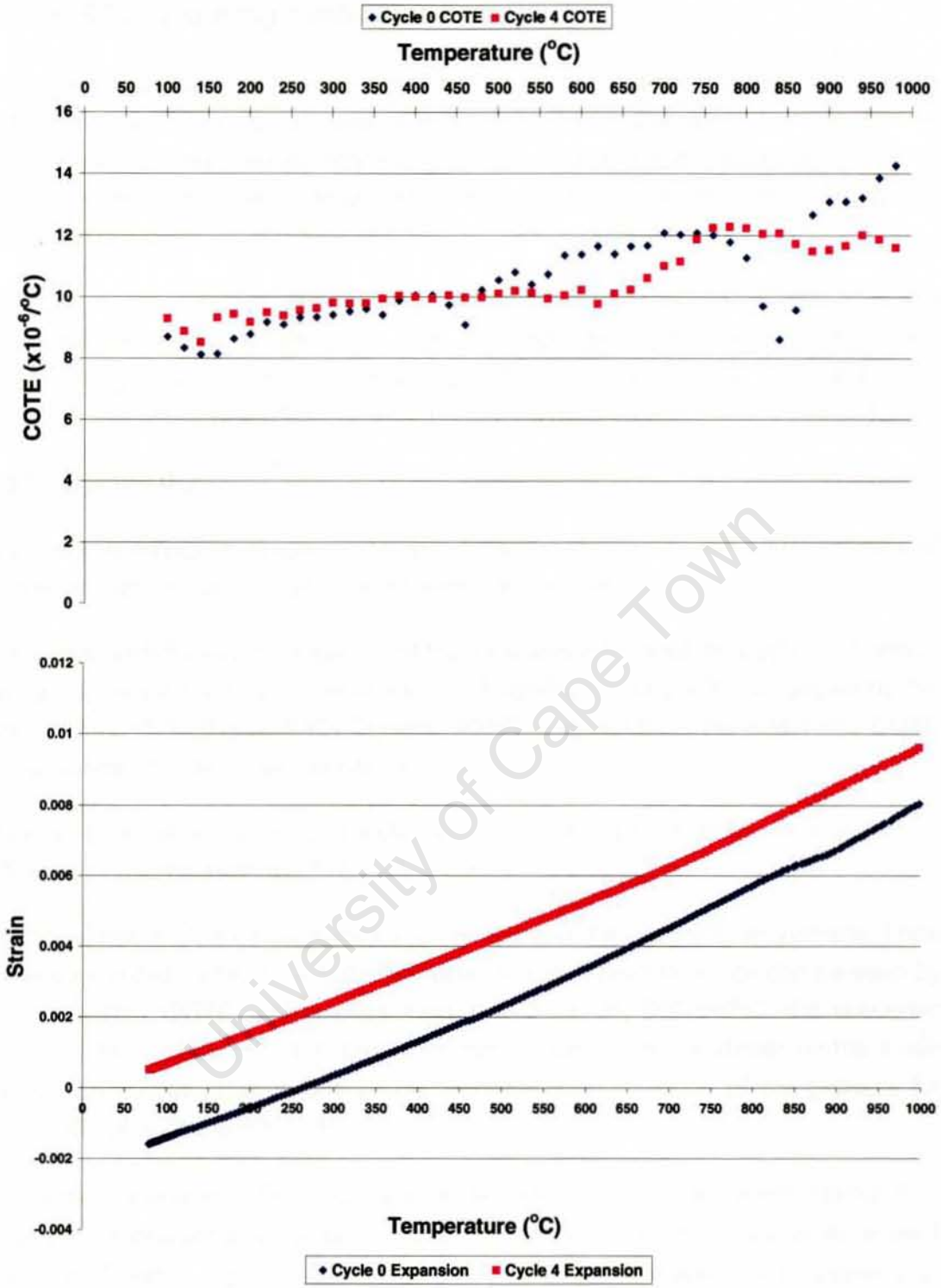

Figure 5.12: *Plot of Strain and COTE vs. temperature, Cycle 0 and 4 during cooling of CP Ti*

5.3 Ti-6Al-4V during heating and cooling

The strain and COTE vs. temperature curves for the following thermal cycles are plotted on the same set of axes: Cycles 0-2, Cycles 2-4 and Cycles 0 and 4. Comparisons between each thermal cycle during heating and cooling are made, in order to monitor the phase transformation behaviour of Ti-6Al-4V before, during and after hydrogenation.

Cycle 0 is the heating and cooling of the alloy in vacuum. Cycle 1 is the hydrogenation step, Cycle 2 is the post-hydrogenation step (in hydrogen environment), Cycle 3 is the dehydrogenation step and Cycle 4 is the post-dehydrogenation step. Cycles 1-4 were performed consecutively (See Section 4.3.1).

5.3.1 Cycles 0-2

This section refers to Figures 5.13 and 5.14, for the strain and COTE curves of Cycles 0, 1 and 2 during heating and cooling respectively.

The phase transformation behaviour of the alloy was monitored for Cycles 0, 1 and 2. The alloy expands due to thermal effects of heating up to 550°C, as shown by the strain curves (See Figure 5.13). Beyond 550°C, a deviation in the strain and COTE curves is seen for the three conditions.

Cycle 0 aims to serve as a benchmark for Cycles 1-4, in order to monitor the influence of hydrogen on the Ti-6Al-4V alloy.

The specimen in Cycle 0 expands from room temperature to 600°C at a constant rate of expansion due to the normal thermal effects during heating, which can be seen by the strain and COTE curves (See Figure 5.13). From 600-840°C, the specimen continues to expand, but at a decreased rate of expansion as shown by the strain and COTE curves. This is due to the increase in the fraction of the β-phase for temperatures above 600°C **[19]**.

The α to β phase transformation is expected to accompany a volume contraction, since the volume per atom of the α phase is larger than the volume per atom of the β phase as shown in Figure 5.1. The specimen experienced a volume contraction over the 860-900°C temperature interval, as shown by the strain and COTE curves. This volume contraction can be attributed to the α to β phase transformation. Above 900°C the specimen expands normally, as shown by the strain and COTE curves up to 1000°C. The COTE curve continues to change quite rapidly beyond 900°C, which indicates that the α to β phase transformation is not yet complete. The β-transus is probably close to 1000°C, but cannot be accurately determined because the specimen was not heated above 1000°C

After heating to 1000°C, the specimen of Cycle 0 is in the β-phase field. During cooling from 1000 to 900°C, the rate of contraction decreases, signifying the β to α phase transformation (See Figure 5.14). Once this transformation is complete, the rate of contraction then increases during cooling from 900°C to 850°C. From 850°C to room temperature the alloy gradually contracts due to thermal effects upon cooling, as shown by the strain and COTE curves. The reverse β to α phase transformation is estimated to be complete by 850°C.

Cycle 1 is the hydrogenation thermal cycle. The specimen in Cycle 1 exhibits the same behaviour as Cycle 0 during heating from room temperature to 550°C, as shown by the strain and COTE curves. The solubility of hydrogen in the α-phase is relatively low in comparison to the solubility in the β-phase, since hydrogen substitutes interstitially into the tetrahedral sites of the titanium lattice and the bcc lattice has more tetrahedral sites than the hcp phase [**9**]. At temperatures lower than 550°C, the high volume fraction of the α-phase produces similar low hydrogen solubility to that indicated for CP-Ti (Cycle 1).

The specimen in Cycle 1 deviates from Cycle 0 at 550°C. The specimen continues to expand, but the rate of expansion increases from 550-750°C, whereas in Cycle 0 the rate of expansion decreases in this temperature interval. The influence of hydrogen is the cause of this deviation from Cycle 0, in that the solubility of hydrogen in both phases causes a volume expansion.

Hydrogen is known to cause an increase in the lattice parameters of the α and β phases and in turn the unit cell volumes of both α and β phase increases, but mainly the β phase by up to 5.35% [**9**]. Furthermore, this increase in the rate of expansion from 550-750°C can also be attributed to the formation of the δ-phase. According to the Ti-6Al-4V-H phase diagram (Figure 2.32a), the formation of hydrides occurs above 600°C with a hydrogen concentration above 15at%. At temperatures above 600°C, titanium and its alloys can absorb hydrogen of up to 60at% [**1**] and thus it is possible that sufficient hydrogen is absorbed to cause hydride formation. The formation of hydrides from the α-phase causes a volume expansion of up to 18% [**9**].

From 750-840°C, the specimen in Cycle 1 continues to expand, but the rate of expansion decreases considerably and a volume contraction is also seen from 860-1000°C, as shown by the strain and COTE curves. This decreased rate of expansion and volume contraction in the respective temperature intervals is due to two reasons: i) the dissolution of the hydride phase, taking into account that at this stage more than 15at% H was absorbed and ii) the transformation of the α to β phase as depicted in Ti-6Al-4V-H phase diagram (Figure 2.32a). The β-transus is difficult to determine, since there are several overlapping changes occurring in the microstructure. The concurrent dissolution of the hydride phase, the formation of the

β-phase and the absorption of hydrogen by the β-phase prevent the β-transus from being identified.

The proposed sequence of phase transformations for Cycle 1 during heating can be summarised as follows:

$$\alpha + \beta \rightarrow \alpha_{II} + \beta_{II} \rightarrow \alpha_{II} + \beta_{II} + \delta \rightarrow \beta_{II} + \delta \rightarrow \beta$$

The strain curve of Cycle 1 is displaced above the strain curve of Cycle 0, due to the presence of hydrogen in solid solution and the δ-phase in Cycle 1 (See Figure 5.13).

As the specimen cools from 1000°C there is a continuous transformation towards a larger volume/atom, which extends down to at least 720°C, as indicated by the rapid change in the COTE values (See Figure 5.14). From the Ti-6Al-4V-H phase diagram (Figure 2.32a) cooling from the β-phase should result in the precipitation of the hydride phase, which in turn leads to a volume expansion i.e. decrease in the contraction rate. Hence, this change can be attributed to the formation of the δ-phase as well as the reverse β to α phase transformation.

From 720°C to room temperature the contraction rate gradually decreases and exhibits the same behaviour as Cycle 0, as seen by the strain and COTE curves, due to thermal effects upon cooling.

The proposed phase transformation sequence for Cycle 1 during cooling can be summarised as follows:

$$\beta_{II} \rightarrow \alpha_{II} + \beta_{II} + \delta$$

At the start of Cycle 2, the phases present at room temperature are α, β and δ with hydrogen in solid solution.

Cycle 2 exhibits a similar behaviour to Cycle 1 during heating, except that the volume expansion from 550-750°C, as seen by the strain and COTE curves, is less pronounced than that of Cycle 1 (See Figure 5.13). This can be attributed to the fact that the rate of absorption of hydrogen in this thermal cycle was lower than that of Cycle 1. This was due to the prior existence of hydrogen within the alloy at the start of Cycle 2. The same phase transformations that occurred in Cycle 1 occurred in Cycle 2, except that at the start of Cycle 2 the δ-phase was already present (formed in Cycle 1). It is expected that the formation of the δ-phase is further increased due to the constant supply of hydrogen that is provided during the entire thermal cycle.

The proposed phase transformation sequence for Cycle 2 during heating can be summarised as follows:

$$\alpha_H + \beta_H + \delta \rightarrow \beta_H + \delta \rightarrow \beta$$

Cycle 2 displays almost identical behaviour to Cycle 1 during cooling as shown by the strain and COTE curves (See Figure 5.14). The strain curves of Cycle 2 during cooling is however, displaced below the strain curve of Cycle 1 during cooling. This suggests that the rate of hydrogen absorption during cooling was greater in Cycle 1 than in Cycle 2. The sequence of phase transformations in Cycle 2 during cooling is the same as Cycle 2 during cooling and can be summarised as follows:

$$\beta_H \rightarrow \alpha_H + \beta_H + \delta$$

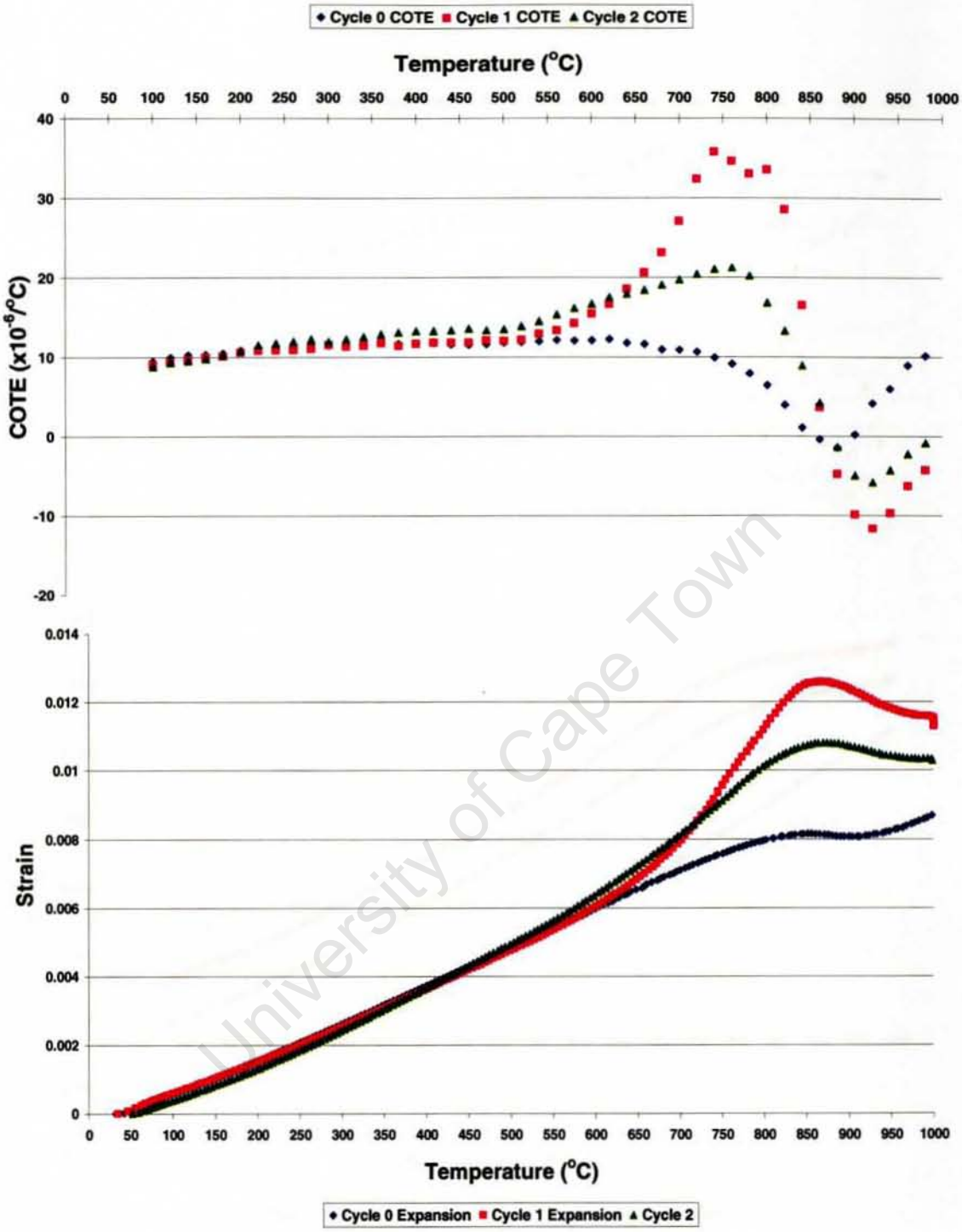

Figure 5.13: *Plot of Strain and COTE graphs, Cycles 0, 1 and 2 during heating of Ti-6Al-4V*

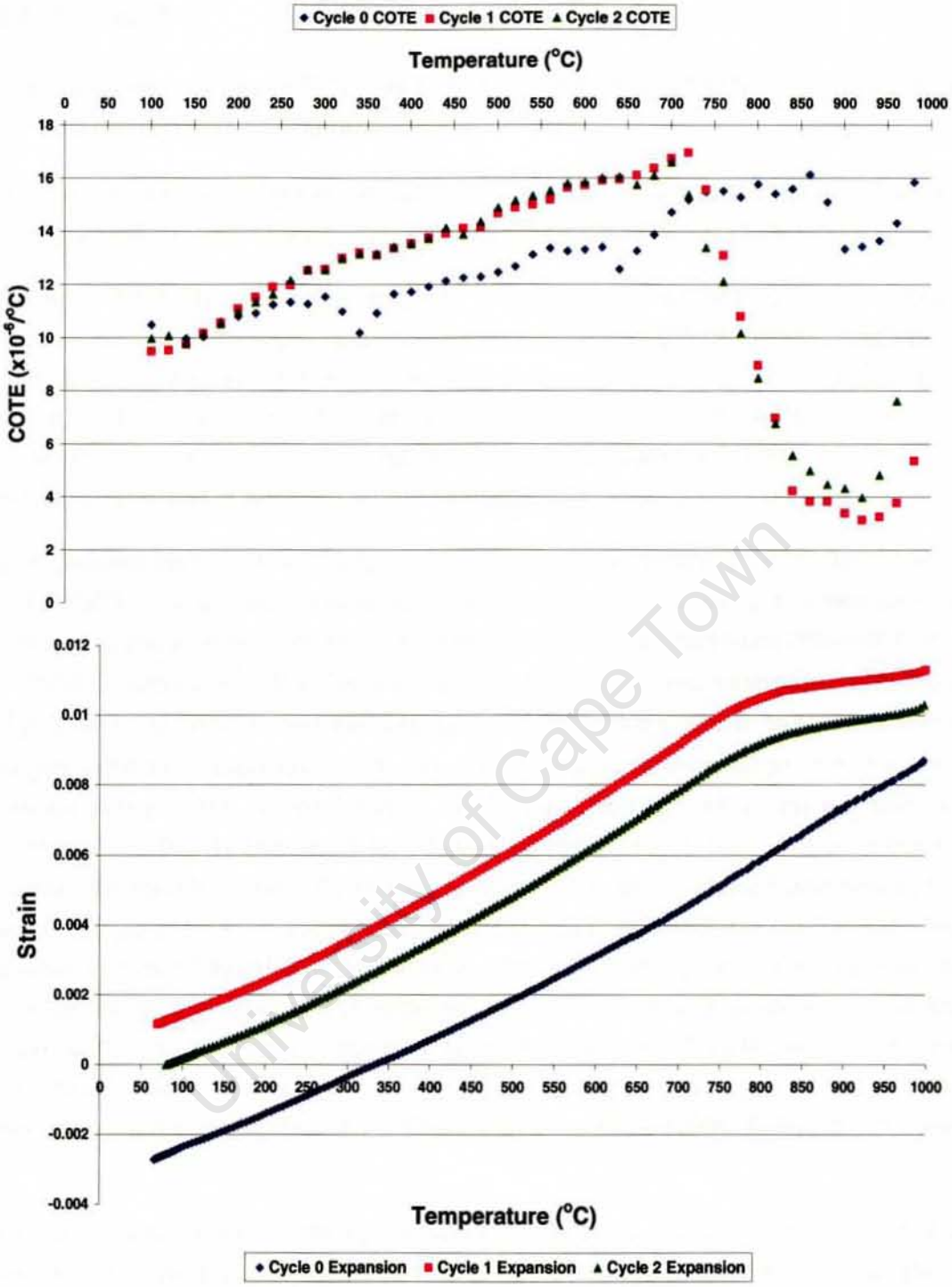

Figure 5.14: *Plot of Strain and COTE vs. temperature, Cycles 0, 1 & 2 during cooling of Ti-6Al-4V*

5.3.2 Cycles 2-4

This section refers to Figure 5.15 and 5.16, for the strain and COTE curves of Cycles 2-4 during heating and cooling respectively.

Cycle 3 is the dehydrogenation step of the alloy. Cycle 3 exhibits the same behaviour as Cycle 2 and 4 during heating from room temperature to 550°C (See Figure 5.15).

From 550-730°C, the specimen in Cycle 3 continues to expand, but at a slightly increased rate of expansion, as shown by the strain and COTE curves. The lattice parameter of the hydride phase is known to increase with an increase in temperature and this explains the change in expansion rate **[56]**. In Cycle 3, the rate of expansion deviates from Cycle 2 at approximately 680°C and the downwards trend suggests the removal of hydrogen in the vacuum environment.

The downward trend in the COTE curve accelerates from about 780°C for Cycle 3 and the COTE values becomes negative above 820°C. In Cycle 2 this decrease in the rate of expansion and volume contraction also occurred, but from 760-850°C and 860-1000°C respectively. For Cycle 2, these two changes were associated with the α to β phase transformation and the dissolution of the hydride phase. In Cycle 3, these changes were also associated with the α to β phase transformation, but the early decrease in the COTE values (starting at 680°C) is likely to reflect the expulsion of hydrogen from the specimen. The addition of hydrogen to the alloy at elevated temperatures results in the volume expansion of the α and β phases and hence, the release of hydrogen from these phases would result in a volume contraction. The decrease in rate of expansion and volume contraction in Cycle 3 can thus also be attributed to: i) hydrogen being expelled from the α and β phases and ii) the decomposition of the hydride phase due to the removal of hydrogen in vacuum. These two reasons also explain why the decrease in the rate of expansion and volume contraction during heating in Cycle 3 was far more pronounced than in Cycle 2.

From 920°C and upwards, the specimen in Cycle 3 then continues to expand at a more or less constant rate, which can be attributed to the presence of the single β-phase.

The proposed phase transformation sequence for Cycle 3 during heating can be summarised as follows:

$$\alpha_H + \beta_H + \delta \rightarrow \beta_H + (\delta) \rightarrow \beta$$

During cooling, Cycle 3 deviates significantly from Cycle 2 due to the different phases present in the specimens (See Figure 5.16).

After heating to 1000°C in Cycle 3, the specimen is in the β-phase field. During cooling from 1000°C, the rate of contraction changes substantially, which signify the β to α transformation. The COTE values become more or less constant below 800°C, which suggests that the bulk of the β to α transformation has been completed.

It is not clear whether all the hydrogen was removed or not at this point and whether all the hydrides had been decomposed. When cooling from 800°C to room temperature, the specimen in Cycle 3 exhibits the same trend as Cycle 2. The specimen continues to contract, with the rate of contraction decreasing gradually due to the normal thermal effects upon cooling.

Cycle 4 is the post dehydrogenation step. The shape of the strain curve for Cycle 4 is the same as that for Cycles 2 and 3, when heating from room temperature to 550°C (See Figure 5.15). For Cycle 4, the specimen continues to expand up to 820°C, with a constant rate in relation to Cycles 2 and 3. This suggests little or no phase transformation occurred from room temperature to 820°C. From 820-900°C, the specimen in Cycle 4 continues to expand, but the rate of expansion decreases slightly, as shown by the strain and COTE curves. This is most likely attributed to the α to β phase transformation.

The behaviour of Cycle 4 is dissimilar to Cycles 2 and 3. In Cycle 3, hydride decomposition and the removal of hydrogen occurred in the 740-900°C temperature interval and if this occurred effectively little no hydrogen or hydrides should be present at the start of Cycle 4. The deviation of Cycle 4 from Cycles 2 and 3 can be attributed to the absence of hydrides and hydrogen in solid solution. If however, residual hydrogen remained after the completion of Cycle 3, then during heating of Cycle 4 hydrogen will continue to be dispelled from the specimen. This may be the case in this study.

After heating to 1000°C, the specimen in Cycle 4 is in the β-phase field. The behaviour of Cycle 4 during cooling is similar to the behaviour of Cycle 3 during cooling (See Figure 5.16). The only difference is that the end of the β to α transformation cannot be identified from the shape of the COTE curve. This observation is surprising and will be discussed further in the next section.

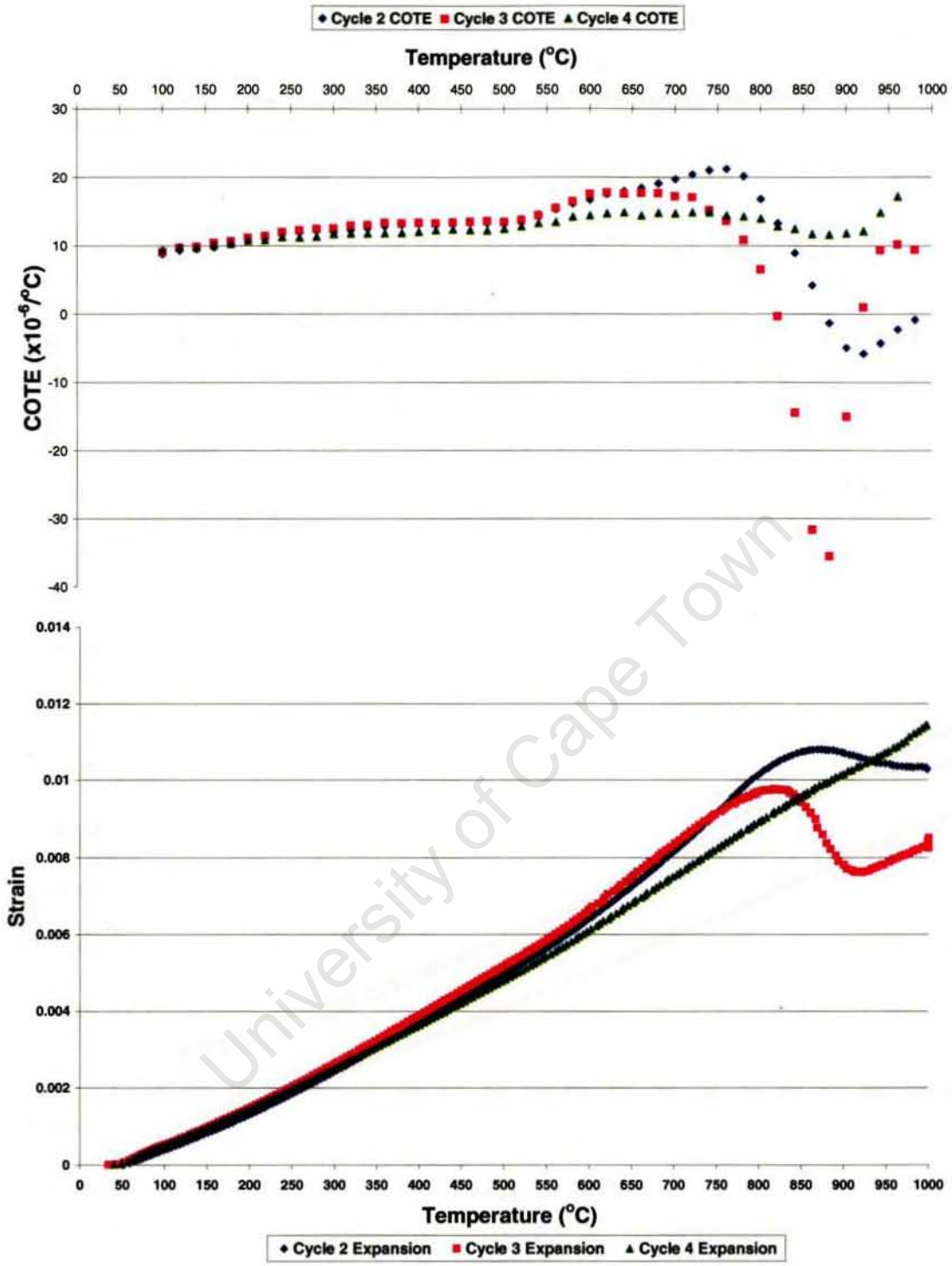

Figure 5.15: *Plot of Strain and COTE vs. temperature, Cycles 2-4 during heating of Ti-6Al-4V*

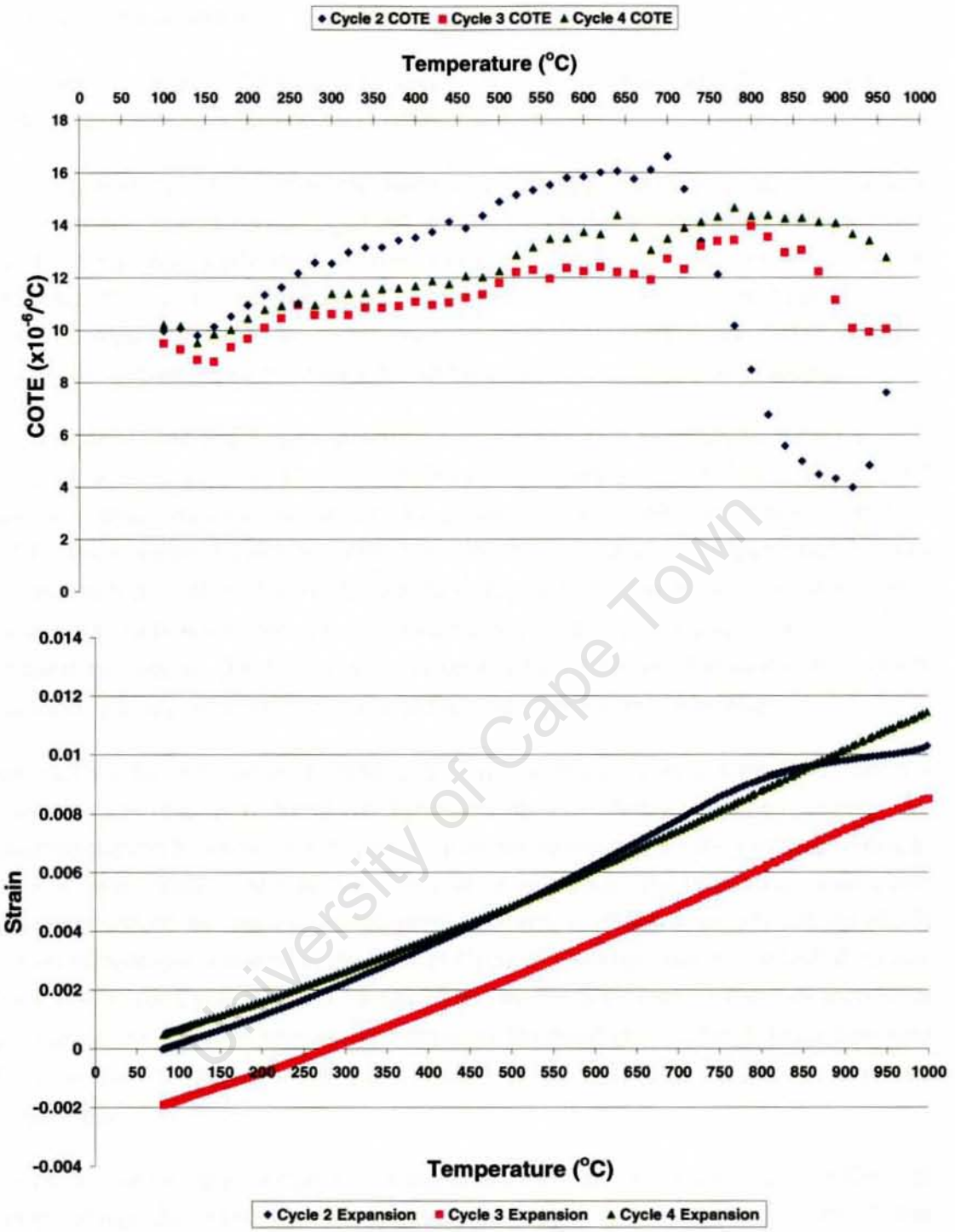

Figure 5.16: *Plot of Strain and COTE vs. temperature, Cycles 2-4, during cooling of Ti-6Al-4V*

5.3.3 Cycles 0 and 4

This section refers to Figures 5.17 and 5.18, for the strain and COTE curves of Cycles 0 and 4, during heating and cooling respectively.

Cycle 0 is hydrogen-free, since the thermal cycle was performed in vacuum. Cycle 4 should contain little or no hydrogen either, due to the dehydrogenation thermal cycle (Cycle 3) that was performed on the specimen. The strain and COTE curves for these two thermal cycles should be identical if the hydrogenation-dehydrogenation cycle is complete. From room temperature to 550°C, the two thermal cycles exhibit a very similar behaviour as shown by the strain and COTE curves (See Figure 5.17).

From temperatures 550°C and upwards, Cycle 4 deviates significantly from Cycle 0. In Cycle 0 from 600-840°C, the specimen continues to expand but the rate of expansion decreases as the fraction of β-phase increases [**19**]. In Cycle 4 (from 600-800°C), the reverse is seen, whereby the specimen continues to expand but the rate of expansion increases. From 860-900°C in Cycle 0, a volume contraction is seen, which is associated with the α to β phase transformation. For Cycle 4 over the same temperature interval, there is no volume contraction; however the rate of expansion decreases slightly, which may be due to the α to β phase transformation.

The reasons for the above deviations of Cycle 4 from Cycle 0 during heating are uncertain. On the one hand, if hydrogen is completely expelled during the dehydrogenation thermal cycle (Cycle 3), then the chemistry for the two specimens in Cycle 0 and Cycle 4 should be identical, and hence the phase transformation behaviour should be the same. However, if there was still a significant (residual) amount of hydrogen present at the start of Cycle 4, the slight rise in the COTE values above 550°C for Cycle 4 could be explained by the presence of residual interstitial hydrogen in the α and β phases. The effect of the hydrogen on the lattice parameter of the α and β phases may be sufficient to partially hide the α to β phase transformation.

The behaviour of Cycle 4 during cooling is also similar to the behaviour of Cycle 0 during cooling (See Figure 5.18). However, the only difference is that in Cycle 0, the β to α phase transformation can be seen (as a change in COTE values during cooling from 1000°C to 880°C), whereas this reaction is not easily identified in Cycle 4 for the reasons same reasons described above.

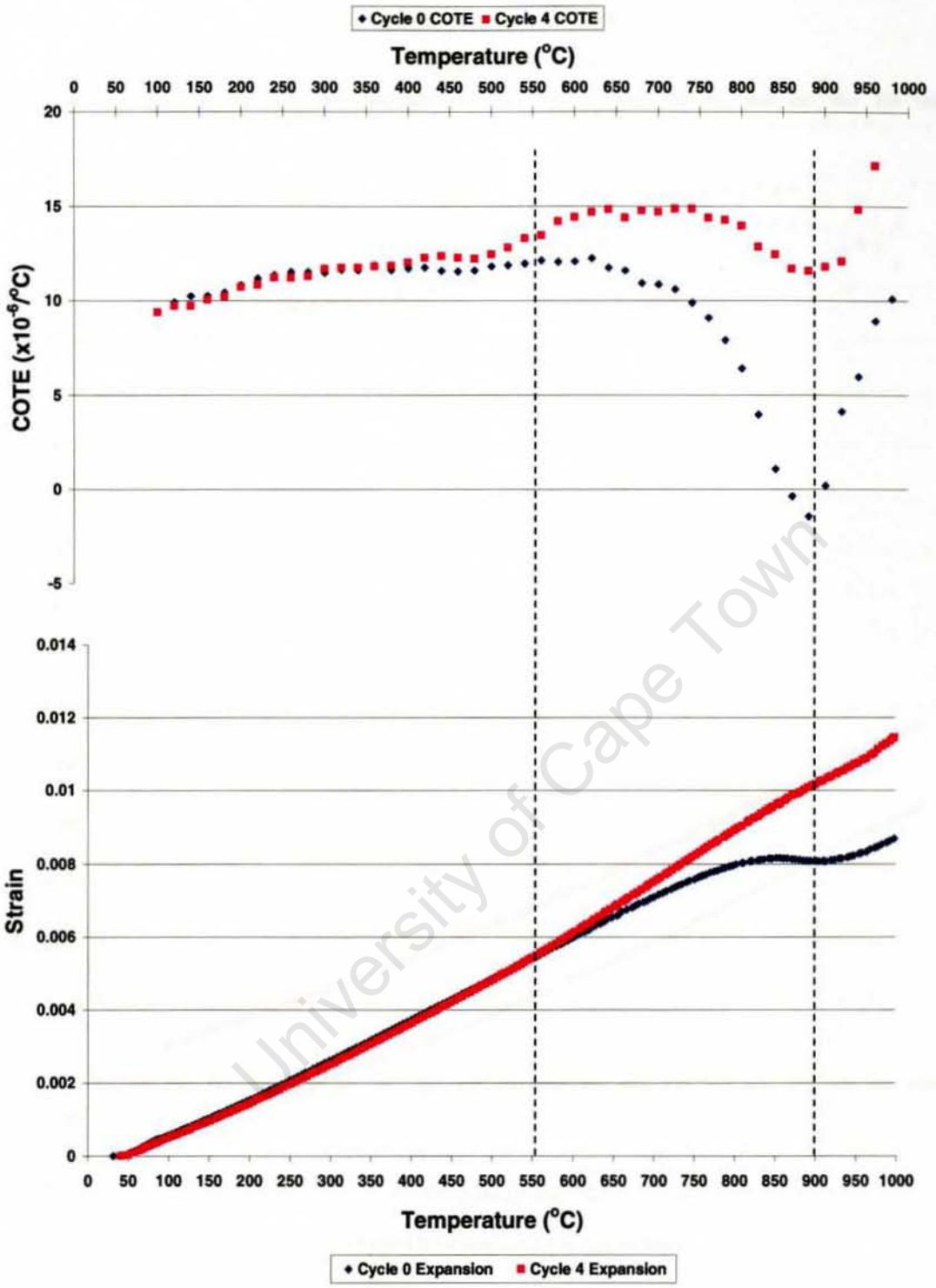

Figure 5.17: *Plot of Strain and COTE vs. temperature, Cycles 0 and 4, during heating of Ti-6Al-4V*

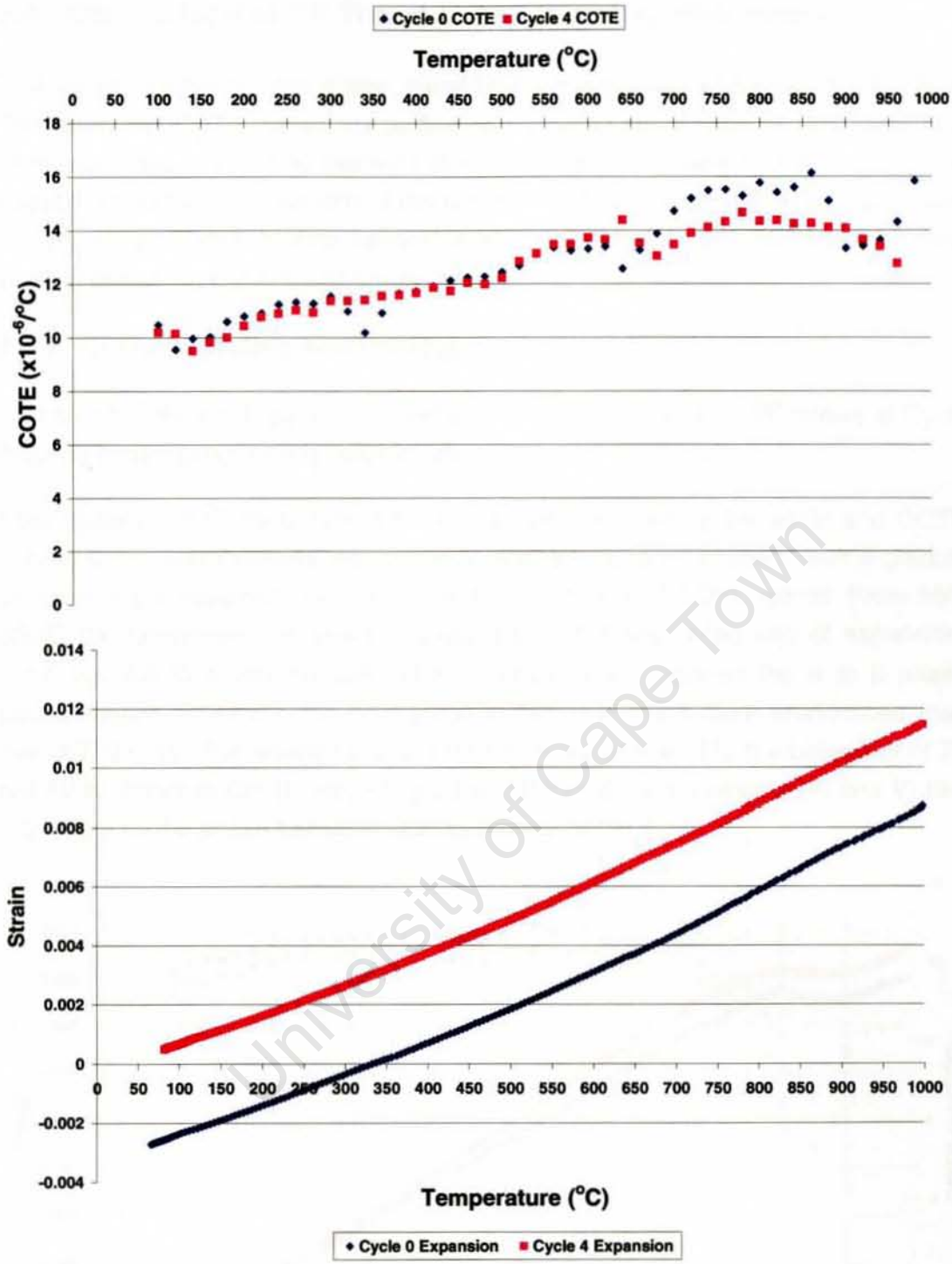

Figure 5.18: *Plot of Strain and COTE vs. temperature, Cycles 0 and 4, during cooling of Ti-6Al-4V*

5.4 Comparison of CP Ti and Ti-6Al-4V using dilatometry

This section compares the phase transformation behaviour of CP Ti and Ti-6Al-V. The strain and COTE curves are plotted on the same set of axes for both materials. This was done in order to highlight the similarities and marked differences in the phase transformation behaviour of the two materials. CP Ti aims to serve as a basis for the phase transformation behaviour of the Ti-6Al-4V alloy during the various thermal cycles i.e. Cycle 0 and Cycles 1-4.

5.4.1 Cycle 0, heating and cooling

This section refers to Figures 5.19 and 5.20, for the strain and COTE curves of Cycle 0 during heating and cooling respectively.

Both materials in Cycle 0 exhibit the same trend as seen by the strain and COTE curves. CP Ti and Ti-6Al-4V expand from room temperature to 650°C with a gradual increase in the expansion rate as shown by the strain and COTE curves. From 650-850°C the specimens continues to expand but at a decreased rate of expansion. From 850-920°C a volume contraction is seen, which signifies the α to β phase transformation. However, the contraction in CP Ti is much more pronounced than that of Ti-6Al-4V. The reason for this is uncertain. Apart from this, the behaviour of Ti-6Al-4V is similar to CP Ti, which suggests that the alloying elements (Al and V) had little effect on the phase transformation behaviour of CP Ti.

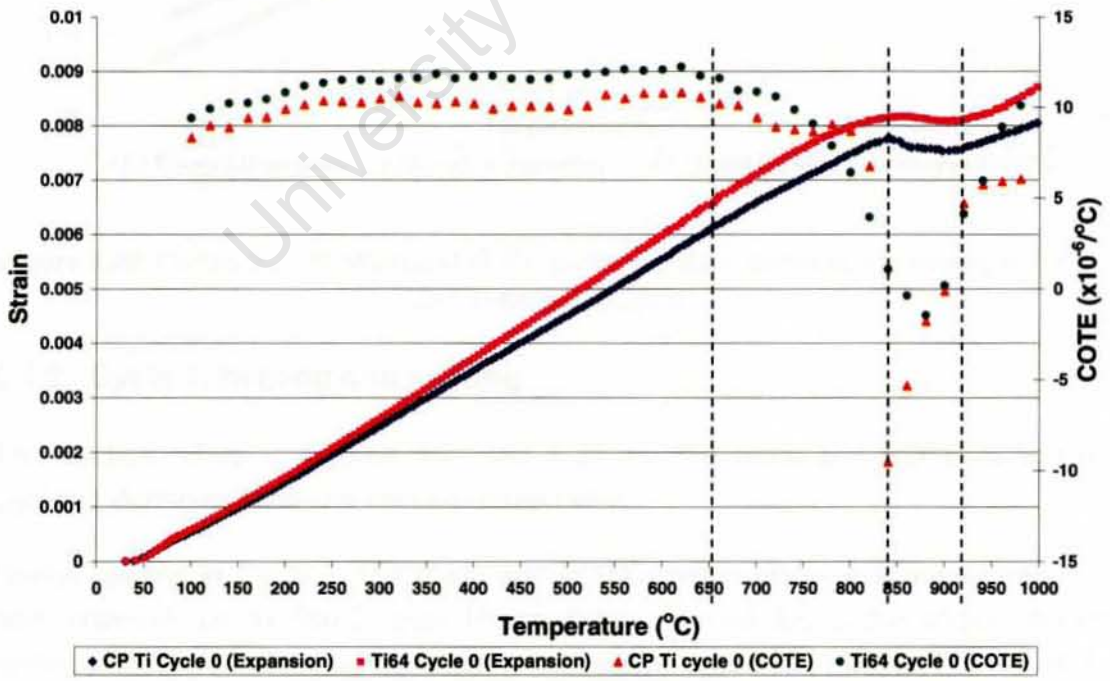

Figure 5.19: *Comparison of Strain and COTE vs. temperature curves during heating of CP Ti and Ti-6Al-4V, Cycle 0*

During the cooling step of Cycle 0, the β to α phase transformation is seen at different temperatures intervals for the two materials (See Figure 5.20). For Ti-6Al-4V this is seen cooling from 1000°C to 880°C, whereas for CP Ti this is seen from 860°C to 780°C, as seen by the strain and COTE curves. This phase transformation temperature interval in CP Ti is seen during the heating cycle as well. This also further implies that the phase diagram for Ti-6Al-4V cannot be solely used to predict the phase transformations of a material, the kinetics also plays a role in predicting phase transformation behaviour and temperatures. After the reverse β to α phase transformation the materials both contract all the way to room temperature due the normal effects upon cooling. The effect of alloying elements is a possible reason for the difference in the behaviour of Ti-6Al-4Vand CP Ti during cooling.

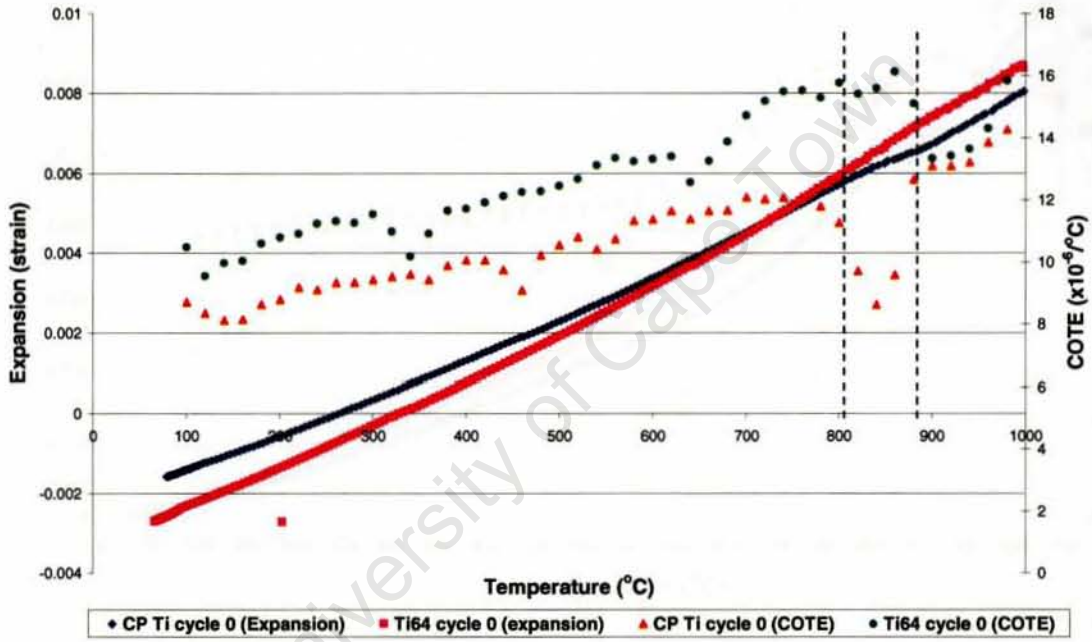

Figure 5.20: *Comparison of Strain and COTE vs. temperature curves during cooling of CP Ti and Ti-6Al-4V, Cycle 0*

5.4.2 Cycle 1, heating and cooling

This section refers to Figures 5.21 and 5.22, for the strain and COTE curves of Cycles 1 during heating and cooling respectively.

During heating in Cycle 1, the strain and COTE curves displays a similar trend in both materials up to 550°C (See Figure 5.21). Beyond 550°C the absorption of hydrogen occurred more rapidly in both materials as reported by Lopez-Suarez et al. **[41]**.

The phase transformations in Ti-6Al-4V and CP Ti, due to the addition of hydrogen to the materials differ. In CP Ti (during heating in Cycle 1) ±40at%H was absorbed and

in Ti-6Al-4V >15at%H was absorbed. This was expected since hydrogen has a greater solubility in CP Ti than in Ti-6Al-4V [39].

For CP Ti the proposed phase transformation sequence during heating was:

$$\alpha \rightarrow \alpha_H \rightarrow \beta_H$$

And for Ti-6Al-4V it was:

$$\alpha + \beta \rightarrow \alpha_H + \beta_H \rightarrow \beta_H \rightarrow \alpha_H + \beta_H + \delta \rightarrow \beta_H + \delta \rightarrow \beta_H$$

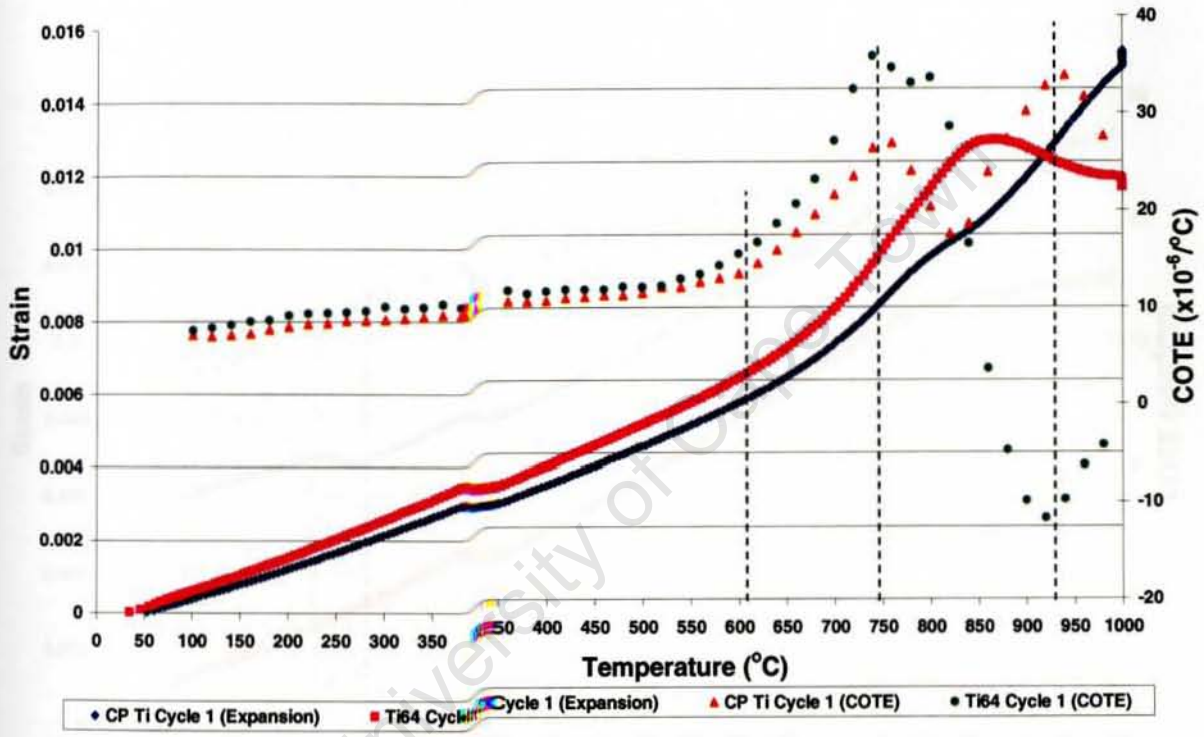

Figure 5.21: *Comparison of Strain and COTE vs. temperature curves during heating of CP Ti and Ti-6Al-4V, Cycle 1*

During cooling in Cycle 1, the two materials exhibits a similar trend cooling from 1000°C to 300°C (See Figure 5.22). A decrease in the contraction rate is seen cooling from 1000°C to 900°C. In Ti-6Al-4V this is due to the reverse transformation of the β to α phase and the precipitation of hydrides (δ-phase) from the single β phase that was present at 1000°C. In CP Ti this is due to the increase in hydrogen uptake. Ti-6Al-4V deviates from CP Ti at 300°C. In CP Ti the rate of contraction decreased during cooling from 300°C and a volume contraction occurred cooling from 275°C to 250°C as shown by the strain and COTE curves. Hydrogen in CP Ti is able to lower the β-transus to 300°C as seen by the Ti-H phase diagram (Figure 2.30b); hence these changes can be attributed to CP Ti experiencing the early β to α phase transformation induced by hydrogen. The addition of hydrogen to the two

materials has different effects on both materials during heating and cooling. The effect of alloying elements may be the cause of this.

For CP Ti the proposed phase transformation sequence during cooling was:

$$\beta_{II} \rightarrow \alpha_{II} + hydride$$

And for Ti-6Al-4V it was:

$$\beta_{II} \rightarrow \alpha_{II} + \beta_{II} + \delta$$

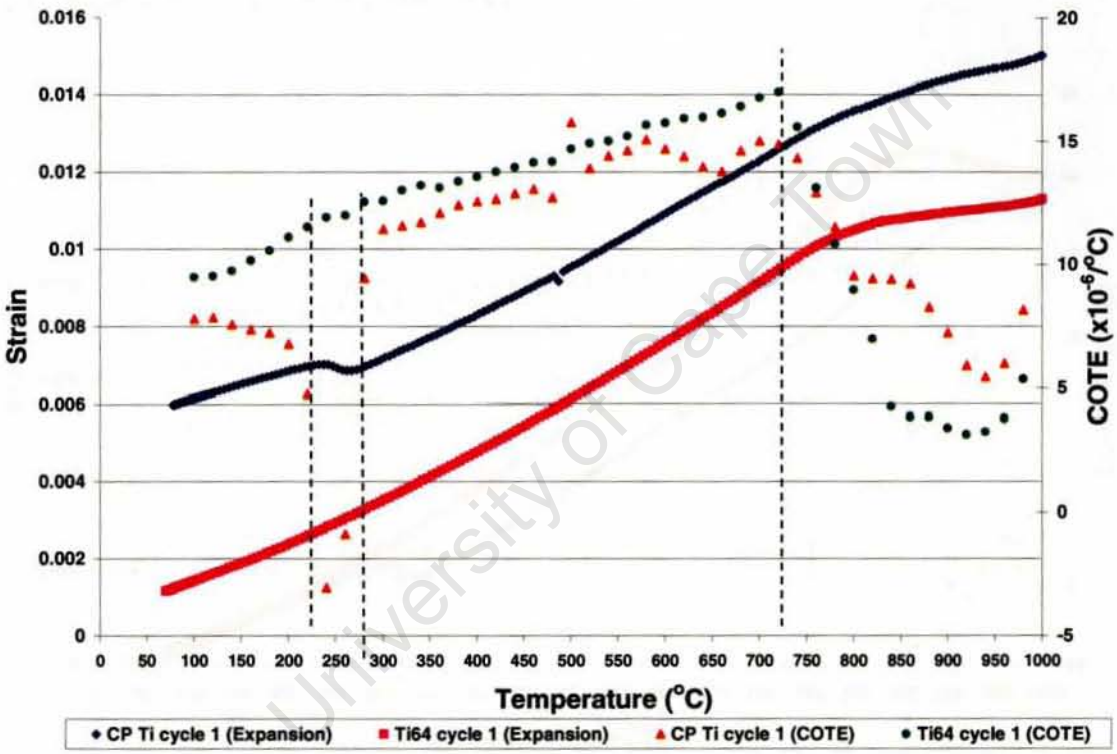

Figure 5.22: *Comparison of Strain and COTE vs. temperature curves during cooling of CP Ti and Ti-6Al-4V, Cycle 1*

5.4.3 Cycle 2, heating and cooling

This section refers to Figures 5.23 and 5.24, for the strain and COTE curves of Cycle 2 during heating and cooling respectively.

During the heating step of Cycle 2, for CP Ti and Ti-6Al-4V, the strain and COTE curves displays key differences (See Figure 5.23). The first difference was the early α to β phase transformation in CP Ti that occurs at 300°C, which is seen as a volume

contraction. This early transformation was also seen in the cooling of Cycle 1 in CP Ti (See Figure 5.22).

The behaviour of two materials as shown by the strain and COTE curves exhibits the same behaviour from 350°C to 550°C, whereby the uptake of hydrogen is minimal. The effect of hydrogen in Ti-6Al-4V differs from CP Ti and hence, at 550°C the behaviour of Ti-6Al-4V deviates from CP Ti. Both materials experiences an increase in the rate of expansion; Ti-6Al-4V from 550-750°C and CP Ti from 650-850°C. This was due to the increase in the uptake of hydrogen. Beyond 850°C in CP Ti, hydrogen was expelled from the specimen, and hence the rate of expansion decreased and a volume contraction was eventually seen. In Ti-6Al-4V the decrease in rate of contraction from 750°C and then volume contraction was due to the dissolution of hydrides and α to β phase transformation.

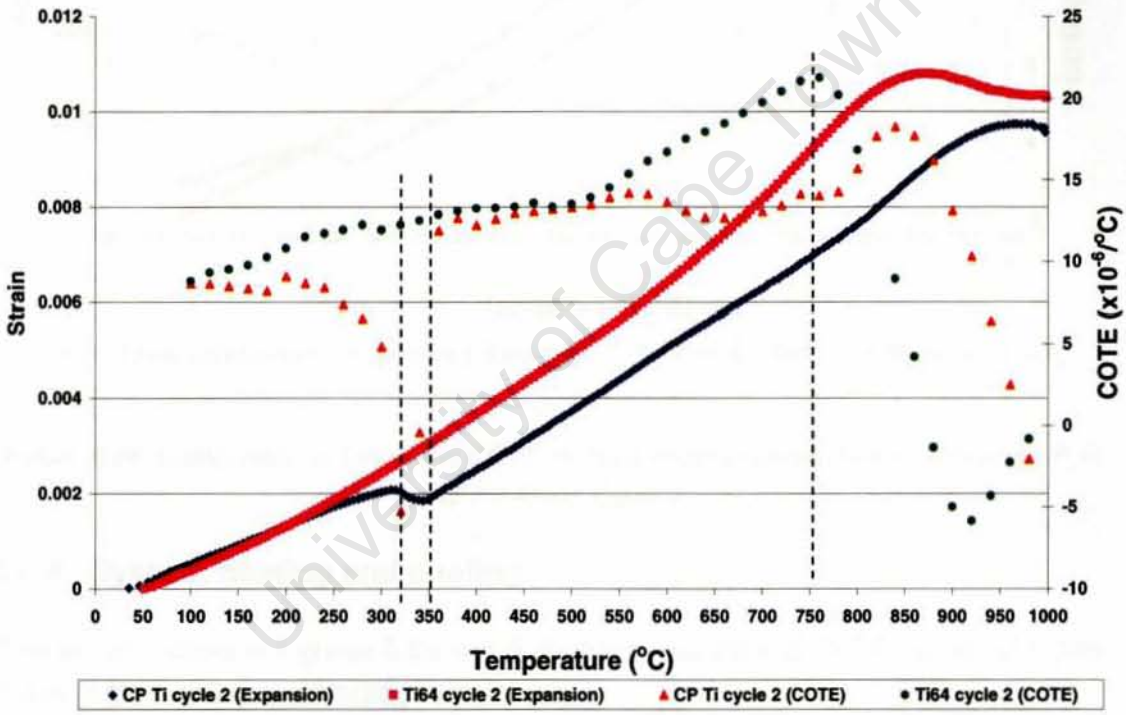

Figure 5.23: *Comparison of Strain and COTE curves during heating of CP Ti and Ti-6Al-4V, Cycle 2*

During the cooling step of Cycle 2, from 1000°C to 300°C, the two materials follow the same trend as shown by the strain and COTE curves (See Figure 5.24). During cooling from 1000°C to 700°C, both materials experiences changes in the COTE values. For CP Ti this is due to the increase in hydrogen uptake, whereas for Ti-6Al-4V this is attributed to the precipitation of hydrides from the β-phase field and the reverse β to α phase transformation during.

During cooling from 700°C to 300°C, CP Ti and Ti-6Al-4V follows the same trend as shown by the strain and COTE curves, which is due to little or no uptake of hydrogen in both materials. At 300°C Ti-6Al-4V deviates from CP Ti, because CP Ti experiences the early reverse β to α phase transformation due to the presence of hydrogen in solid solution.

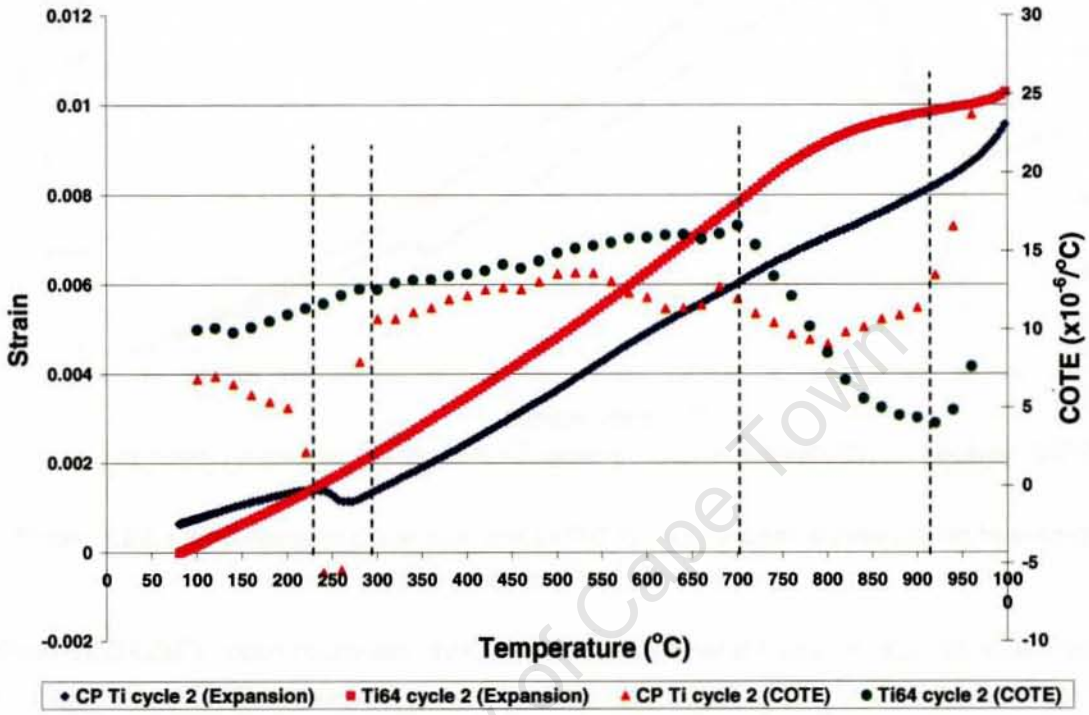

Figure 5.24: *Comparison of Strain and COTE vs. temperature curves during cooling of CP Ti and Ti-6Al-4V, Cycle 2*

5.4.4 Cycle 3, heating and cooling

This section refers to Figures 5.25 and 5.26, for the strain and COTE curves of Cycle 3 during the heating and cooling respectively.

During heating in Cycle 3, Ti-6Al-4V exhibits the same trend as CP Ti, as shown by the strain and COTE curves (See Figure 5.25). The major difference however, is the early β-transus in CP Ti, which is seen in 300-350°C. For Ti-6Al-4V the β-transus is seen at higher temperatures. The early, hydrogen induced β-transus in CP Ti is a recurring phase transformation, which was also seen from the cooling step in Cycle 1 and Cycle 2 (heating and cooling). This can be attributed to the presence of hydrogen in solid solution, which lowered the β-transus.

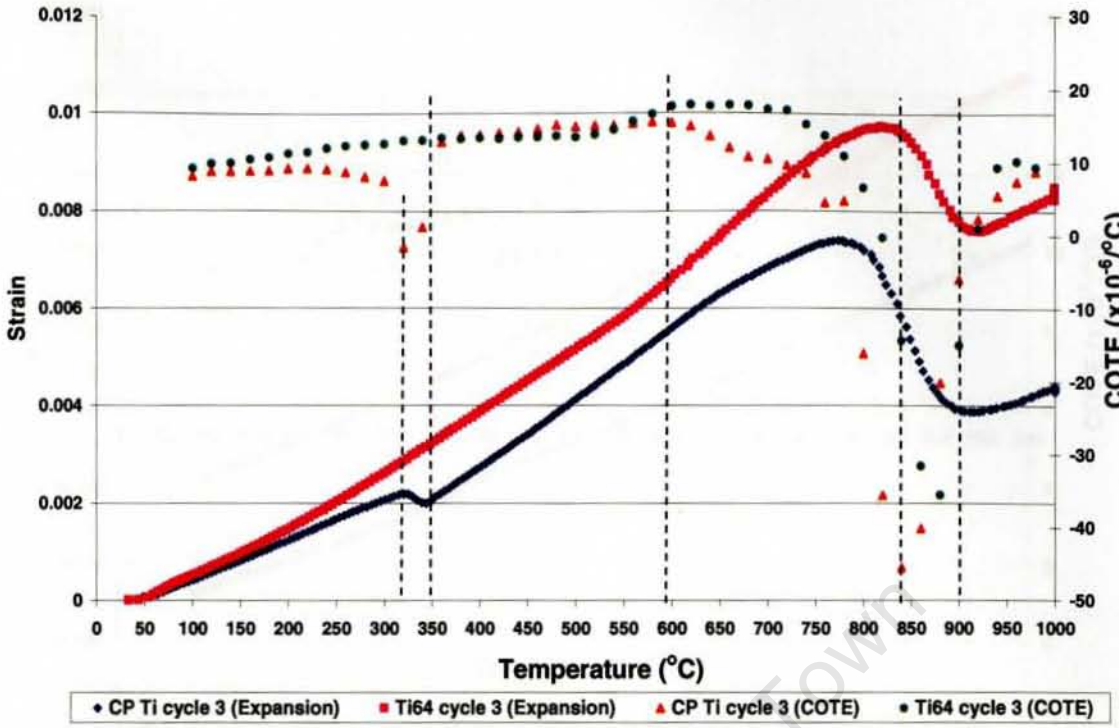

Figure 5.25: *Comparison of Expansion and COTE vs. temperature curves during heating of CP Ti and Ti-6Al-4V, Cycle 3*

From 350-650°C both materials continues to expand at a more or less constant rate of expansion. This is due to the fact that prior to 650°C, little or no hydrogen gets expelled from the specimen, since optimum removal of hydrogen in titanium and its alloys occurs from 650-850°C. In both materials the rate of expansion decreased from 600-810°C due to the expulsion of hydrogen in this temperature interval. The rate of expansion continued to decrease resulting in a volume contraction from 800-900°C in both materials. For Ti-6Al-4V this is attributed to three reasons: i) the dissolution of the hydride phase in Ti-6Al-4V ii) the α to β phase transformation and iii) the continued expulsion of hydrogen from the specimen. For CP Ti this continued decrease in the rate of contraction was only due to the continued expulsion of hydrogen. At the start of Cycle 3, CP Ti contained much more hydrogen than Ti-6Al-4V, and hence the volume contraction (from 800-900°C) in CP Ti is much more pronounced than in Ti-6Al-4V.

During the cooling step of Cycle 3, the behaviour of Ti-6Al-4V follows the same trend as CP Ti (See Figure 5.26). The rate of contraction decreases cooling from 1000°C to 920°C, which is due to the β to α phase transformation. An increase in the rate of contraction is seen cooling from 900°C to 800°C, signifying end of the β to α phase transformation.

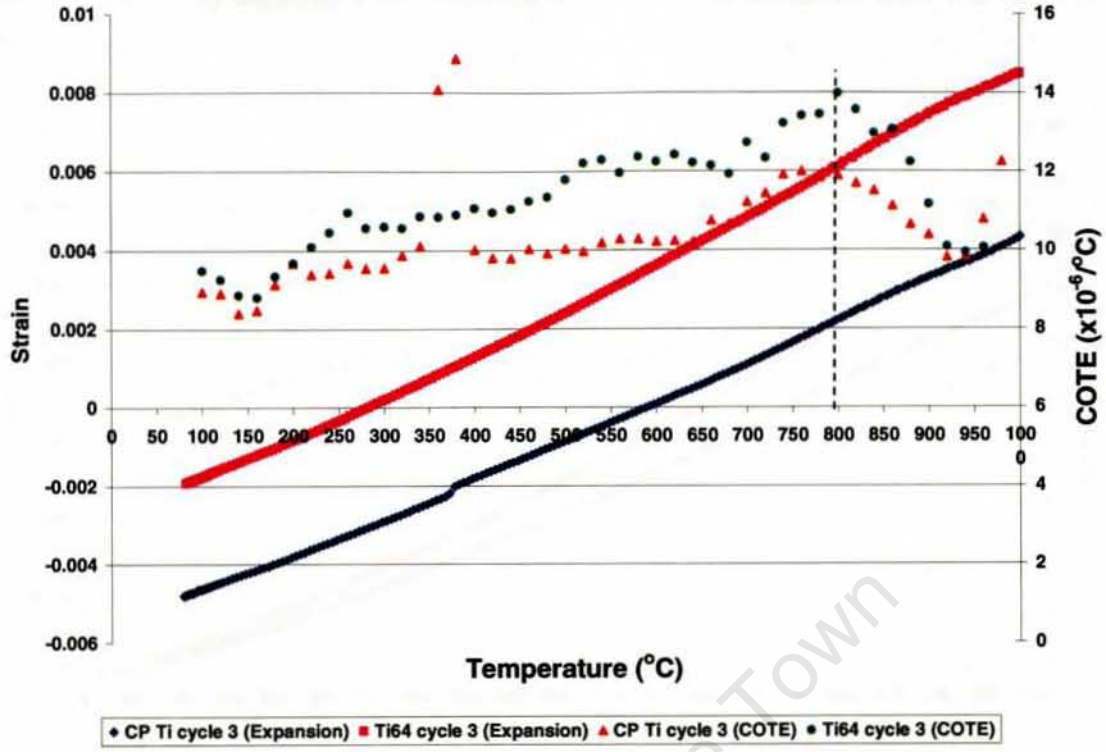

Figure 5.26: *Comparison of Strain and COTE vs. temperature curves during cooling of CP Ti and Ti-6Al-4V, Cycle 3*

5.4.5 Cycle 4, heating and cooling

This section refers to Figures 5.27 and 5.28, for the strain and COTE curves of Cycle 4 during the heating and cooling respectively.

During the heating step of Cycle 4, both materials expands up to 750°C as seen by the strain and COTE curves, due to normal thermal effects during heating (See Figure 5.27). Possible α to β phase transformations occurred from 820-925°C and 820-880°C for CP Ti and Ti-6Al-4V respectively. It is however, unclear as to whether the decrease in the rate of expansion in both materials is significant to attribute it to the α to β phase transformation, since the change in COTE values are very minor. Residual hydrogen, which may be present in CP Ti and Ti-6Al-4V at the start of Cycle 4, may have partially hidden the β-transus in both materials. The two materials, generally exhibits the same trend and it is not clear in both materials whether all the hydrogen had been expelled from the specimens during the dehydrogenation cycle.

During the cooling step in Cycle 4, both materials exhibit the same trend (See Figure 5.28). From the strain curves (that appear relatively linear), it appears as if little or no phase transformation occurred during cooling in both materials. Hence, the reverse β to α transformation could not be identified for the same reasons as explained in the heating step of Cycle 4. During cooling in both materials it is also unclear whether

hydrogen is being expelled if any residual hydrogen had remained after the heating step in Cycle 4.

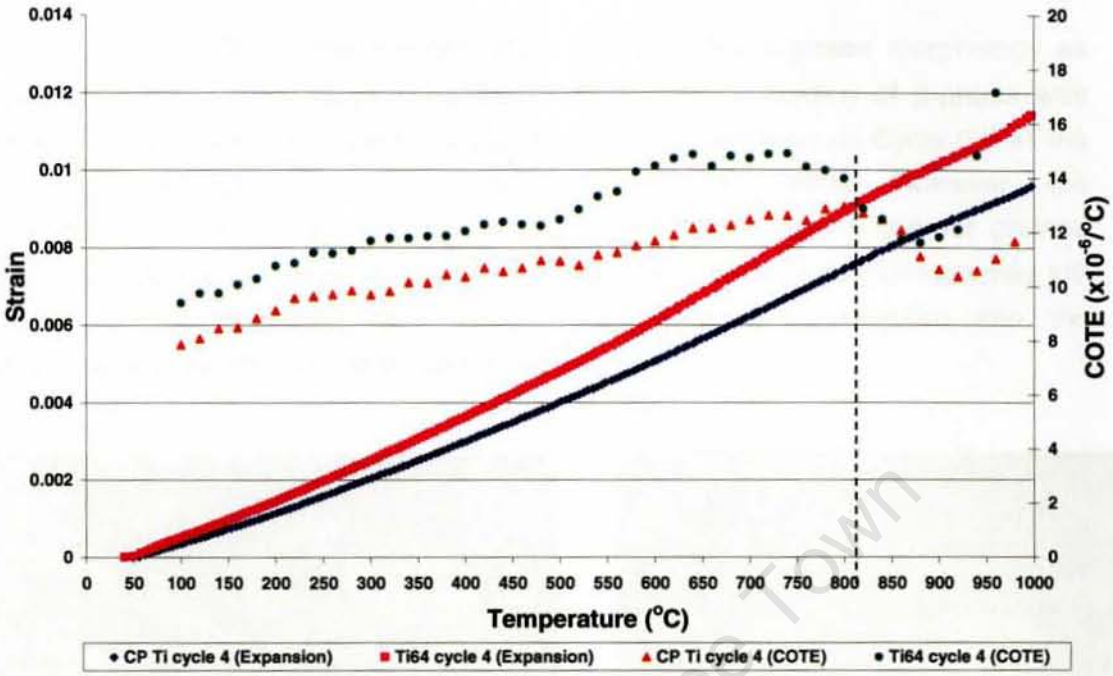

Figure 5.27: *Comparison of Strain and COTE vs. temperature curves during heating for CP Ti and Ti-6Al-4V, Cycle 4*

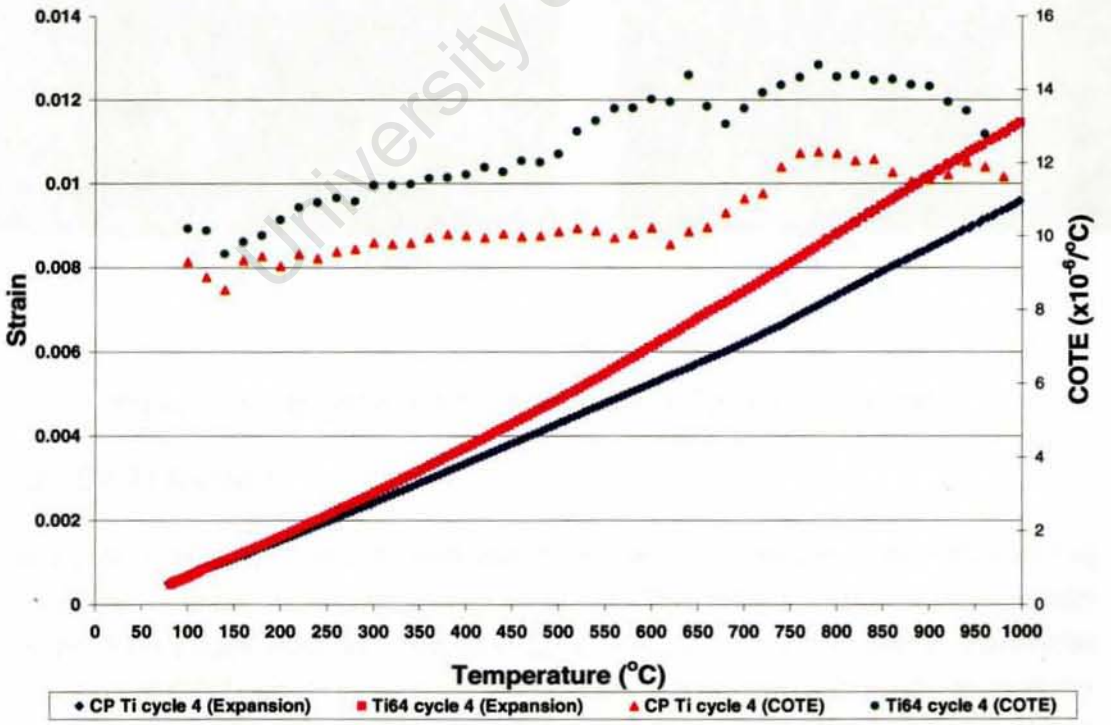

Figure 5.28: *Comparison of Strain and COTE vs. temperature curves during cooling for CP Ti and Ti-6Al-4V, Cycle 4*

5.5 Microstructure analysis

5.5.1 CP Ti Cycles 0 and 4

After Cycle 0 of CP Ti, the microstructure exhibited the α-phase morphology as expected in the α-type alloys (See Figure 5.29a). No indication of β-phase was present. Cycle 4 was expected to display the same morphology as Cycle 0 if all the hydrogen was removed during the dehydrogenation cycle. However, the microstructure of Cycle 4, as shown in Figure 5.29b, displays a coarser grained structure composed of the α-phase. It is unclear as to whether the specimen may still contain residual hydrogen, and hence more detailed investigation into the microstructural constitution would be required.

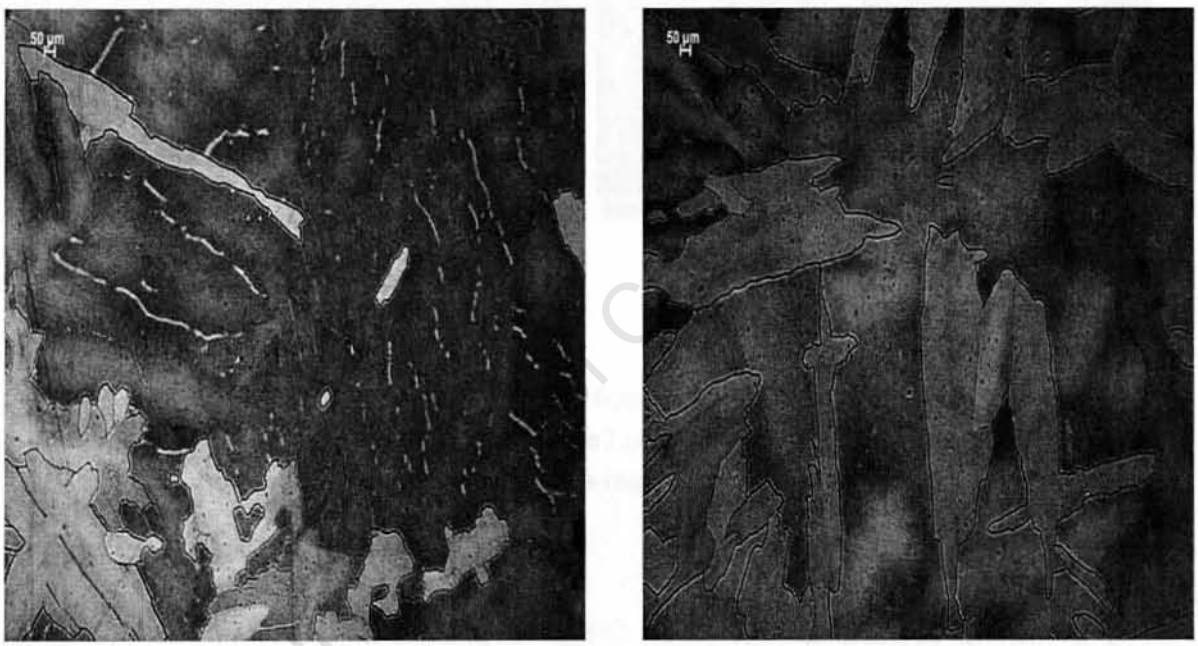

a) b)

Figure 5.29: *Light micrographs of CP Ti after a) Cycle 0 and b) Cycle 4*

5.5.2 CP Ti Cycle 1

After Cycle 1 of CP Ti, the microstructure displayed a mixture of two phases i.e. hydride and α laths, as shown in Figure 5.30a. This microstructure was expected from the Ti-H phase diagram (Figure 2.32b), since after hydrogenation the phase constitution of CP Ti would have been altered due to hydrogen absorption to form the hydride phases during the cooling step of Cycle 1. Figure 5.30b is the corresponding EBSD map, which shows that the dominant phase present after the completion of Cycle 1 is the hcp phase and that two types of hydrides (δ and ε) are present, as

indicated by the yellow and blue regions. Since the crystallography of α and α' (hcp martensite) are the same, it is uncertain as to whether the α' may be present or not after Cycle 1.

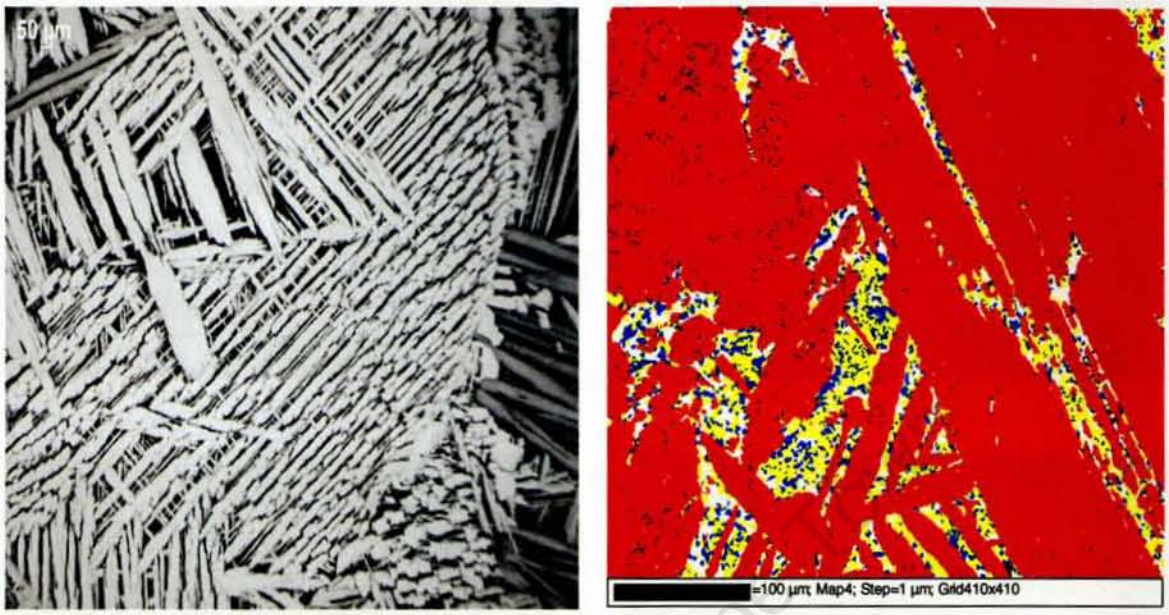

a) b)

Figure 5.30: *a) Light micrograph of CP Ti after Cycle1, showing a mixture of hydride and α phases and b) EBSD map, red regions: hcp (α/α') phase, yellow and blue regions: two forms of hydride phases (δ and ε), white regions: non-indexed regions*

5.5.3 CP Ti 325°C quench at cooling

Heating to 1000°C and quenching at 325°C upon cooling displays a mixture of phases i.e. hydride and α laths as shown in Figure 5.31a and b. From the strain and COTE curves of Cycle 1 (during cooling), at 325°C it was expected that the transformation from β to α had not occurred yet (See Figure 5.5), hence β-phase and not α-phase was expected in this microstructure. This particular microstructure resembles that of Cycle 1 (Figure 5.30a), which means that the process to quench at 325°C was not quick enough and consequently the specimen was cooled to below 325°C before quenching. A SEM image (Figure 5.31c) of the specimen revealed hydride laths and an overlay of the scanned region showed the existence of hydride phases. The corresponding EBSD map (Figure 5.31d) of the scanned region displays two forms of hydrides (δ and ε as seen in Figure 5.30b). This region scanned by the EBSD unit is most likely a region within a hydride lath and does not reflect the overall phase constitution.

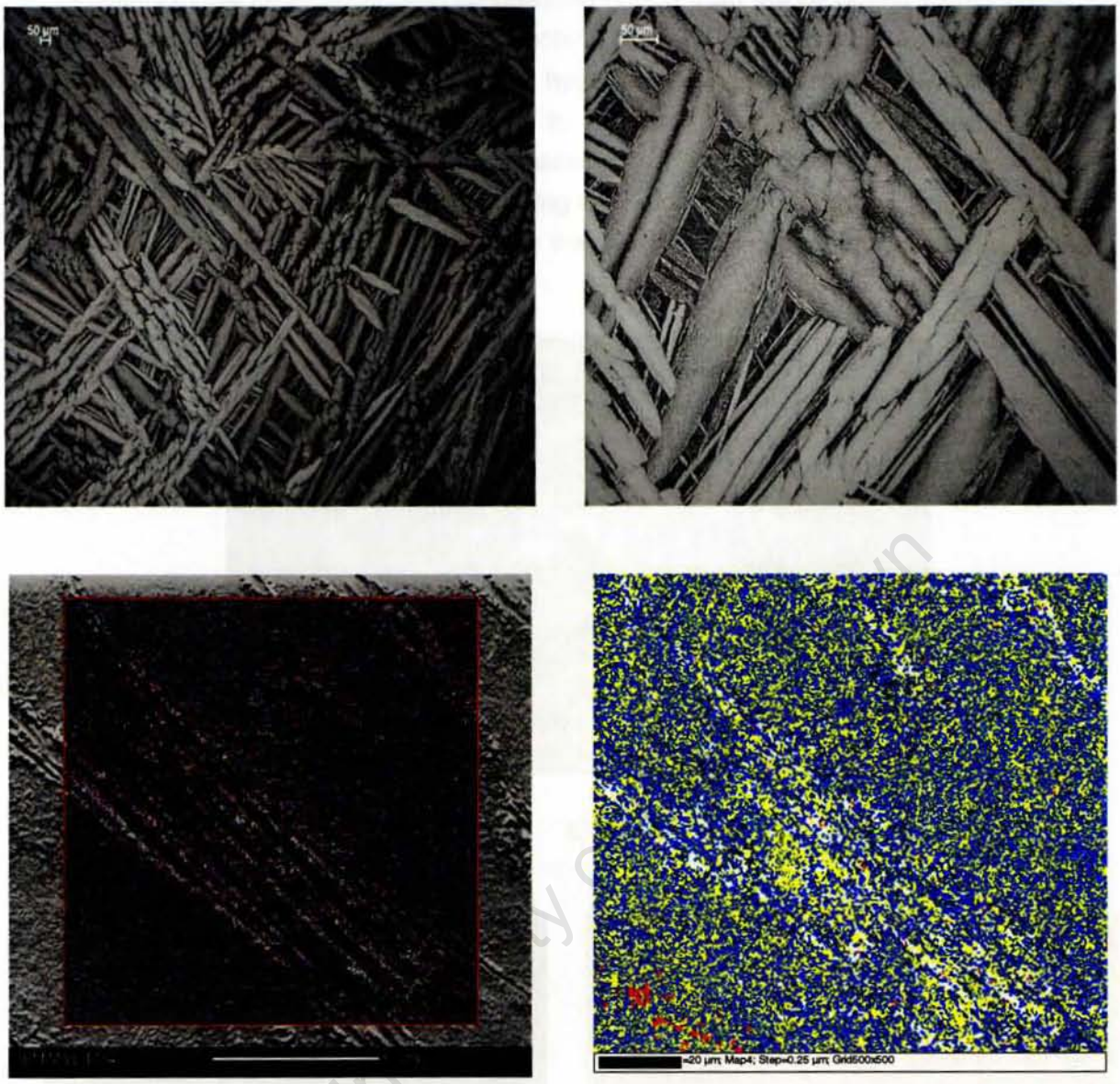

Figure 5.31: *CP Ti after 325°C quench during cooling a) Light micrograph at low magnification b) high magnification displaying and hcp and hydride phases c) SEM image of scanned region (selected region highlighted in red) and d) EBSD map of scanned region, blue and yellow regions: two forms of hydrides (δ and ε)*

5.5.4 CP Ti 750°C quench

Heating to 750°C in a hydrogen environment and quenching in water displayed a large grained structure. Quenching at 750°C was aimed at "freezing" the microstructure at this temperature. From Figure 5.4, at 750°C, the specimen was on the α/β phase boundary, and hence was in a transition state i.e. in the process of transforming from $\alpha_H \rightarrow \alpha_H + \beta_H$. Figure 5.32a exhibits a microstructure which displays that some of the large α-grains had transformed to the smaller β-grains, but is mainly

composed the large α-grains. The scanned region from the SEM and EBSD images (Figures 5.32b and c) shows that quenching from 750°C resulted in a mixture of hcp (either the α or α') and two forms of hydrides (δ and ε) dispersed within the hcp phase. Hydrides were not expected to be present at room temperature, since quenching at 750°C was meant to "freeze" the microstructure at this temperature. This suggests that the cooling rate during quenching was not fast enough in order to "freeze" the microstructure, and hence the precipitation of hydrides occurred during cooling.

a)

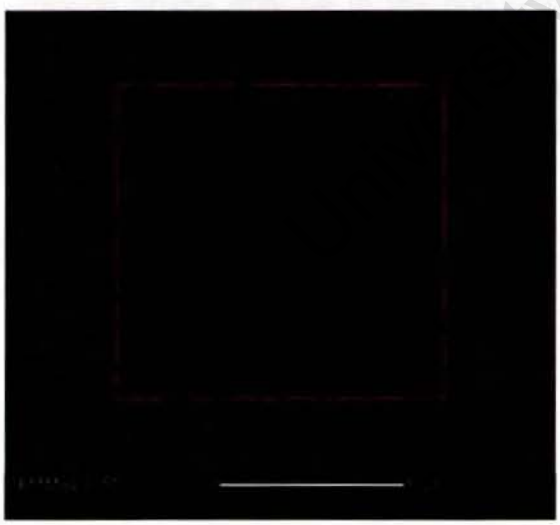

b)

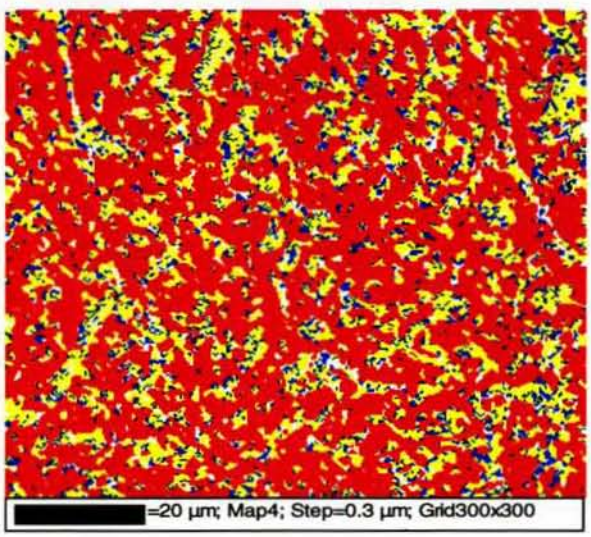

c)

Figure 5.32: *CP Ti after 750°C quench a) Light micrograph at low magnification displaying large α-grains and smaller β-grains b) SEM image of scanned region (selected region highlighted in red) and c) EBSD map of scanned region, red region: hcp phase (α/α'), yellow and blue regions: two forms of hydrides (δ and ε)*

5.5.5 CP Ti, 825°C quench

The microstructure after quenching from 825°C is composed of an equiaxed prior β-phase grain structure, which transformed to the hcp phase during cooling. The grain size is much smaller than that of the specimen quenched at 750°C (Figure 5.32a). This is due to the fact that the specimen at 825°C had transformed from the large grained α-phase to the smaller grained fully β-phase, as explained by the analysis of the strain and COTE curves of Cycle 1 (heating) (See section 5.2.1). The SEM and EBSD images, (Figures 5.33b and c) displays equiaxed hcp grains, which contains a large volume of intragranular hydride precipitates. It is uncertain if the hcp phase is α-phase or the α'-martensite, since the crystallography of α and α' is the similar, and hence EBSD detects α and α' as the same phase.

5.5.6 CP Ti quenched at 940°C during heating (Cycle 1-hydrogenation)

After quenching from 940°C, the microstructure displays a lamellar-type morphology (See Figures 5.34a and b). The lamellar structure exhibits alternating hcp (α/α') and hydride phases, whereby the hydrides formed during cooling. At 940°C, the specimen contained far more hydrogen than at 825°C (See Figure 5.4), which resulted in this lamellar-type morphology.

The presence of hydrides was not detected because the EBSD software was only requested to identify the α and β phases during indexing. The presence of the hydride phase may be in the non-indexed regions. As a result of this, the non-indexed region indicated that a phase(s) other than the hcp phase was also present. At higher magnification, in a different region within the specimen, Figures 5.34e and f shows that this other phase(s) were two forms of hydrides (δ and ε).

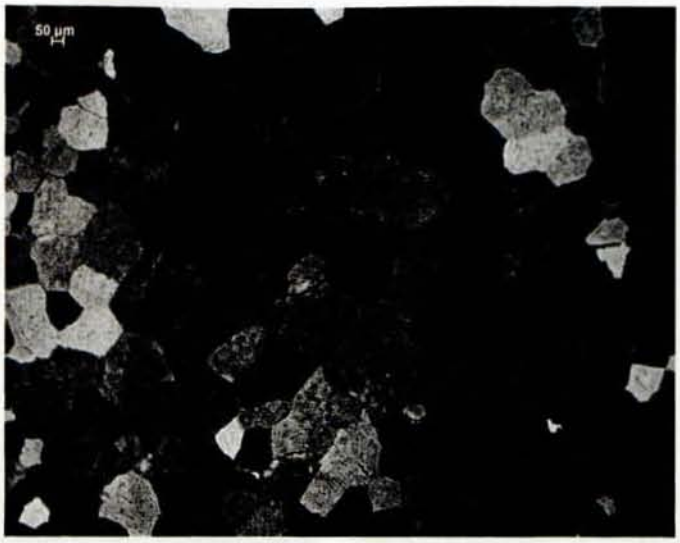

a)

b)

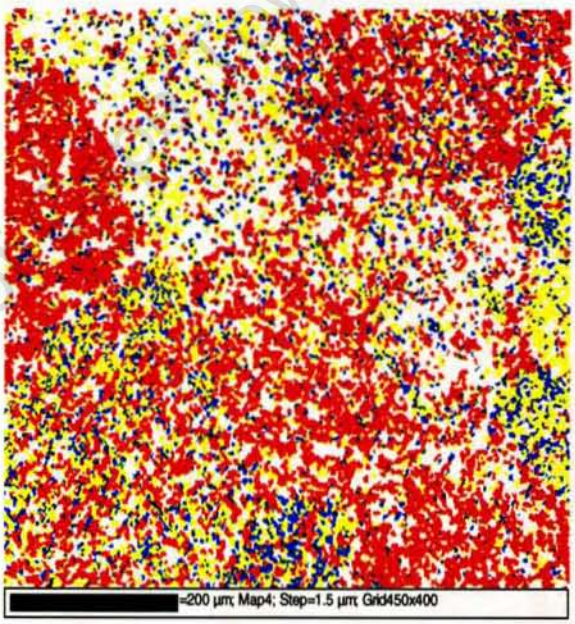

c)

Figure 5.33: *a) Light micrograph of CP Ti after 825°C quench, displaying an equiaxed grain structure with a mixture of a hcp (α/α') and hydride phases b) SEM image of scanned region (selected region highlighted in red) displaying distinct grains and c) EBSD map of scanned region displaying the composition of the grains, red regions: hcp (α/α') phase, yellow and blue regions: two forms of hydride phases (δ and ε), and white regions: non indexed regions*

a)

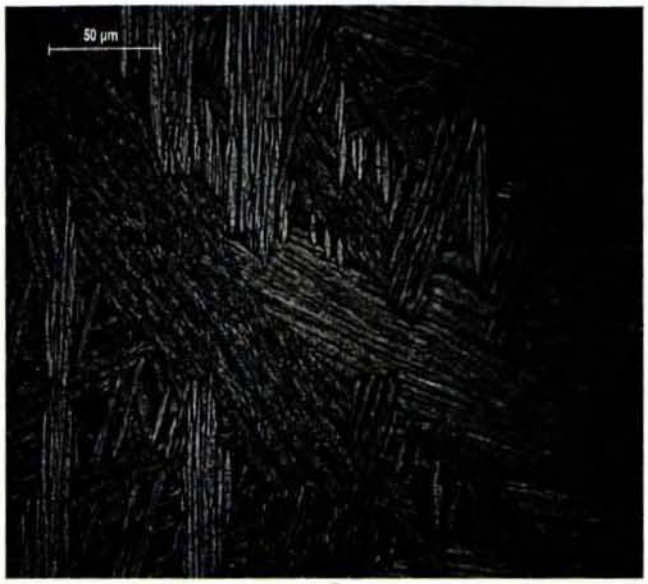

b)

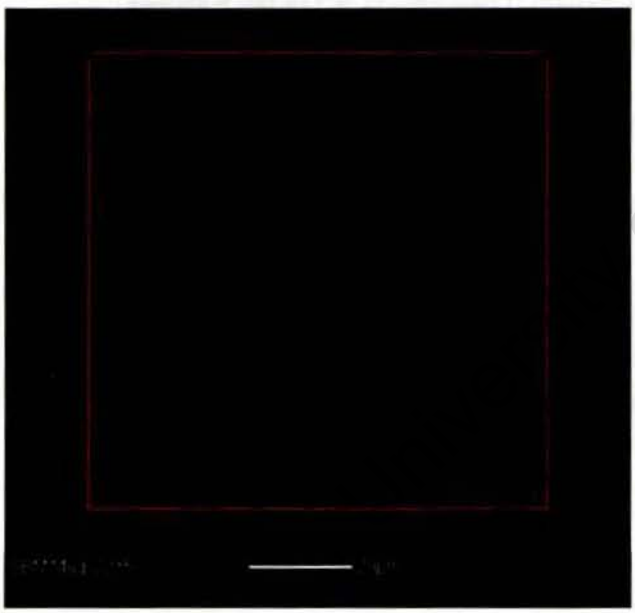

c)

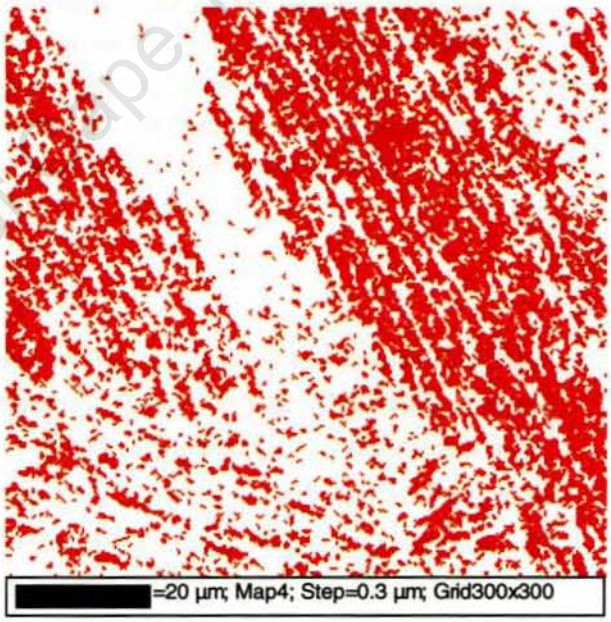

d)

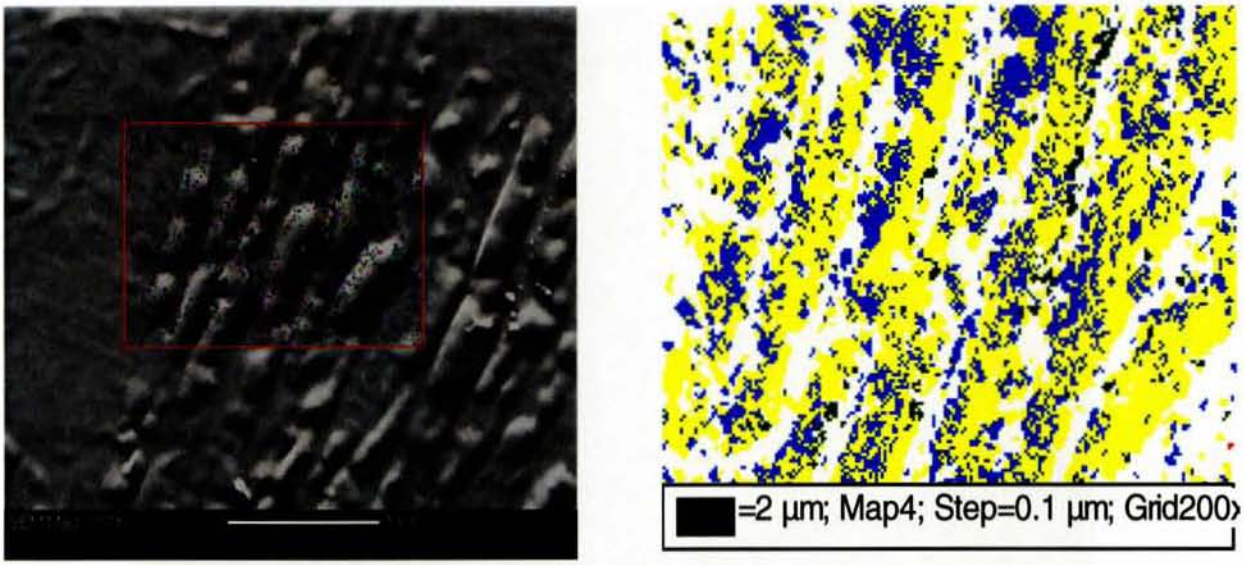

e) f)

Figure 5.34: *a) CP Ti after 940°C quench a) Light Micrograph at low magnification and b) high magnification c) SEM image of scanned region (selected region highlighted in red), d) EBSD image of scanned region in (c), red region: hcp (α/α') phase, white regions: non-indexed regions, e) SEM image of a different region within the specimen (at higher magnification) and f) EBSD image of scanned region in (e), yellow and blue regions: two forms of hydride phases (δ and ε)*

5.5.7 Ti-6Al-4V Cycle 0

After Cycle 0 of Ti-6Al-4V, the Widmanstätten microstructure formed due to the slow cooling from 1000°C to room temperature (heating and cooling rate 1°C/min). A slow cooling rate results in β decomposition by a diffusional process i.e. nucleation and growth in the solid state. The structures formed are primary α-particles on the grain boundaries and Widmanstätten α-plates. These Widmanstätten plates nucleated at the α-allotromorphous and growth to the matrix. The prior β grain boundary remains visible even after cooling to room temperature, as shown in Figure 5.35.

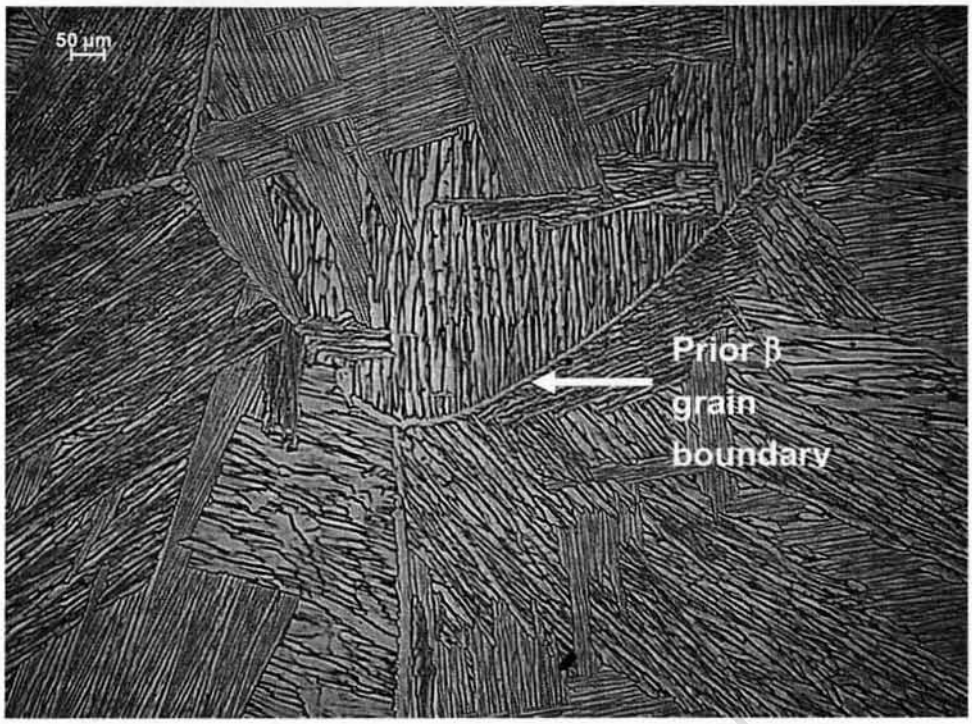

Figure 5.35: *Light micrograph of Ti-6Al-4V after Cycle 0, displaying Widmanstätten plates and the prior β grain boundary*

5.5.8 Ti-6Al-4V quenched at 1000°C during heating (Cycle 1-hydrogenation)

Quenching from 1000°C during hydrogenation resulted in a needle like martensite structure (α'), whereby the prior grain β grain boundary can still be seen. The only phase that can be identified in the microstructure is the martensite (α') type structure, which is characteristic of Ti-6Al-4V during fast cooling from its parent phase (β). The prior β grain boundary can also still be seen as shown in Figure 5.36. This suggests that at 1000°C the specimen was in the single β-phase field as indicated by the Ti-6Al-4V phase diagram (Figure 2.32a). No hydride phase can be seen in the microstructure.

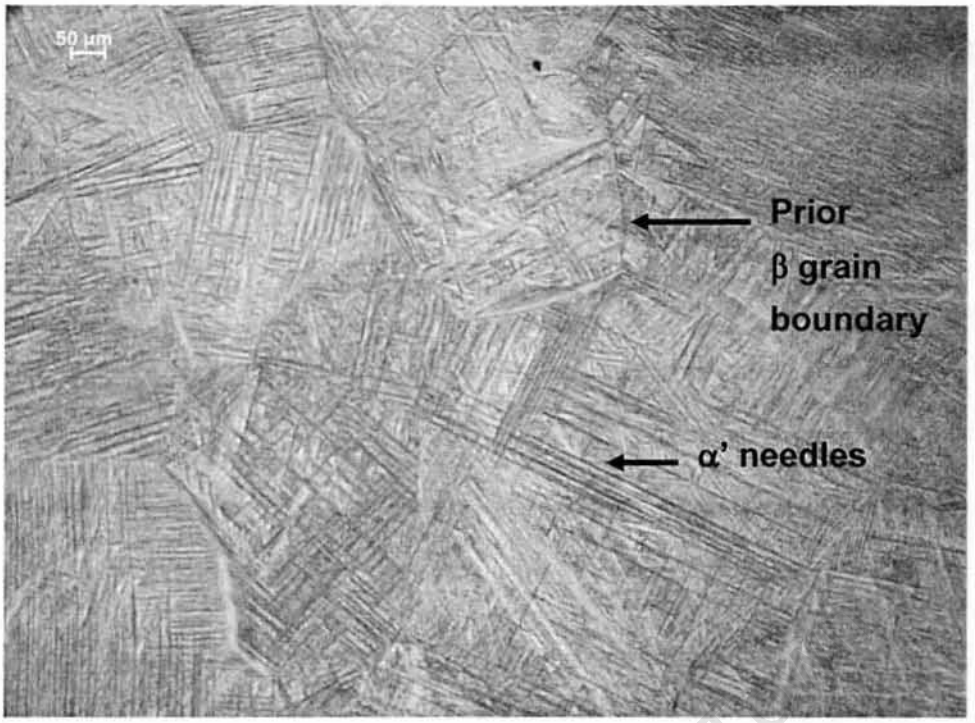

Figure 5.36: *Light micrograph of Ti-6Al-4V after 1000°C quench, displaying martensite (α') needles*

5.5.9 Ti-6Al-4V Cycle 1

After Cycle 1 a basket-weave type structure is seen with α laths in a β matrix, as shown by Figure 5.37a and the EBSD map (Figure 5.37b). The presence of hydrides was not detected because the EBSD software was only requested to identify the α and β phases during indexing. The presence of the hydride phase may be in the non-indexed regions. Furthermore, EBSD could not identify α' because it has a similar crystallography as α, and hence α' might have been detected as α during indexing. As established from Figure 5.36, at 1000°C the single β-phase existed, hence cooling from this region will lead to a mixture of α+β+δ as predicted by the Ti-6Al-4V phase diagram (Figure 2.32a).

a) b)

Figure 5.37: *Ti-6Al-4V after Cycle 1 a) Light micrograph and b) EBSD map, red regions: hcp (α/α') phase, yellow regions: β phase, white regions: non-indexed regions*

5.5.10 Ti-6Al-4V Cycle 2

Cycle 2 was the reheating and cooling of the hydrogenated specimen (after Cycle 1) in a hydrogen environment, hence the hydrogen content is greater in Cycle 2 than in Cycle 1. However, from Figures 5.13 and 5.14 the strain and COTE curves (of the two thermal cycles) were fairly similar, and hence it is not surprising that the microstructure after Cycle 2 is the same as that of Cycle 1 (See Figures 5.37a and 5.38a). From Figure 5.38a, the same basket-weave type structure consisting of the α and β phases is seen, which is similar to Figure 5.37a. The EBSD map (Figure 5.38b) also displays the presence of the basket-weave type structure (α-phase in a β matrix). The presence of hydrides was not detected because the EBSD software was only requested to identify the α and β phases during indexing (as in Cycle 1). The presence of the hydride phase may be in the non-indexed regions. Furthermore, EBSD could not identify α' because it has a similar crystallography as α, and hence α' might have been detected as α during indexing.

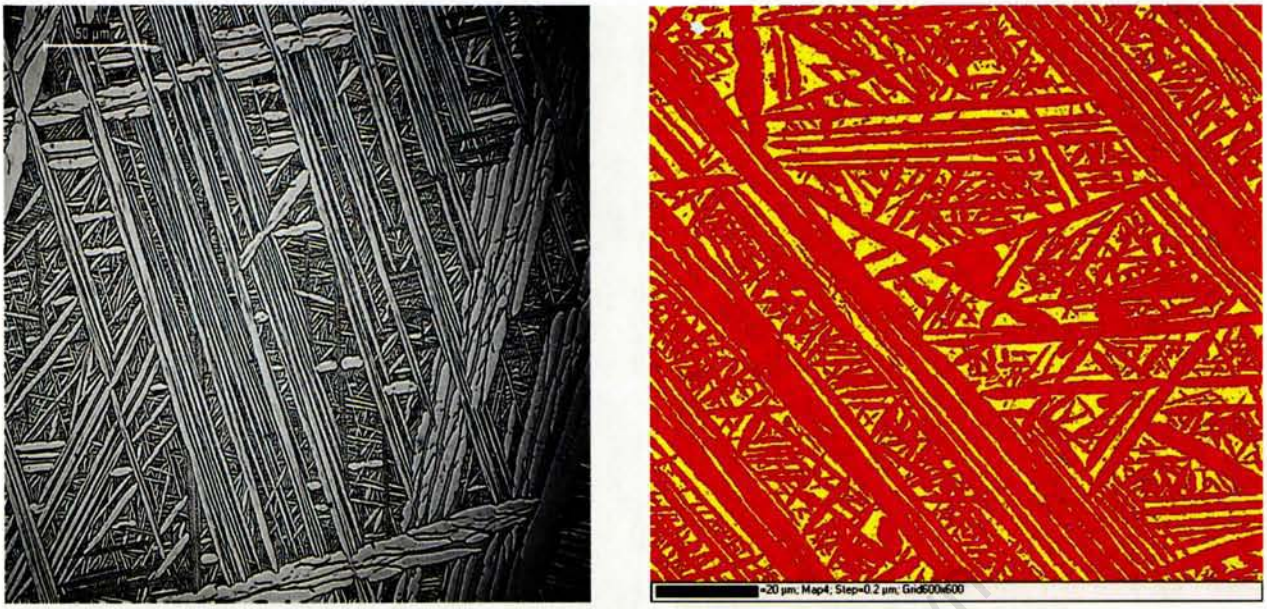

a) b)

Figure 5.38: *Ti-6Al-4V after Cycle 2 a) Light micrograph b) EBSD map, red regions: hcp (α/α') phase, yellow regions: β phase, white regions: non-indexed regions*

5.5.11 Ti-6Al-4V Cycle 3

The microstructure of Cycle 3 (dehydrogenation cycle), as seen in Figure 5.39a, displays a similar morphology as that of Cycle 0 (Ti-6Al-4V heated in vacuum), without any indication of the presence of a hydride phase. This suggests that the dehydrogenation process removed a substantial amount of hydrogen with the decomposition of the hydride phase, which was present after Cycle 2. The non-indexed regions in the shown in Figure 5.39b suggest that a phase other than the α and β phase could exist within the specimen. The presence of hydrides was not detected because the EBSD software was only requested to identify the α and β phases during indexing. The presence of the hydride phase may be in the non-indexed regions.

a) b)

Figure 5.39: *Ti-6Al-4V after Cycle 3 a) Light micrograph b) EBSD map, red regions: hcp (α/α') phase, yellow regions: β phase, white regions: non-indexed regions*

5.5.12 Ti-6Al-4V Cycle 4

Cycle 4 (the post-dehydrogenation step in vacuum) exhibited a similar microstructure as that of Cycle 3 (Figure 5.39a), as seen in Figure 5.40a. This suggests that the specimen could have a similar phase constitution as Cycle 3 (after heating and cooling) i.e. Widmanstätten laths in a β matrix. Figure 5.40b is the corresponding EBSD map, the black regions signifying the grain boundaries. The grains are much coarser than that of Cycle 3. The reason for this is uncertain and would require more detailed investigation into the microstructural constitution and evolution.

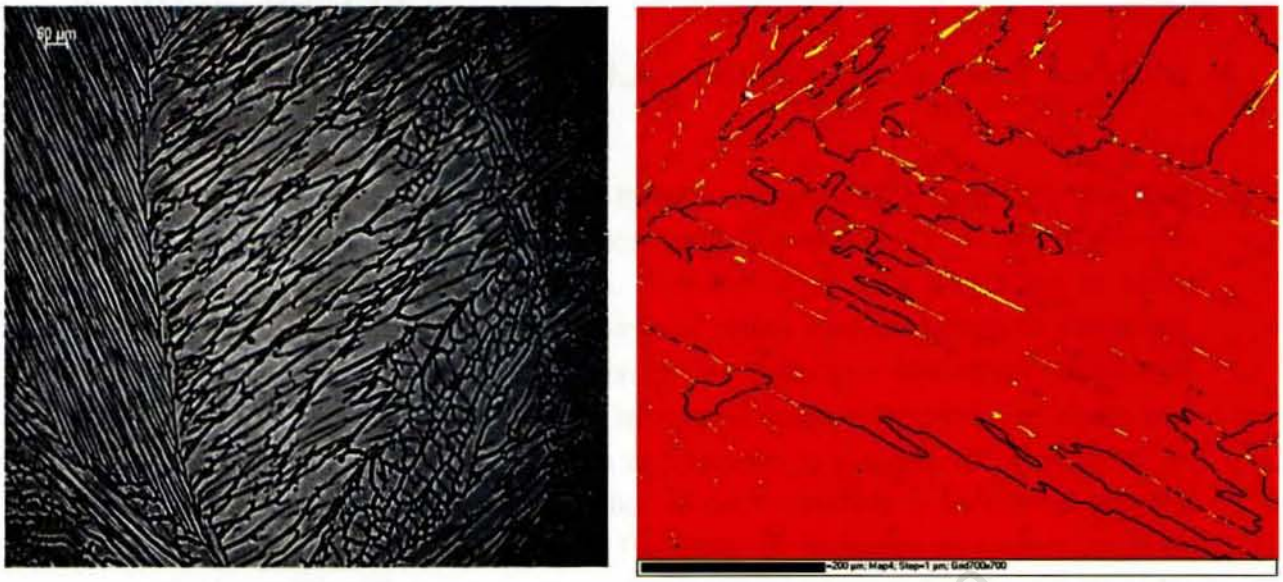

Figure 5.40: *Ti-6Al-4V after Cycle 4 a) Light micrograph showing coarse α grains in a β matrix b) EBSD map, red regions: hcp (α/α') phase, yellow regions: β phase, white regions: non-indexed regions and black regions: grain boundaries*

6 CONCLUSIONS

The push-rod dilatometer was successfully modified to act as a dual functioning dilatometer/hydrogen furnace.

Dilatometry with *in-situ* hydrogenation thermal cycles was successfully used to monitor the real-time phase transformation behaviour of both CP Ti and Ti-6Al-4V, before, during and after hydrogenation. This technique was also used to show marked differences and similarities in terms of phase transformations of these two materials. Dilatometry was used to monitor the hydrogen absorption (uptake of hydrogen) and desorption (expulsion of hydrogen) process by means of strain and COTE curves. Furthermore, the addition of hydrogen to a stable CP Ti and the Ti-6Al-4V alloy caused the phase composition of both materials to be altered coupled with the formation of hydride phases. The level of hydrogen absorption in both materials during the different thermal cycles could be estimated. This was done by combining the output of the dilatometry and SEM/EBSD analysis with the published phase diagrams.

A series of specific conclusions were drawn:

- Dilatometry was able to estimate the limit of hydrogen absorbed during the hydrogenation cycle; in CP Ti this was ±40at%H and in Ti-6Al-4V it was >15at%H

- The sequence of phase transformations for CP Ti during and hydrogenation differed significantly from Ti-6Al-4V

- During hydrogenation (Cycle 1) in CP Ti, the phase transformation sequence during heating could be summarised as follows:

$$\alpha \rightarrow \alpha_H \rightarrow \alpha_H + \beta_H \rightarrow \beta_H \rightarrow \beta_H + (G)$$

- During hydrogenation (Cycle 1) in CP Ti, the phase transformation sequence during cooling could be summarised as follows:

$$\beta_H \rightarrow \alpha_H + hydride$$

- During hydrogenation (Cycle 1) in Ti-6Al-4V the phase transformation sequence during heating could be summarised as follows:

$$\alpha + \beta \rightarrow \alpha_H + \beta_H \rightarrow \alpha_H + \beta_H + \delta \rightarrow \beta_H$$

- During hydrogenation (Cycle 1) in Ti-6Al-4V the phase transformation sequence during cooling could be summarised as follows:

$$\beta_H \rightarrow \alpha_H + \beta_H + \delta$$

- The uptake of hydrogen only occurred from ±550°C for both CP Ti and Ti-6Al-4V
- Hydrogen caused the lattice expansion of CP Ti and Ti-6Al-4V during hydrogenation (Cycle 1), which was seen by the strain and COTE curves
- Hydrogen in solid solution lowered the β-transus of CP Ti to ~ 300°C as predicted by the Ti-H phase diagram.

7 FUTURE WORK

The following recommendations are made in order to further understand the phase transformation behaviour during each thermal cycle for both CP Ti and Ti-6Al-4V:

- Water quench experiments during each thermal cycle at pertinent temperatures should be devised in order to monitor phase transformations at critical temperatures

- Since this project only focussed on non-isothermal phase transformations, TTT curves could not be constructed during each thermal cycle. Hence, a series of isothermal treatments should be performed for each thermal cycle at pertinent temperatures. This will allow for the further monitoring the kinetics of phase transformations of CP Ti and Ti-6Al-4V before, during after hydrogenation

- Since the amount of hydrogen could not be accurately quantified during the hydrogen absorption and desorption process, the phase diagrams for Ti-H and Ti-6Al-4V could not be accurately used to quantify the phases present using the lever rule. Hence, a technique should be devised to accurately quantify the amount of hydrogen present in the specimen

- Quantitative phase analysis should be performed on the EBSD maps in order to understand how the addition of hydrogen altered the phase composition of CP Ti and Ti-6Al-4V during and after hydrogenation. This would require more extensive EBSD sampling of the microstructure

- Further quantitative phase and hydrogen content analysis should be performed on Cycle 4 in order to understand the post-hydrogenation behaviour of CP Ti and Ti-6Al-4V and to ascertain whether dehydrogenation was successful in removing all the hydrogen from the specimen

8 REFERENCES

1. O.N. Senkov and F. H. Froes, *Thermohydrogen processing of titanium alloys*, International Journal of Hydrogen Energy **24** (1999), 565-576.

2. H. Wipf (Editor), *Hydrogen in metals iii*, Springer, 1997.

3. A. D. Mcquillian, *An experimental and thermodynamic investigations of the hydrogen-titanium system*, Proceedings of the Royal Society of London Series A **204** (1951), 309-322.

4. A. San-Martin and F. D. Manchester, *The H-Ti (hydrogen-titanium) system*, Journal of Phase Equilibria **8** (1987), 30-42.

5. B. A. Kolachev, *Reversible alloying of titanium alloys with hydrogen*, Metal Science and Heat treatment **35** (1993), 586-596.

6. J.I. Qazi, O. N. Senkov, J. Rahim and A. Genc, *Phase transformations in Ti-6Al-4V-xH alloys*, Metallurgical and Materials Transactions A **32A** (2001), 2453-2463.

7. A. Guitar, G. Vigna and M. I. Luppo, *Microstructure and tensile properties after thermohydrogen processing of Ti-6Al-4V*, Journal of Mechanical behaviour of Biomedical Materials **2** (2009), 156-163.

8. K. L. Housley, *Black sand: The history of titanium*, Metal Management Aerospace, Inc., 2007.

9. E. Tal-Gautelmacher and D.Eliezer, *The hydrogen embrittlement of titanium-based alloys*, JOM Journal of Minerals, Metals and Materials Society **57** (2005), no. 9, 46-49

10. S. Lathabai, B. L. Jarvis and K. J. Barton, *Comparison of keyhole and conventional gas tungsten arc welds in commercially pure titanium*, Materials Science and Engineering **A299** (2001), 81-93.

11. R.R. Pawar and V. T. Deshpande, *The anisotropy of the thermal expansion of α-titanium*, Acta Crystallography **A24** (1968), 316-317.

12. R. Boyer, E. W. Collings and G. Welsch, *Materials properties handbook: Titanium alloys*, Materials Park (OH): ASM International, 1994.

13. C. Wu, V. Kumar, J. Liau, F. L'Esperance and G. Baker, "99.0ti," eFunda (Engineering Fundamentals) online, 2010.

14. W. F. Smith, "Structure and properties of engineering alloys," McGraw-Hill Publishing Co., 1981.

15. H. K. D. H. Bhadeshia, "Metallurgy of titanium and its alloys," University of Cambridge, Cambridge, 2004.

16. C. Leyens and M.Peters, *Titanium and titanium alloys: Fundamentals and applications*, Wiley-VCH Verlag GmbH & Co, 2003.

17. J. L. Murray (Editor), *The Al-Ti (Aluminium-Titanium) phase system. Phase diagrams of binary titanium alloys*, ASM, 1987.

18. D. R. Askerland, *The science and engineering of materials*, Stanely Thornes Ltd, 1998.

19. J.W. Elmer, T. A. Palmer and S. S. Babu, *In situ observations of lattice expansion and transformation rates of α and β phases in Ti-6Al-4V*, Materials Science and Engineering **A 391** (2005), 104-113.

20. C. Wu, V. Kumar, J. Liau, F. L'Esperance and G. Baker, "Ti-6Al-4V," eFunda (engineering fundamentals) online, 2010.

21. C. Garcia de Andries, F. G. Caballero, C. Capdevila and L. F. Alvarez, *Application of dilatometric analysis to the study of solid-solid phase transformations in steels*, Materials Characterization **48** (2002), 101-111.

22. M. Motyka and J. Sieniawski, *The influence of initial plastic deformation on microstructure and hot plasticity of α+β titanium alloys*, Archives of Materials Science and Engineering **41** (2010), 95-103.

23. N.S. Reddy, C. S. Lee, J.H. Kim and S. L. Semiatin, *Determination of the beta-approach curve and the beta-transus temperature for the titanium alloys using sensitivity analysis of a trained neural network*, Materials Science and Engineering **A434** (2006), 218-226.

24. M. Wei, A. J. Ruys and M. V. Swain, *Interfacial bond strength of electrophoretically deposited hydroxyapatite coatings on metals*, Journal of Materials Science: Materials in Medicine **10** (1999), 401-409.

25. S. Tamirisakandala, R. B. Bhat and D. B. Miracle, *Effect of boron on the beta transus of Ti-6Al-4V alloy*, Scripta Materialia **53** (2005), 217-222.

26. S. Malinov, Z.Guo, W. Sha and A. Wilson, *Differential scanning calorimetry study and computer modelling of β to α phase transformation in a Ti-6Al-4V alloy*, Metallurgical and Materials Transactions **32A** (2001), 879-887.

27. A. A. Ilyin, B. A. Kolachev and A. M. Mamanov, "Titanium '92: Science and technology," F. H. Froes and I. Caplan (Editors), vol. 1, TMS, Warrendale, PA, 1992, pp. 941-947.

28. W. R. Kerr, P. R. Smith, M. E. Rosenblum, F. J. Gurney, Y. R. Mahajan and L. R. Bidwell, "Titanium 80: Science and technology," H. Kimura and O. Izumi (Editors), vol. 4, TMS, Warrendale, PA, 1980, pp. 2477-2486.

29. R. Shivpuri, J. Hua, P. Mittal and A. K. Srivastava, "Industrial,welding and systems engineering," The Ohio State University, Columbus, USA, 2002, pp. 1-4.

30. S.L. Semiatin, S. L. Knisley, P. N. Fagin, F. Zhang and D. R. Barker, *Microstructure evolution during alpha-beta heat treatment of Ti-6Al-4V*, Metallurgical and Materials Transactions A **34A** (2003), 2377-2386.

31. W. Sha and Z.Guo, *Letter: Phase evolution of Ti-6Al-4V during continuous heating*, Journal of Alloys and Compounds **290** (1999), L3-L7.

32. R. Filip, K. Kubiak, W. Ziaja and J. Sieniawski, *The effect of the microstructure on the mechanical properties of the two-phase titanium alloys*, Journal of Materials Processing Technology **133** (2003), 84-89.

33. D. Phelan, M. Reid, N. Stanford and R. Dippenaar, *In-situ observations of phase transformations in titanium*, JOM Journal of Minerals, Metals and Materials Society **58** (2006), 67-69.

34. T. Ahmed and H. J. Jack, *Phase transformation during cooling in α+β titanium alloys*, Materials Science and Engineering A **243** (1998), 206-211.

35. M. R. Plichta, J. C. Williams and H. I. Aaronson, *On the existence of β to α_m transformation in the alloy systems Ti-Ag, Ti-Au and Ti-Si*, Metallurgical and Materials Transactions A **8** (1977), 1885-1892.

36. E. W. C. R. Boyer, and G. Welsch (Editor), *Material properties handbook: Titanium alloys*, ASM International, 1994.

37. X.L. Han, Q. Wang, D. L. Sun, T. Sun and Q. Guo, *First principle study of hydrogen diffusion in alpha Ti*, International Journal of Hydrogen Energy **34** (2009), 3983-3987.

38. C.P. Liang and H. R. Gong, *Fundamental influence of hydrogen on the various properties of α-titanium*, International Journal of Hydrogen Energy **35** (2010), 3812-3816.

39. D. Eliezer, N. Eliaz, O. N. Senkov and F. H. Froes, *Positive effects of hydrogen in metals*, Materials Science and Engineering A **280** (2000), 220-224.

40. E. Tal-Gautelmacher, D. Eliezer and D. Eylon, *The effects of low fugacity hydrogen in duplex and beta-annealed Ti-6Al-4V alloy*, Materials Science and Engineering A **381** (2004), 230-236.

41. A. Lopez-Suarez, J. Rickards and R. Trejo-Luna, *Analysis of hydrogen absorption by Ti and Ti-6Al-4V using the ERDA technique*, International Journal of Hydrogen Energy **28** (2003), 1107-1113.

42. W. R. Kerr, *The effect of hydrogen as a temporary alloying element on the microstructure and tensile properties of Ti-6Al-4V*, Metallurgical and Materials Transactions A **16** (1981), 1077-1087.

43. R. J. Smickley and L. E. Darid, US Patent no: 4505746 1985.

44. L. Levin, R. G. Vogt, D. Eylon and F. H. Froes, 5th International conference on Titanium. In, Deutsche Gesellshaft fur Metallkunde, 1984, p.^pp. 2107-2114.

45. C. F. Yolton and F. H. Froes, vol. US Patent no: 4219357, 1980.

46. 6th International conference on Titanium. In, Les Editions de Physique, 1988, p.^pp. 1641-1646.

47. N. Ninomi, B. Gong, T. Kobayashi, T. Ohyabu and O. Toriyama, *Fracture characteristics of Ti-6Al-4V and Ti-5Al-2.5Fe with refined microstructure using hydrogen*, Metallurgical and Materials Transactions A **26** (1995), 1141-1151.

48. A. A. Ilyin, I. S. Polkin, A. M. Mamonov and V. K. Nosov, "Thermohydrogen treatment- the base of hydrogen technology of titanium alloys," *Titanium '95: Science and Technology*, vol. 4, 1995.

49. H. Okamoto, *H-Ti (hydrogen-titanium)*, Journal of Phase Equilibria and Diffusion: Supplemental Literature Review: Section III (2011).

50. J.I. Qazi, O. N. Senkov, J. Rahim and F. H. S. Froes, *Kinetics of martensite decomposition in Ti-6Al-4V-xH*, Materials Science and Engineering A **359** (2003), 137-149.

51. Z. Sun, H. Hou, W. Zhou, Y. Wang and Z. Li, *The effect of hydrogen on microstructures evolution and deformation behaviour of Ti-6Al-4V alloys,* Journals of Alloys and Compounds **476** (2009), 550-555.

52. J. Zhao, H. Ding, W. Zhao, X. Tian, H. Hou and Y. Wang, *Influence of hydrogenation on microstructures and microhardness of Ti-6Al-4V alloy*, Transactions Nonferrous Metals Society of China **18** (2008), 506-511.

53. D.B. Shan, Y. Y. Zong, T. F. Lu and Y. Lv, *Microstructural evolution and formation mechanism of fcc titanium hydride in Ti-6Al-4V-xH alloys*, Journal of Alloys and Compounds **427** (2007), no. 229-234.

54. G. Domizzi, M. I. Luppo and G. Vigna, *Microstructural features of the hydrogenation process in Ti grade 2*, Journal of Alloys and Compounds **424** (2006), 193-198.

55. C.C. Shen and T. P. Perng, *Pressure-composition isotherms and reversible hydrogen-induced phase transformations in Ti-6Al-4V*, Acta Materialia **55** (2007), 1053-1058.

56. D. Setoyama, J. Matsunaga, H. Muta, M. Uno and S. Yamanaka, *Mechanical properties of titanium hydride*, Journal of Alloys and Compounds **381** (2004), 215-220.

57. L. Luo, Y. Su, J. Guo and H. Fu, *Formation of titanium hydride in Ti-6Al-4V alloy*, Journal of Alloys and Compounds **45** (2006), no. 140-144.

58. H. K. D. H. Bhadeshia, *Bainite: Overall transformation kinetics*, Journal de Physique Archives **43** (1982), no. C4, 433-448.

59. F. J. Humpreys, *Review grain and sub grain characterization by electron back scatter diffraction*, Journal of Materials Science **36** (2001), 3833-3854.

60. "Basics of EBSD," vol. 2010, Oxford instruments PLC, Oxfordshire, 2005.

61. O. N. Senkov, B. C. Chakoumakos, J. J. Jonas and F. H. Froes, *Effect of temperature and hydrogen concentration on the lattice parameter of the beta titanium*, Materials Research Bulletin **36** (2001), 1431-1440.

9 APPENDIX

PRO E drawings for modification of dilatometer (Shaft 1)

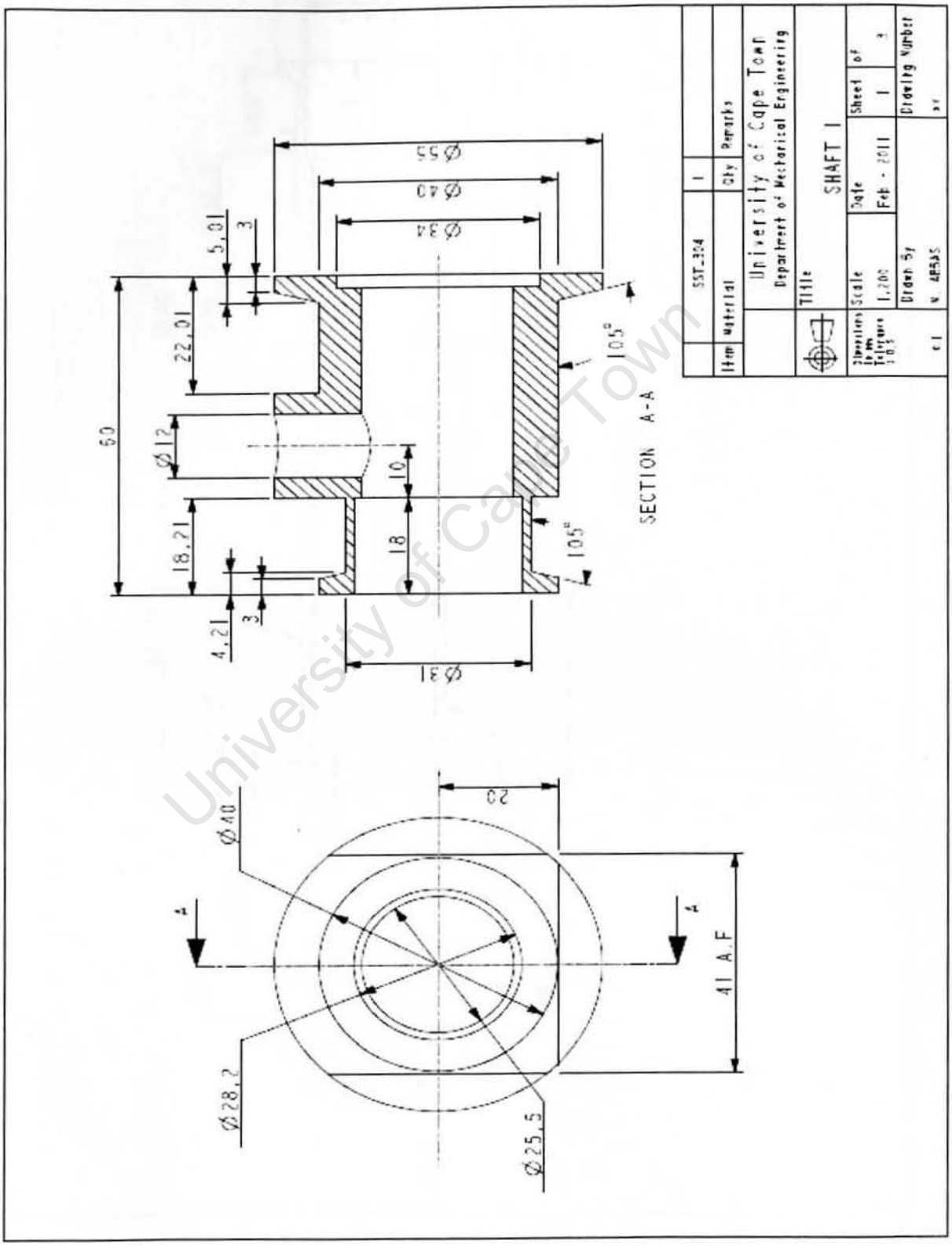

Shaft 2

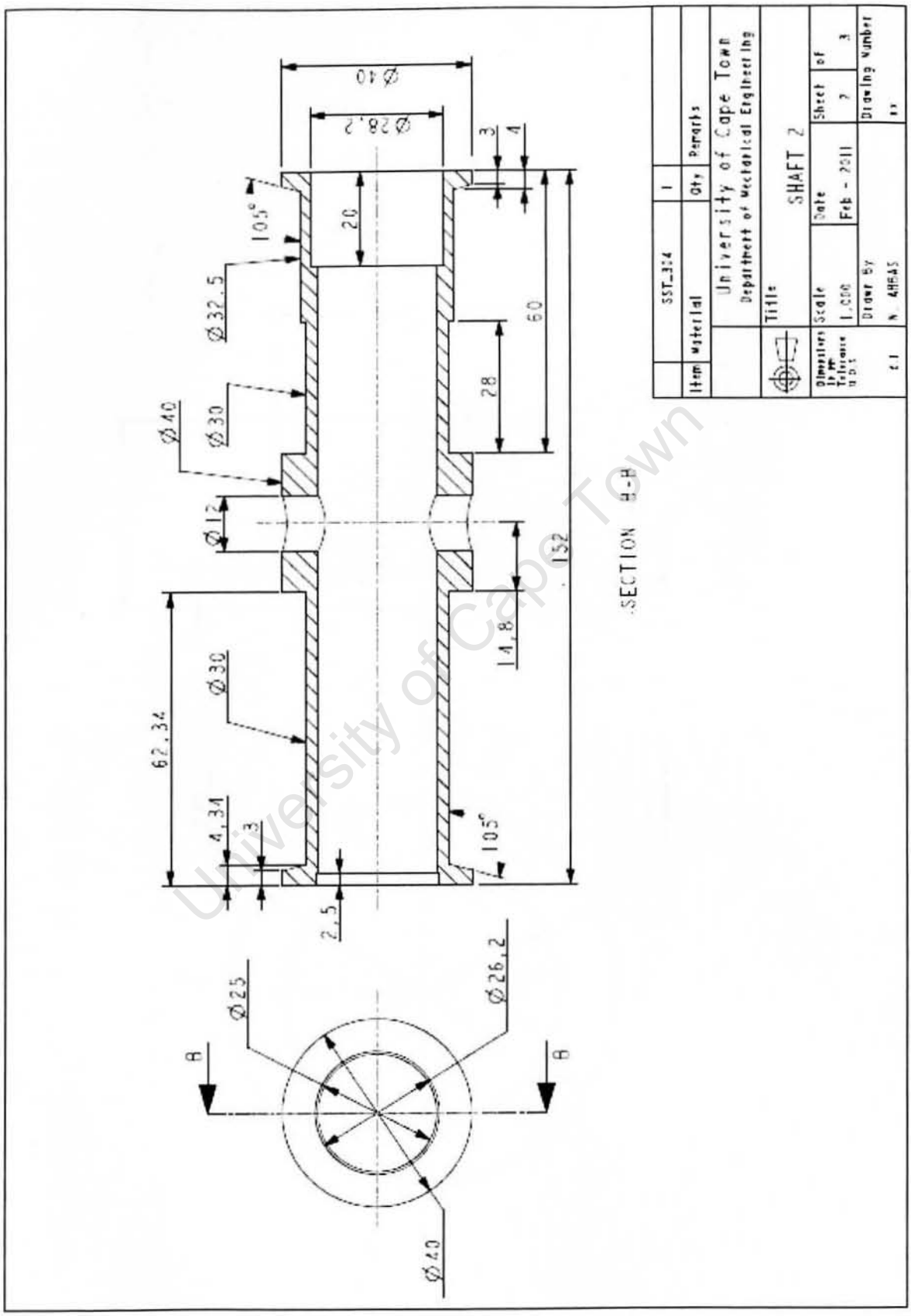

Flanges

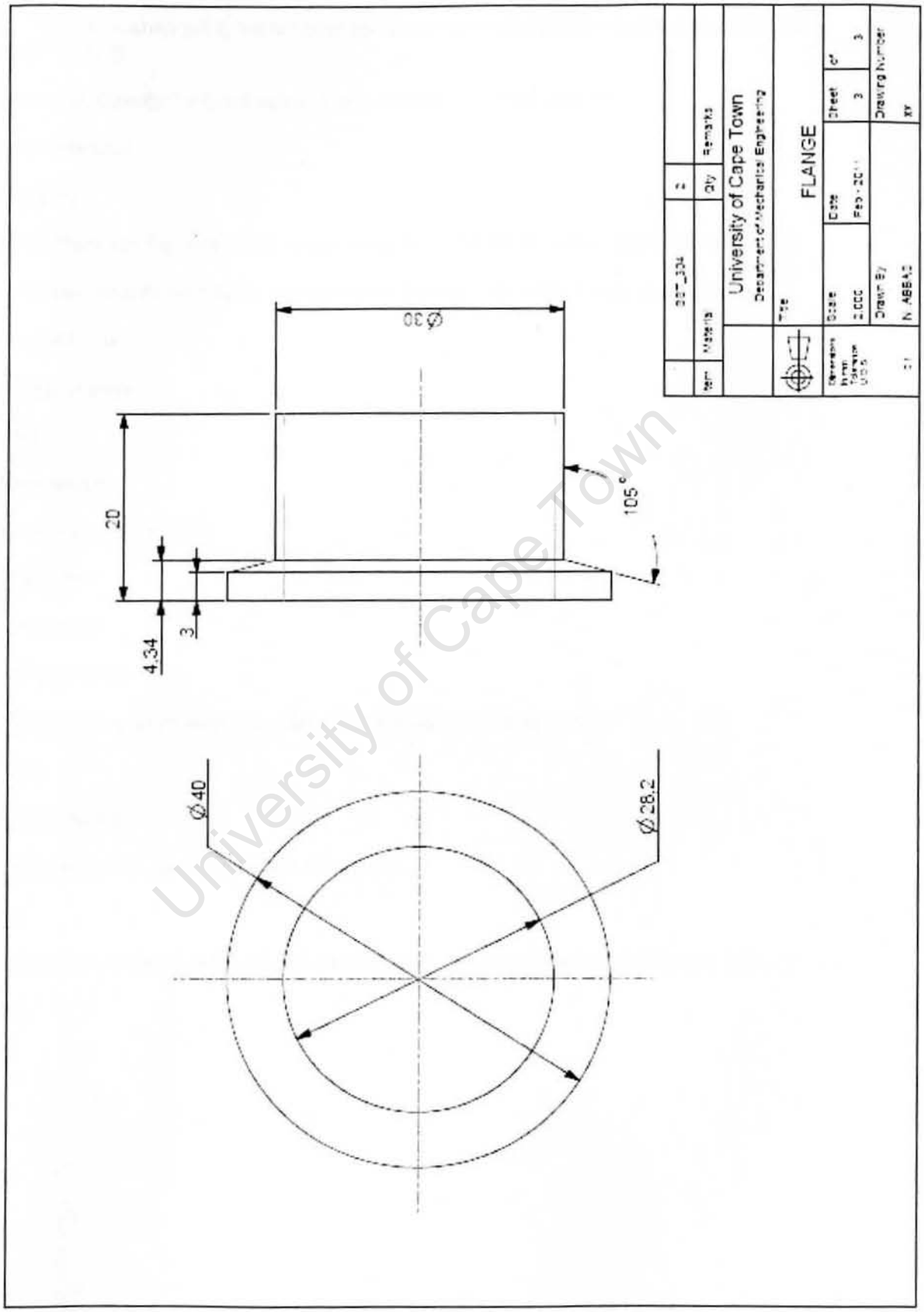

MATLAB CODE FOR AVERAGE STRAIN AND TEMPERATURE CALCULATIONS

```
disp('Note that when using the program the excel spreadsheet to be analysed must be in the
same folder. ');

data=input('Specify the excel spreadsheet, include extension (e.g .xls): ','s');

y=xlsread(data);

f=length(y);

fprintf('There are %g data points in your excel file. This value is your data point max.  \n',f);

limit=input('Specify the closest number below the data point max that is divisible by 5: ');

newy=y(1:limit);

g=length(newy);

inc=g/5;

check=limit/5;

check2=isinteger(check);

if check2==1

   for i=1:inc

   k=1+((i-1)*5);

   yavg(i)=(newy(k)+newy(k+1)+newy(k+2)+newy(k+3)+newy(k+4))/5;

   end

   yavg2=yavg.';

   xlswrite('5point_output_average.xls',yavg2);

else

   disp('The number specified is not divisible by 5, restart application and choose again. ');

end
```

VOLUME CALCULATION FOR α AND β PHASES (PER ATOM) DURING HEATING TO 1050°C

The volume of hcp phase (per atom)

The factor of 6 in the denominator of Equation (a) arises because the unit cell of the α (hcp) consists of 6 atoms whereas that of β (bcc) consists of four atoms.

$$V_\alpha = \frac{a^2 c 3\sqrt{3}}{2 \times 6} \text{ (a)}$$

$$a = a_o[1 + \alpha_{\alpha a}(T - 20)] \text{ (b)}$$

$$c = c_o[1 + \alpha_{\alpha c}(T - 20)] \text{ (c)}$$

- V_α = volume of the α phase
- a_o = lattice parameter (basal plane) of titanium at room temperature (α phase): 2.95Å
- T = temperature
- $\alpha_{\alpha a}$ = coefficient of thermal expansion of α phase along a-axis at room temperature: 10.5×10^{-6}/°C
- $\alpha_{\alpha c}$ = coefficient of thermal expansion of α phase along c-axis at room temperature: 5.6×10^{-6}/°C
- c_o = lattice parameter of titanium (adjacent plane) at room temperature (α phase): 4.66Å

The volume of bcc phase (per atom)

The factor of 2 in the denominator of Equation (d) arises because the unit cell of the α (hcp) consists of 6 atoms whereas that of β (bcc) consists of four.

$$V_\beta = \frac{b^3}{2} \text{ (d)}$$

$$b = b_o[1 + \alpha_\beta(T - 20)] \text{ (e)}$$

- V_β = volume of the β phase
- b_o = lattice parameter titanium in the bcc phase: 3.27Å

- T = temperature (increasing at increments of 10°C)
- α_β = coefficient of thermal expansion of β phase: 14.1×10^{-6}/°C